DISSERTATION | DOCTORAL THESIS

Titel | Title

The role of sister chromatid conformation during homology-directed repair of DNA double-strand breaks

verfasst von | submitted by

Inès Prlesi L M

angestrebter akademischer Grad | in partial fulfilment of the requirements for the degree of

Doctor of Philosophy (PhD)

Wien | Vienna, 2025

Studienkennzahl lt. Studienblatt | Degree programme code as it appears on the student record sheet:	UA 794 620 490
Dissertationsgebiet lt. Studienblatt | Field of study as it appears on the student record sheet:	Molekulare Biologie
Betreut von | Supervisor:	Dipl.-Biol. Dr. Daniel Wolfram Gerlich

Table of Contents

Contribution statement

The research presented in this thesis was carried out at the Institute of Molecular Biotechnology of the Austrian Academy of Sciences (IMBA), in Vienna, as part of the Vienna Bio Center (VBC) PhD program, in the laboratory of Daniel Gerlich and under his supervision.

Data acquisition and experimental procedures were conducted solely by myself (Inès Prlesi). The experimental data were processed using a preprocessing and analysis pipeline originally developed by Vincent Reuter, and subsequent data analysis was conducted using scripts and tools provided by Thomas Steinacker. Both the processing pipeline and the analysis scripts were adapted and applied by me to the specific research questions of this thesis. No other collaborators, technicians, or supervisors directly carried out experiments or primary data collection on behalf of myself.

Any additional contributions by supervisors, collaborators, and technicians were limited to scientific discussion, conceptual guidance, feedback on data interpretation, and editorial comments on the text.

Use of Algorithms and AI-based Tools

In accordance with the university's AI policy, the following algorithms and tools were used in the preparation of this thesis:

- Automated spelling and grammar checking was performed using standard language tools (e.g., the built-in spelling and grammar checkers in Microsoft Word).
- AI-based language models (e.g., ChatGPT) were used for improving the fluency and clarity of some paragraphs. These tools were not used for generating original scientific content, designing experiments, producing or altering data, or performing statistical analyses. All scientific ideas, interpretations, and conclusions are my own.

No algorithm or AI-based tool was used to fabricate, manipulate, or falsify data or results. All reported experiments, analyses, and conclusions are based on my original work and genuine research activities.

Vienna, 25.11.2025

Inès Prlesi

Acknowledgments

I would like to thank **Daniel Gerlich** for being my thesis supervisor and for giving me the opportunity to work on such an exciting project, surrounded and supported by excellent scientists, in an incredible institute with remarkable resources and infrastructure. I also would like to thank **Andrea Pauli** and **Joao Matos** for being part of my thesis committee and providing guidance and support in this experience.

I want to thank the people in Vienna who accompanied me during my thesis by sharing the everyday reality of my PhD with me. I am deeply grateful to **Thomas** and **Federico** for their guidance and supervision, and for creating an environment where collaborative work and friendship naturally came together. I am thankful to all of my other **colleagues** in the Gerlich Lab for the great lab atmosphere, for the many coffee breaks, and for the numerous hangouts that made everyday life in the lab very enjoyable. My heartfelt thanks go to **my friends** in Vienna for making my time here feel like home throughout my PhD. I am especially grateful to **Barbara** for her emotional support and solidarity throughout the ups and downs of the PhD experience. I would like to thank my **cats**, especially **Yuzu**, who was with me in Vienna and helped me keep perspective and focus on the small joys in life. Finally, to my **partner**, thank you for making life extra exciting even when times were hard, and for all the laughter, lightness, and support that made this journey so much brighter.

I also need to thank all my loved ones in France, whom I did not get the chance to see very often but who were on my mind the whole time. I want to thank **Kim**, my best friend, for always being there for me, whether from a distance in Paris, during one of her numerous trips to Vienna, or during my trips back home. I also want to thank **Jilann** who has been a precious friend for so many years, and even though we don't get to be together as often as we'd like, I have always felt her support. I would like to thank my **parents** for their endless support during this adventure, which turned out to be more intense than any of us expected. I have missed them dearly and am excited to return to them. Above all, to my **sister**, thank you for being my rock in life and throughout this PhD, always there with infinite support and understanding.

Zusammenfassung

Während der G2-Phase müssen Zellen DNA-Doppelstrangbrüche (DSBs) präzise mithilfe der Schwesterchromatide reparieren. Wie die lokale Chromatinarchitektur und die Doppelrolle von Cohesin diesen Prozess steuern, war jedoch unklar. In meiner Dissertation habe ich einen Einzelzellansatz mit „Vier-Enden"-RASER-FISH entwickelt, der gleichzeitig beide DSB-Enden auf der gebrochenen Chromatide und die entsprechenden Loci auf der intakten Schwester an definierten, Cas9-induzierten Bruchstellen auflöst. In Kombination mit Zellzyklus-Synchronisation, quantitativer Bildgebung und akuten Perturbationen von Cohesin- und Homologiereparaturfaktoren zeige ich, dass G2-DSBs konsequent eine Disjunktion der Enden in cis und eine verstärkte Annäherung der Schwestern erfahren. Die End-Separation erfordert loop-extrudierendes Cohesin, jedoch nicht kohäsives, Sororin-gebundenes Cohesin, während die Annäherung der Schwesterloci auch ohne Cohesin und zentrale HR-Faktoren erfolgt, was auf einen Cohesin- und HR-unabhängigen Kompaktierungsmechanismus hinweist. Meine Arbeit legt damit offen, wie die lokale 3D-Genomorganisation um DSBs herum orchestriert wird, und etabliert einen vielseitigen Rahmen, um reparaturassoziierte Chromatindynamik an einzelnen Loci zu untersuchen.

Summary

During G2, cells must repair DNA double-strand breaks (DSBs) accurately using the sister chromatid as a template. However, how local chromatin architecture and cohesin's dual roles shape this process remain unclear. In my thesis, I developed a single-cell, "four-end" RASER-FISH assay that simultaneously resolves both DSB ends on the broken chromatid and the corresponding loci on the intact sister at defined Cas9-induced breaks. Combining this with cell-cycle synchronization, quantitative imaging, and acute perturbations of cohesin and homologous recombination factors, I show that G2 DSBs robustly undergo cis end disjunction and increased sister proximity. End separation requires loop-extruding cohesin but not cohesive, Sororin-bound cohesin, whereas sister engagement occurs even in the absence of cohesin and key HR factors, indicating a cohesin- and HR-independent compaction mechanism. My work thus uncovers how local 3D genome reorganization around DSBs is orchestrated and establishes a versatile framework to dissect repair-related chromatin dynamics at single loci.

1. Introduction

1.1. Safeguarding Genome Integrity: Double-Strand Break Repair Pathways

DNA is a molecule that provides the blueprint for all biological processes an organism needs for its life, therefore maintaining its integrity is a crucial stake. If the DNA is not safeguarded accurately, proper function of the organism is compromised and issues in cell proliferation can arise. This can eventually lead to deadly diseases, such as cancer (Jackson & Bartek, 2009; Lukas et al., 2011). Many lesions can threaten the DNA, and among them the most threatening lesions are DNA double-strand breaks. These breaks cause physical disruption of the DNA double helix, severing its continuity. Multiple repair pathways have evolved to safeguard genome stability and are thus deployed by eukaryotic cells to repair these breaks (Hartlerode & Scully, 2009). Two canonical repair pathways predominate: non-homologous end-joining and homologous recombination. Other alternative pathways such as single-strand annealing and alternative end-joining can act as additional routes in specific exceptional contexts (Figure 1.1.1). Each pathway affects differently the mutational outcomes and chromosome structure, but they share the same starting point, among which is the phosphorylation of the histone H2A (γH2AX) (Rogakou et al., 1998; Scully & Xie, 2013). This chromatin mark specific to the repair of double-strand breaks is deposited by the Ataxia-telangiectasia mutated (ATM) kinase (Burma et al., 2001). Despite their similar starting point, the usage of each of these pathways depends on the cell cycle stage (Hustedt & Durocher, 2016; Scully et al., 2019). This reflects the availability and presence of the factors required for each of these pathways, as well as the accessibility to a homologous template.

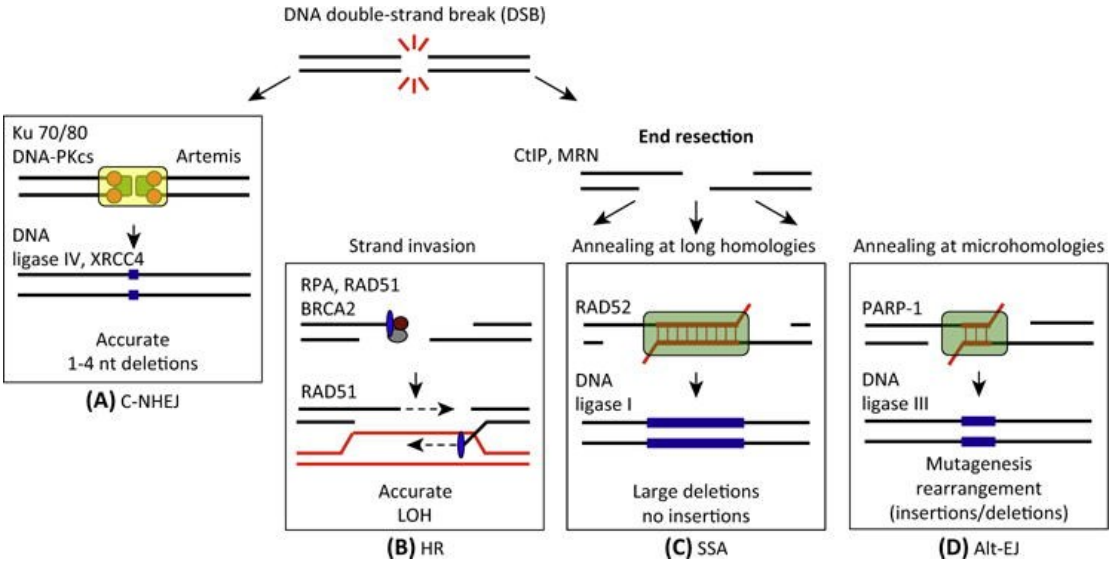

Figure 1.1.1. Repair pathways for DNA double-strand breaks. Here are depicted the two major repair pathways, namely canonical non-homologous end-joining (C-NHEJ; A) and homologous recombination (HR; B). Alternatively, two other repair pathways also occur: single-strand annealing (SSA; C) and alternative end-joining (alt-EJ; D). The main factors are indicated for each pathway. Figure from (Ceccaldi et al., 2016).

In the G1 phase of the cell cycle, the principal repair pathway for DNA double-strand breaks is non-homologous end-joining (Pannunzio et al., 2018) (Figure 1.1.2). The blunt broken ends are recognized by the Ku70/Ku80 complex, that in turn recruits other factors such as DNA-dependent protein kinase catalytic subunit (DNA-PKcs) leading to DNA end tethering (Graham et al., 2016). In this pathway, the DNA ends are protected from resection and are quickly aligned and religated by DNA ligase IV (LIG4) (Nick McElhinny et al., 2000; Wilson et al., 1997).

While it is fast and effective, this pathway can be error-prone and potentially lead to inversions or deletions of base pairs surrounding the DNA break (Guirouilh-Barbat et al., 2004) since it does not rely on any type of homology.

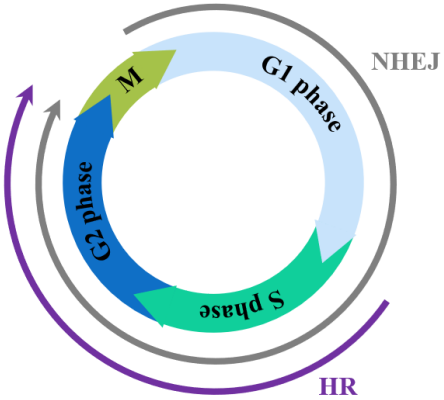

Figure 1.1.2. Eukayotic cell cycle. Cells undergo consecutively G1 phase, S phase, G2 phase and M. In G1, a single copy of the genome is present. S phase is the replicative phase, where the DNA is progressively doubled. In G2 phase, the genome is present fully replicated. M stands for mitosis, where the duplicated genomes faithfully segregate at two opposites poles of the cell. During cytokinesis, the original G1-phase mother cell gives rise to two daughter cells with the same genetic information. The major repair pathways of double-strand breaks in each phase are also depicted: non-homologous end-joining (NHEJ) happens throughout the cycle, while homologous recombination (HR) only occurs in replicated genomes, namely during S and G2 phases. Inspired from (Hochegger et al., 2008).

By contrast, the S and G2 phases of the cell cycle are permissive for homologous recombination, making it a canonical repair pathway in this context (Mao et al., 2008; Saleh-Gohari & Helleday, 2004). Indeed, these phases are characterized by the presence of a sister chromatid, as DNA is replicated. In mitotic cells, the repair happens mostly between sister chromatids and not between homologous chromosomes (Johnson & Jasin, 2000; Nakamura et al., 2019). Therefore, having an intact homologous repair template in the nucleus enables this generally high-fidelity repair process. Homologous recombination requires 5'-3' end resection at the double-strand break site, a process enabled in S/G2 phases and coordinated by the MRN complex (MRE11-RAD50-NBS1 triad), CtIP (CtBP-Interacting Protein), BRCA1 (Breast cancer 1), and exonucleases such as EXO1. Resection generates single-stranded DNA overhangs that are initially bound by Replication Protein A (RPA), a trimer that allows single-stranded DNA from winding back on itself. This protein is subsequently exchanged for the protein RAD51,

with the help of BRCA2 (Breast cancer 2), forming a nucleoprotein filament, that I will refer to as "RAD51 filament". The RAD51 filament, or presynaptic filament, will conduct homology search by probing the surrounding DNA and thus forming intermediate eight-nucleotide long semi-stable complexes (Qi et al., 2015). Also, due to structural differences between RPA and RAD51, RAD51-coated DNA generates a stiffer filament in comparison to RPA, which facilitates the search activity (Lee et al., 2013). Once homology is found, the RAD51 filament performs strand invasion into the sister chromatid, displacing the original DNA strand which causes the formation of a displacement loop (D-loop). This will trigger the unloading of RAD51 by the protein RAD54 (Mason et al., 2015) and initiate the repair process with DNA synthesis and eventually completion of recombination.(Figure 1.1.3.)

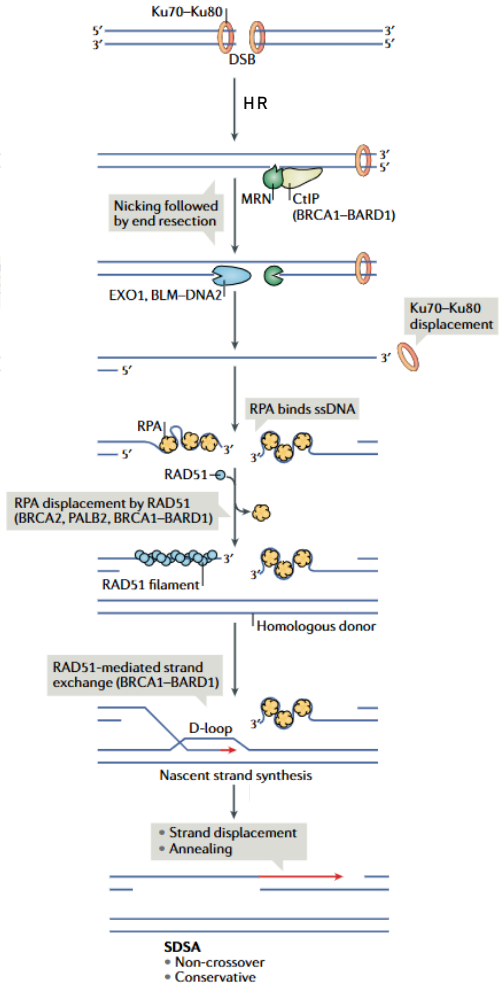

Figure 1.1.3. Homologous recombination (HR) steps in somatic cells, and its different actors. Adapted from (Scully et al., 2019), only displaying the case where

homologous recombination ends with synthesis-dependent strand annealing (SDSA), which is the predominant pathway in somatic cells.

1.2. Three-Dimensional Genome Architecture and the Cohesin Complex

Packing nearly two meters of DNA into a nucleus that is only ~10 μm in diameter constitutes an extraordinary organizational challenge. Eukaryotic genomes must be condensed enough to fit in the physical constraints of the nuclear envelope, but almost as importantly they should remain readable by the cell. Indeed, accessibility of the genome is crucial for transcription, replication and repair, which are all factors supporting and allowing cell survival. Finding the right balance between compaction and accessibility is ensured by folding chromatin into a highly organized and hierarchical three-dimensional architecture.

This hierarchical organization spans several scales (Cremer & Cremer, 2010) (Fig. 1.2.1). At the megabase scale, chromosomes occupy distinct territories within the nucleus (Khalil et al., 2007). Within each territory, chromatin segregates into compartments, which further subdivide into topologically associating domains (TADs). At the sub-megabase level, individual chromatin loops form between specific loci (Rao et al., 2014). Together, these layers of organization define the three-dimensional context in which DNA repair takes place.

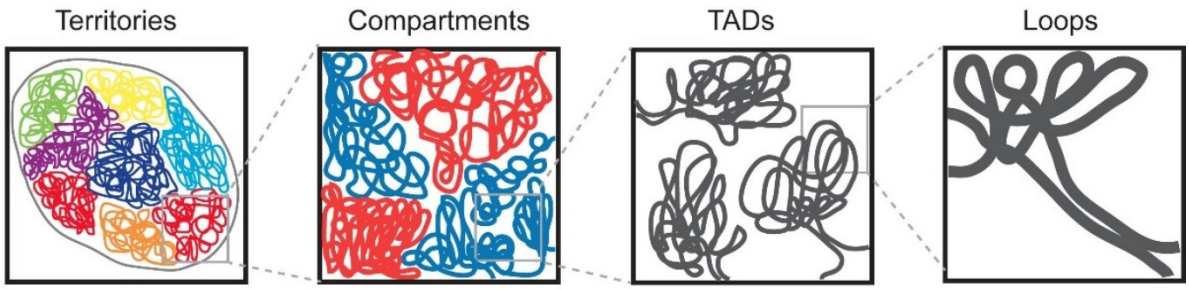

Figure 1.2.1. Hierarchical chromatin folding. Here are depicted the different scales at which the chromatin is folded in eukaryotic cells. Every level of compaction allows for preferential DNA interactions within it, and decreased DNA interactions across

them. Territories are defined by the chromosomes' position in the nucleus, while compartments are functionally described as generally transcriptionally active or inactive. Topologically-associated domains (TADs) are regions where physical genomic contact occurs more often than between TADs. At the finest scale, DNA loops form and increase contacts between two elements, such promoter-enhancer interactions. Adapted from (Sikorska & Sexton, 2020).

A central organizer of three-dimensional genome architecture is the cohesin complex, a ring-shaped protein complex that belongs to the family of Structural Maintenance of Chromosomes (SMC) (Michaelis et al., 1997; Rao et al., 2017) (Figure 1.2.2). This highly conserved complex is composed of the SMC1 and SMC3 ATPases, whose two coiled proteins dimerize at their hinge domains. They are bridged by the kleisin subunit RAD21, "closing" the ring. An additional subunit, STAG1 or STAG2 (also known as SA1/SA2), binds RAD21, and can serve as an interaction platform for other regulators.

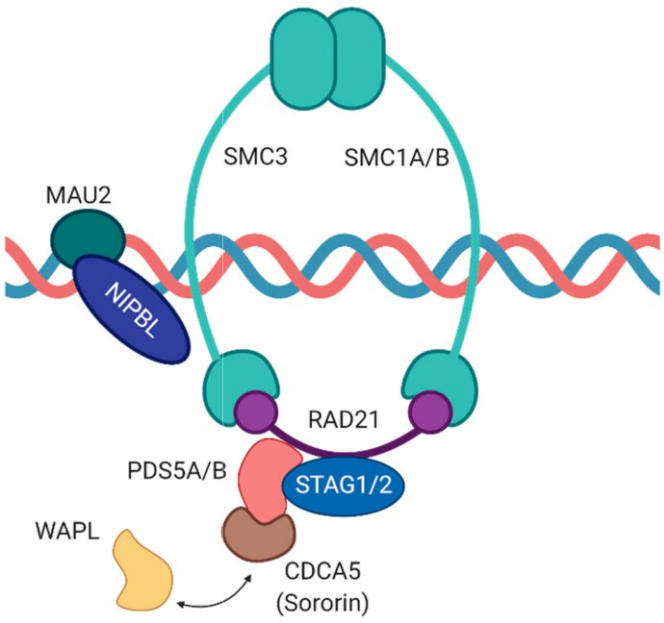

Figure 1.2.2. The cohesin complex and its associated proteins. The core is formed of four proteins: SMC3, SMC1, RAD21 and STAG1/2; there are five regulators of cohesin: NIPBL and MAU2, PDS5A/B, WAPL, and Sororin. The last two compete for binding to PDS5, WAPL favoring release of cohesin from the DNA and Sororin inducing sister chromatid cohesion. Figure from (Kuru-Schors et al., 2021).

Cohesin is loaded onto chromosomes by NIPBL (Nipped-B-like protein) associated with the MAU2 protein, which in an ATP-dependent manner, extrudes DNA to form loops. Its residence time and processivity are regulated by binding subunits, namely by the release factor WAPL (Wings apart-like protein homolog) and modulated by PDS5 (Sister chromatid cohesion protein PDS5 homolog B/A). Loop growth is also constrained in size by boundary elements enriched for CTCF (CCCTC-binding factor). This factor binds to convergently oriented CTCF-binding sites, which act as a strong stopper, limiting loop size and contributing to the formation TADs (Wutz et al., 2017). These domains thus represent genomic regions within which DNA contacts are more frequent than across boundaries, and they provide a modular framework that influences a multitude of cellular processes, such as gene regulation, replication timing, and DNA repair.

1.3. Cohesin Functions Across the Cell Cycle: The Dual Role in G2

Already in G1, cohesin finds itself playing crucial roles in the architecture of the genome and its function. By extruding loops of chromatin, cohesin compacts chromosomes and brings distant loci into proximity (Schwarzer et al., 2017). The organization of the genome into loops influences many cellular processes, namely transcription. Loops both increase proximity between promoters and enhancers, but they also can in return insulate specific regions from enhancers, overall shaping the transcriptional landscape of cells. Replication timing is also affected by looping of the chromatin, with each loop often forming regions of coordinated replication origin firing. In this context, cohesin acts as a dynamic loop-extruder which is going through cycles of loading, sliding and releasing from the chromatin.

When the genome is replicated in S phase, cell nuclei contain twice as many chromatids, increasing crowding. In this architectural challenge, cells are still able to maintain their nuclear functions properly, among which transcription and replication. It is during replication that a fraction of cohesins is converted into a new form, referred to as cohesive cohesin. The cohesion factor Sororin binds to the cohesin complex and promotes its stable association with chromatin by preventing WAPL-mediated release

(Nishiyama et al., 2010). At the same time, ESCO acetyltransferases acetylate the SMC3 subunit of cohesins, further increasing their stability. This stable cohesin form will remain bound to the sister chromatids, holding them together until mitosis (Gerlich et al., 2006). The other cohesin complexes remain dynamic and continue to extrude loops along the DNA fiber.

As a result, cohesins perform two mechanistically distinct functions on the same genome: one pool of cohesins extrudes loops that tend to structure each chromatid independently, and another pool maintains cohesion between sister chromatids (Figure 1.3.1). The dual activity of cohesins shape a complex pattern of sister chromatid conformations (Mitter et al., 2020), creating two spatial axes that are central for our understanding of chromatin dynamics in an intricately organized nucleus.

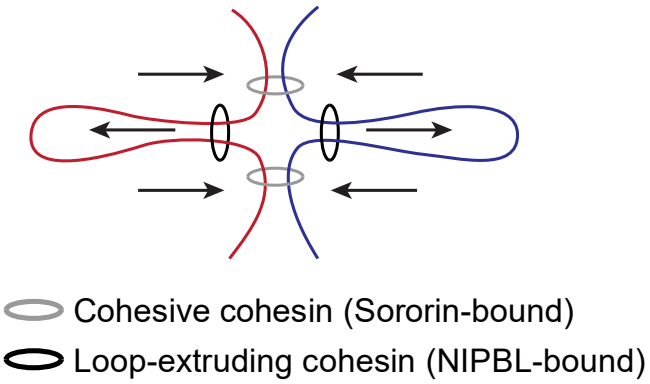

Figure 1.3.1. Opposing actions of cohesins on replicated genomes. Cohesins have different effects on sister chromatid proximity, depending on their bound partner. Sororin-bound cohesin creates linkages that keep sisters in close proximity, whereas NIPBL-bound cohesins extrude loops on the same chromatid, causing extremities of the loop to be further away. Adapted from (Batty et al., 2023).

Notably, loop extrusion has been proposed to increase separation between sister loci in replicated chromosomes, by structuring each chromatid independently (Batty et al., 2023). In the context of DNA double-strand break repair during G2, this implies that if a break happens inside a loop, or even at the loop extremity, the broken ends will find themselves to be far away from the template locus on the intact sister chromatid. Homologous recombination cannot proceed with faithful repair in contexts where the

homologous template is not found. This makes the looping activity of cohesins a potentially detrimental characteristic for homology-mediated DNA repair.

On the other hand, Sororin-stabilized cohesive cohesin could restrain the diffusion of broken ends and therefore favor accurate repair. Indeed, by clamping the sisters together throughout the genome, the proximity between the damaged locus and the sister template is maintained.

Thus, in a G2 nucleus, the same cohesin machinery can in principle both constrain and remodel the spatial environment of a DSB. Disentangling how these two activities affect end behavior in cis and sister-template engagement in trans is a central aim of this thesis and is explored in more detail in the following sections.

1.4. Cohesin and Double-Strand Break Repair: Current Perspectives and Open Questions

Interestingly, RAD21 was first identified for its role in DNA double-strand break repair (Birkenbihl & Subramani, 1992), before its canonical role in sister chromatid cohesion was discovered (Michaelis et al., 1997). It was indeed shown that RAD21-defective yeast had more difficulties in repairing ionizing-radiation-induced DNA double-strand breaks. This underlines the importance of the cohesin complex in double-strand break repair. Cohesin has now been found to participate in multiple facets of double-strand break repair (Litwin et al., 2018), yet its precise contributions to homologous recombination remain debated.

1.4.1. Cohesin accumulation and domain-scale organization near double-strand breaks

Cohesins have long been known to accumulate around double-strand breaks (Ström et al., 2004; Unal et al., 2007), but only more recently has the attention shifted to the functional consequences of such an observation. The architectural changes induced by cohesin accumulation results in the formation of “repair domains” which are enriched

for repair factors (Arnould et al., 2021; de Luca et al., 2024; Sanders et al., 2020). Thanks to their loop extrusion activity and the constraint by boundary elements, cohesins can increase local contact frequency (Rao et al., 2014; Schwarzer et al., 2017). This is hypothesized to concentrate the homologous recombination machinery and modulate access to the donor template.

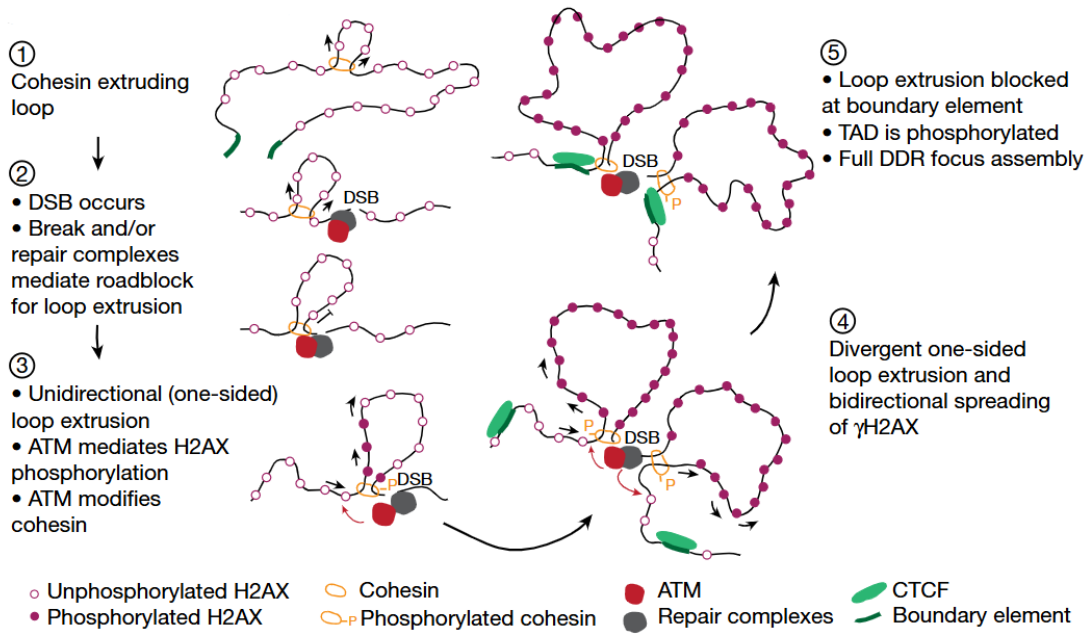

Figure 1.4.1. Model for cohesin-mediated formation of repair domains. The authors propose that γH2AX deposition in response to a DNA double-strand break is ATM-dependent, and that it relies on the loop-extruding function of cohesin. Figure from (Arnould et al., 2021)

These observations support a view in which cohesins participate in the organization of a microenvironment that is favorable for repair, rather than directly catalyzing steps of homologous recombination.

1.4.2. End tethering and coordinated dynamics of double-strand break ends

Cohesins have been proposed to act as a tether on broken DNA ends, maintaining their proximity and thereby favoring accurate repair (Yang et al., 2023). In budding yeast,

microscopy and genetics showed that cohesin tethers double-strand break ends through oligomerization or pairing of cohesin complexes (Phipps et al., 2025).

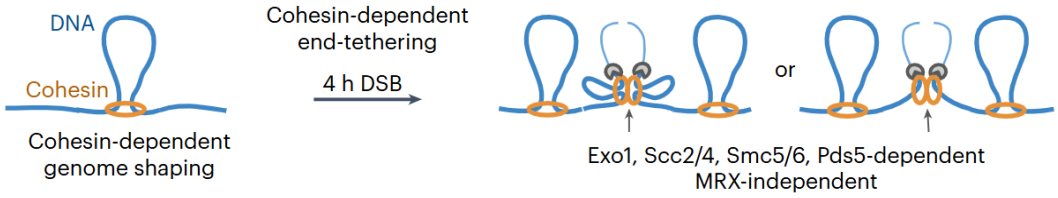

Figure 1.4.2.1. Oligomerization of cohesins to act as a tether around double-strand break ends. Figure from (Phipps et al., 2025)

Other studies in yeast have reported other factors than cohesins to be responsible for double-strand break end tethering, such as MRX (the yeast equivalent of the MRN complex), Exo1 and the 9-1-1 clamp (Piazza et al., 2021). Instead, it has been shown that RAD51-mediated stiffening of the resected ssDNA at double-strand break ends results in a coordinated homology search by both ends. In this model, cohesin is thought to be responsible for the restriction and focusing of the local search range (Dumont et al., 2024).

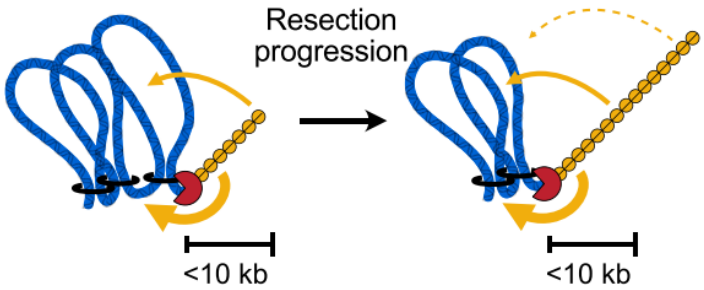

Figure 1.4.2.2. Model for the interaction of the RAD51-coated ssDNA and cohesin-mediated loops on the same chromatid. Figure from (Dumont et al., 2024)

End tethering has also been proposed as a mechanism of double-strand break end dynamics in human cells (Friskes et al., 2025). Altogether, these findings raise the possibility that the behavior of broken DNA ends reflects a balance between cohesin-mediated constraints and changes in the physical properties of the DNA fiber induced by resection and RAD51 loading.

1.4.3. Chromatin mobility and template search

Double-strand breaks have also been shown to increase overall chromatin mobility (Dion et al., 2012; Miné-Hattab & Rothstein, 2012), and while this may facilitate homology search, it also increases the risk of ectopic interactions (Aten et al., 2004; Roukos et al., 2013). Cohesins can both restrict motion of damaged DNA by loop extrusion and sister cohesion (Arnould et al., 2023; Dion et al., 2013; Yang et al., 2023), and in other contexts promote chromatin reorganization by redistributing contacts (Piazza et al., 2021; Teloni et al., 2025) (Figure 1.4.3). Whether cohesins primarily aid contacting the sister chromatid (trans proximity) (Covo et al., 2010) or mainly limits mis-joining by constraining ends (cis control) (Gelot et al., 2016) likely depends on cell type, genomic context, and time within S/G2.

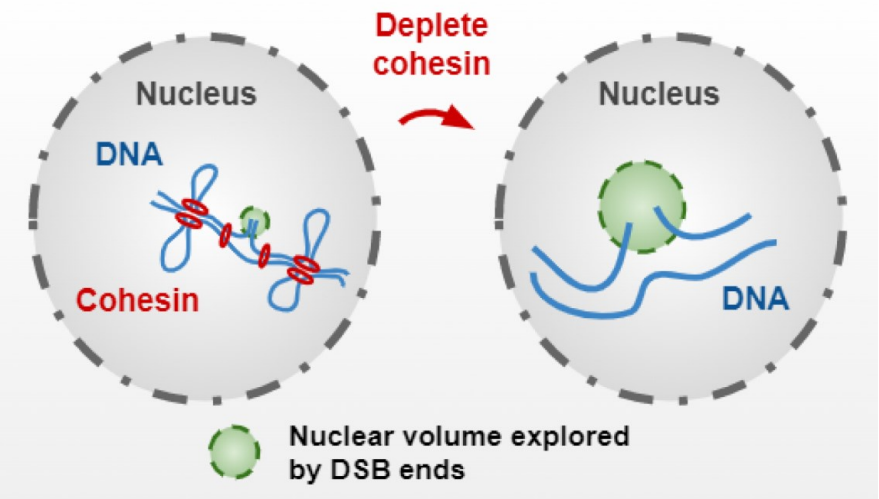

Figure 1.4.3. Cohesin contributes to restrict chromatin mobility in the context of DNA double-strand break repair. Adapted from (Phipps & Dubrana, 2022)

Some questions thus remain unresolved, namely questions about double-strand break ends behavior in cis and trans (disjunction or tethering), the contribution of cohesins in homologous recombination, and the coordination of spatial organization and RAD51 loading.

Addressing these questions requires single-cell, site-specific measurements that simultaneously resolve the two ends on the damaged chromatid (cis) and the position

of the sister template (trans) — a view that population-averaged sequencing approaches (e.g., ChIP-seq and Hi-C) cannot provide. Our approach was designed to obtain this missing perspective.

1.5. Bridging the Conceptual Gap: A Single-Cell, Four-End Approach to Study G2 DSB Repair

Most evidence on cohesin and repair of double-strand breaks through homologous recombination comes from population-averaged assays, such as ChIP-seq and CUT&Run for factor accumulation, Hi-C/3C for contact frequencies, END-seq/BLISS for end processing. While these approaches provide enormous amounts of data and thus strongly highlight reoccurring patterns, they have two key limitations:

First, they average across cells and loci, which obscures the heterogeneity caused by variable cutting efficiency, locus context, and sometimes even cell-cycle phase (especially the G2-specific architectural state). This limitation can be resolved by imaging assays, combined with immunofluorescence, where we can access the single-cell level.

Another limitation is that they mainly rely on the inference of spatial organization indirectly (via contact probabilities or factor occupancy) rather than on the direct measurement of physical distances. This can skew the interpretation of results, since the genomic landscape is not accurately represented.

Although they allow us to uncover a lot of knowledge about genomic contacts during double-strand break repair, both sequencing and imaging-based approaches so far share the same shortcomings. Differentiating the sister chromatids to detect which one is undergoing repair is not possible, due to their sharing of the same DNA sequence or their spatial proximity. On a smaller scale, the DNA ends of a single double-strand break are not simultaneously resolved, on the damaged chromatid (in cis) and on the corresponding loci on the sister chromatid (in trans) in the same cell. This currently prevents us from discovering the intricate DNA movements that occur during homologous recombination.

It is for this reason that I want to address these fundamental questions that were not tackled previously:

- To what extent does cohesin drive cis end disjunction versus end tethering at mammalian double-strand breaks in G2?
- How do cohesins contribute to sister-template proximity during homologous recombination: through their cohesive function, their loop-extruding activity, or neither?
- How are these spatial behaviors temporally ordered with respect to resection and RAD51 loading?

Our approach to close the gap

To obtain this missing perspective and address these questions, we developed a site-specific and time-resolved assay in G2 that directly measures both cis end behavior and trans sister engagement:

- Cells in G2 phase: Synchronization protocol to obtain cell-cycle specificity in our readout, capturing the complex organization of the DNA at this stage
- Cas9-induced DSBs: Targeted breaks at defined loci with controlled timing, alongside quantification of cutting efficiency.
- Orthogonal readouts of homologous recombination engagement: Immunofluorescence for 53BP1 and RAD51 to track pathway choice and timing relative to spatial changes.
- "Four-end" resolution with RASER-FISH: An oligonucleotide pool design that labels each of the four ends of a double-strand break (two per sister) so we can identify and measure:
    - Cis distances: separation of the two ends on the damaged chromatid.
    - Trans distances: proximity between corresponding loci on sister chromatids.
- Mechanistic perturbations: Acute depletion of cohesin subunits (RAD21) and cohesion stabilizer (Sororin) to separate loop-extruding versus cohesive

functions; depletion of homologous-recombination-specific factors (BRCA1 and BRCA2) to test the dependency of homology-directed repair to spatial dynamics.

- Single-cell, single-locus quantifications: 3D distance measurements and distributional analyses that capture heterogeneity and effect sizes rather than only mean shifts.

Together, these features allow us to directly test whether cohesin is required for cis end disjunction versus sister-template proximity, and whether these spatial reorganizations depend on the function of homologous recombination, within the distinct architectural context of G2.

2. Methods overview

To study chromosome conformation in the context of homologous recombination, we established multi-site induction of DNA double-strand breaks to analyze the organization of DNA break ends and their homologous region on the sister chromatid using FISH and determine the type and organization of repair machinery using immunofluorescence. We are using a synthetic single-guide RNA (sgRNA) targeting 23 genomic sites (the sgRNA HS17 from (van den Berg et al., 2018) and out of these 23 sites, I designed 21 corresponding FISH probes to visualize chromatin in their vicinity. By detecting 53BP1 as a general double-strand break repair marker, we can assess the induction of breaks, to then study whether the homologous recombination-specific repair component RAD51 has formed filaments on DNA. The conformation of the filaments and adjacent 30kb-long regions are then determined by multiplexed FISH. Through these experiments, the project allows us to assess how the chromosome conformation prior to double-strand break induction affects homologous recombination efficiency, and how sister chromatids reorganize during DNA repair. The three main technologies we are using are explained below.

2.1. Time-controlled Cas9-mediated double-strand break induction

For time-controlled multi-site induction of DNA double-strand breaks we use a human cancer cell line (HeLa cells) that contains an inducible expression construct of Cas9 and transfect synthetic gRNAs (sgRNAs) that target 23 sites in the human genome. This core technology, along with its combination with a synchronization protocol ensuring most cells are in G2 (when homologous recombination is active), has already been established and validated in the lab by a post-doc, **Federico Teloni**, with whom I collaborated to further improve the system.

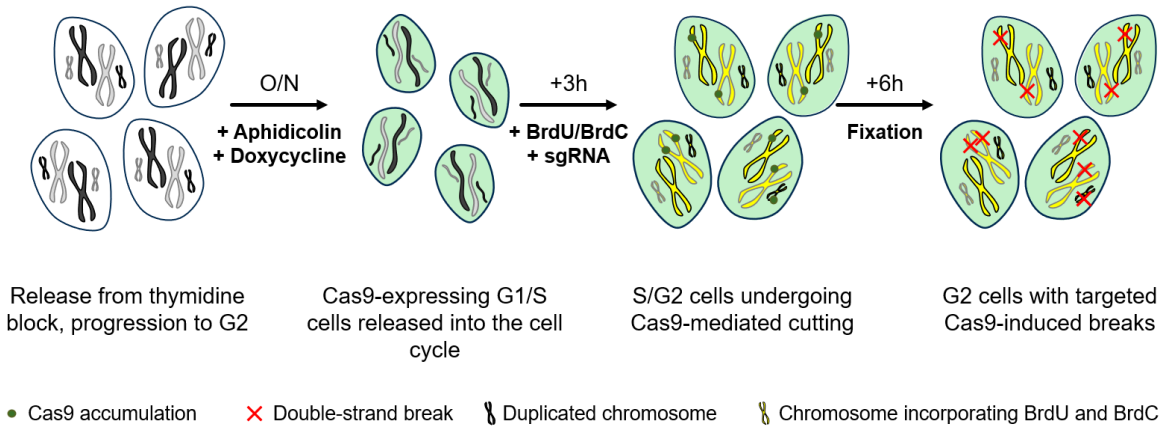

Figure 2.1. Synchronization protocol for double-strand break induction in G2. This is a simplified version where the main steps are detailed. More precise information can be found in the materials and methods section. Addition of aphidicolin results in cell cycle arrest at the G1/S boundary. Addition of doxycycline triggers Cas9-expression in the cells. BrdU and BrdC are the nucleotide analogs that we use for the RASER-FISH procedure. The sgRNAs are transfected three hours after release.

2.2. Sister chromatid fiber tracing by multiplexed RASER-FISH

Visualization of DNA loci around the Cas9/gRNA target regions will be achieved with an improved version of the fluorescence in situ hybridization (FISH) protocol. Standard FISH procedures require harsh denaturing conditions that perturb the fine structure of chromatin, and they cannot distinguish between sister chromatids owing to their identical DNA sequence and close proximity. For this project, we use a new version of FISH that overcomes both limitations: Resolution After Single-strand Exonuclease Resection-FISH (RASER-FISH) (Beckwith et al., 2025; Brown et al., 2022; Goodwin & Meyne, 1993). RASER-FISH is based on DNA labeling with nucleotide analogues, which are incorporated into a different DNA strand in each sister chromatid during one round of DNA replication. Subsequent illumination by ultraviolet light induces DNA nicks, followed by exonuclease digestion with ExoIII, such that each sister chromatid contains a distinct single-stranded DNA molecule that can be detected by specific oligonucleotide probe sets. Indeed, by designing reverse complementary probes in a staggered manner, it is possible to target the sisters differently with our probes. This project was carried out in collaboration with **Thomas Steinacker**, a post-doc in the lab, who had already implemented a multiplexed version of sister-chromatid-specific RASER-FISH (scsRASER-FISH) to resolve sister chromatid fibers with super-resolution on a microscope (Figure 2.2.).

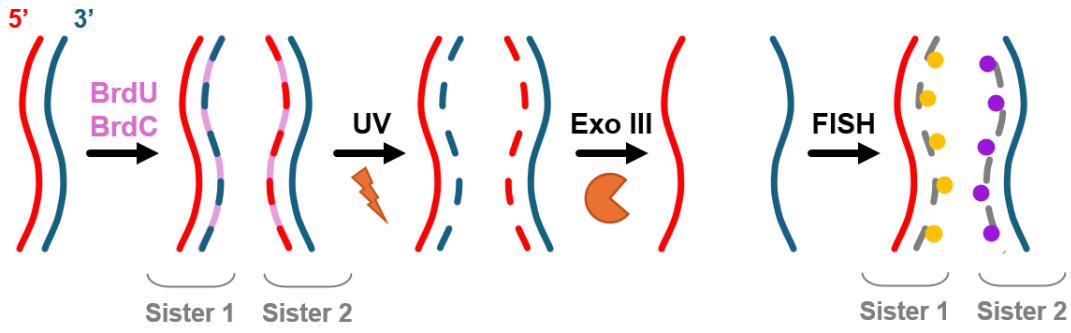

Figure 2.2. Sister-chromatid-sensitive RASER-FISH. The main steps of the scsRASER-FISH procedure are demonstrated here.

This procedure integrates automated imaging and liquid handling devices for sequential FISH experiments. This powerful scsRASER-FISH system provides the core

technology allowing us to probe sister chromatid conformation in the context of homologous recombination of DNA double-strand breaks.

2.3. "Super-resolution" imaging of DNA double-strand break ends

Precise localization of the scsRASER-FISH signal is achieved through a complex processing pipeline, embedded in a software initially built by collaborators in the Ellenberg lab (Beckwith et al., 2025), but further solidified and developed by **Vincent Reuter**, the bioinformatician in the lab who oversees this part of the project. The Looptrace software is based on a similar principle as for super-resolution microscopy such as STORM, except that our "blinking" signal comes from DNA oligonucleotide probes. With a two-step hybridization strategy, primary probes are stably bound to the sample for the duration of imaging, while secondary fluorescent probes are going through repeated steps of automated flow through, hybridization and washing away. We rely on the sequential illumination of different FISH loci, to be able to fit gaussian curves over the signal and infer precise coordinates for each locus, with sub-pixel resolution. The imaging system we are using is a widefield microscope, which allows us to capture the maximum amount of light and thus detect even loci with faint signal. By processing the data through our LoopTrace-derived analysis software, we obtain the coordinates of each of the imaged FISH loci, namely up- and downstream sites of 21 break sites, and with sister-specificity (Figure 3.3.1).

3. Results

3.1. Locus- and time-controlled induction of DNA double-strand breaks in synchronized cells

Double-strand breaks occur within an organized three-dimensional chromatin architecture that could, in principle, exert a decisive influence on how these breaks are repaired. DNA conformation at break sites could either promote accurate repair or constitute a predisposition to mis-repair and genome instability. Despite major advances in our understanding of chromosome folding, the extent to which chromatin organization constrains or biases repair outcomes at individual breaks remains insufficiently understood. Most recent knowledge about this question is often derived from sequencing approaches and more specifically thanks to high throughput chromosome conformation capture methods such as HiC. These techniques provide robust contact probability patterns, averaging millions of cells to deduce contact probabilities, but come with the downside of erasing subtler aspects of chromosome conformation. For instance, they do not provide precise information about the distances between genomic loci, especially in the case when they are too far apart to be considered as “in contact”. The question I want to address with this project is: how does the three-dimensional configuration of chromosomes influence the repair of individual DNA double-strand breaks, specifically during homologous recombination?

For this, we need to be able to induce breaks at specific loci, with temporal control to target only G2 when homologous recombination occurs, and we need a way to resolve sister chromatids and DNA break ends to study their relative positions. Thus, we induce Cas9-mediated breaks to gain locus specificity, that we trigger in G2 cells through a strictly timed synchronization protocol, since it is during this cell stage that homologous recombination is active. We then combine this with immunofluorescence of repair proteins (we use 53BP1 as a general marker of repair and RAD51 as a factor specific to homologous recombination) to identify the DNA damage response and the chosen repair pathway. Finally, we perform sister-chromatid sensitive RASER-FISH to detect the targeted break sites, with the possibility to specifically image upstream or

downstream regions of the break, on different sisters. We thus access all four positions from the same structure, at the single-cell resolution.

We first assessed whether the staging of the cells was correct by assessing the DNA content of the cells by quantitative image-based cytometry during an EdU incorporation assay (Figure 3.1.1).

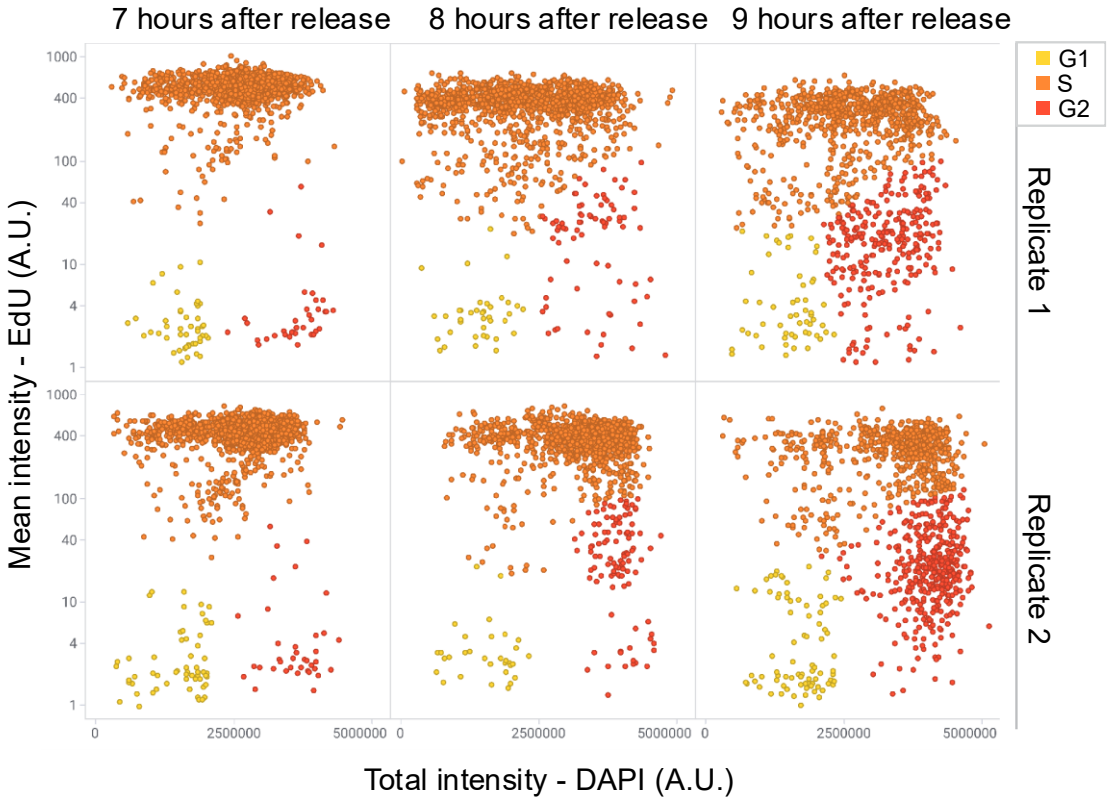

Figure 3.1.1. EdU incorporation assay. EdU incorporation profiles of two replicates. Double-strand breaks are induced in the cells, using a sgRNA concentration of 27.5 nM, 3 hours after their release in the cell cycle from an aphidicolin block. 20 minutes before fixation, EdU is added in the medium to mark the replicative state of the cells in the population. Fixation occurs at different times, after the release of the cells in the cell cycle. Given that the timing of transfection is the same in all conditions, the indicated time points correspond to the time after the release, and not after transfection.

We do this by measuring the signal intensity of the nuclear stain DAPI as well as the incorporation of oligonucleotides (in this case, EdU) as an identifier of the replicative state at the time of fixation. The cells in the bottom left corner represent G1 cells, with low DNA content and low incorporation of EdU; the cells at the top are cells in S phase, with a very high incorporation of EdU; finally the cells in the bottom right corner are the G2 cells (or end of S phase): their DNA content is doubled compared to the G1 cells and their EdU incorporation is low. We also compare different fixation timings, after release of the cells from G1/S into G2, and after DNA double-strand break induction. Indeed, we can see that at 9 hours after release (the optimized timing for our protocol) we have the most S and G2 cells compared to earlier time points.

The DNA content profiles confirm this observation, we can see that in the 7 and 8 hours conditions the prevalent cell cycle stage is S phase, whereas in 9 hours after release we have a mixture of S phase and G2 cells (Figure 3.1.2). This means that the synchronization protocol provides the right setting to study homologous recombination.

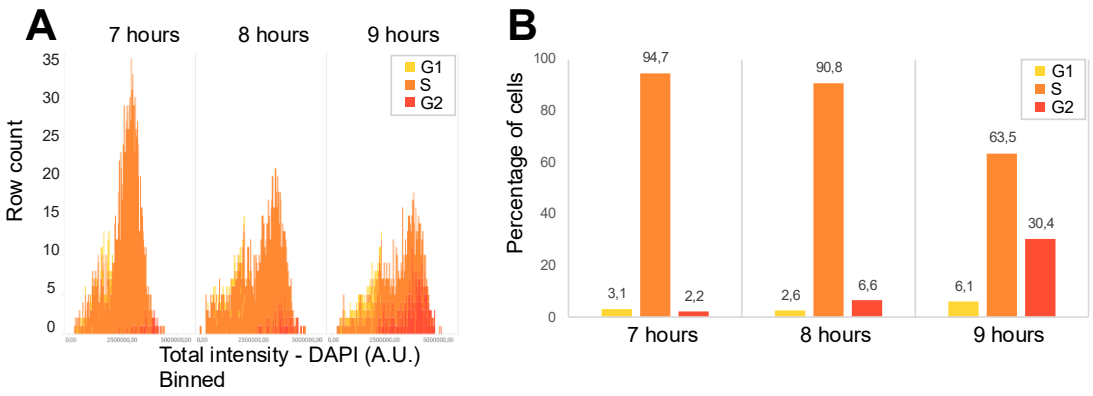

Figure 3.1.2. Cell cycle stages in synchronized cells. (A) DNA content profiles, for three time points, displaying the cell-cycle stage tags attributed with the EdU incorporation assay. **(B)** Quantification of the cell stage composition at different fixation times.

Another aspect of the protocol we wanted to confirm from previous implementations by Federico Teloni, was the concentration of the sgRNA we use to transfect our Cas9-expressing cells. For this, we performed a titration assay, where the cells were transfected with variable concentrations of sgRNA (ranging from 0,1375 nM to 110 nM) (Figure 3.1.3). We assessed the number of repair foci per cell, via 53BP1 labeling, and the number of foci undergoing homologous recombination, via RAD51 labeling. We saw that the DNA damage response was saturated around 27.5 nM, which confirms that using it as a transfection concentration ensures that the cells are properly induced for DNA double-strand breaks.

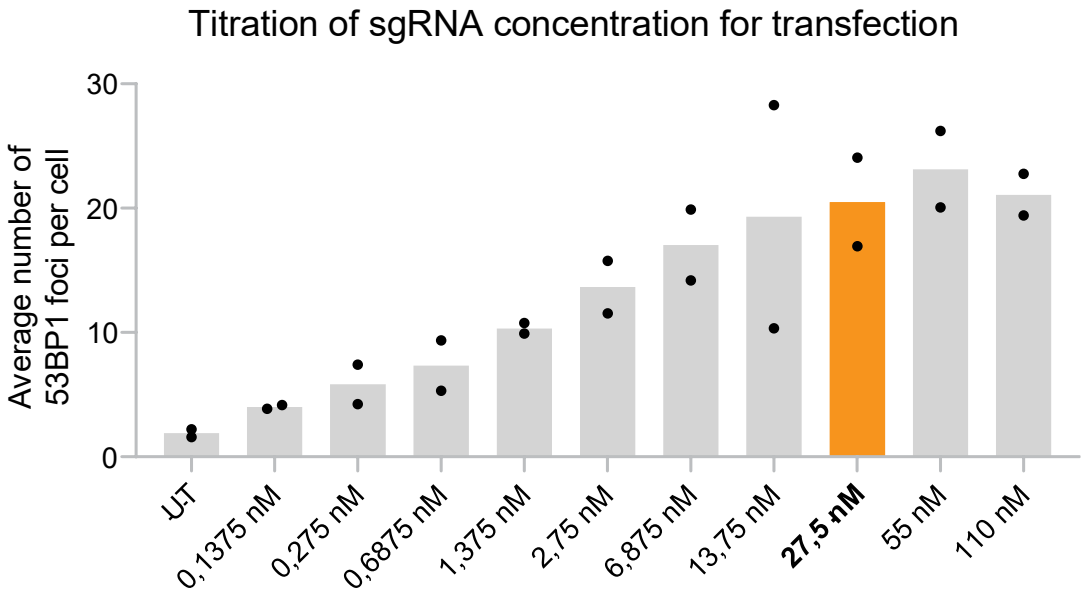

Figure 3.1.3. Titration of sgRNA concentration. Transfection of sgRNA into Cas9-expressing cells with increasing concentrations leads to an increased number of DNA breaks, here assessed through the number of 53BP1 foci per cell. Two experimental replicates are shown here, the bar representing the mean. In orange is the concentration that is used for the rest of this study.

We are thus showing that we can successfully reconstitute the right experimental conditions for our project, adapting the protocol from previous research in the lab. This includes the enrichment of cells with replicated genomes in our sample, in which we consistently induce DNA double-strand breaks, mediated by Cas9 after its conjugation with transfected sgRNAs.

3.2. Cas9-induced DNA double-strand breaks are efficiently repaired by homologous recombination

With a solid and reproducible protocol to induce time-resolved targeted DNA double-strand breaks in G2 cells, we wanted to then focus on the specificity of the breaks and investigate if our system allows for preferential induction of homology-directed repair. To determine that, we performed RASER-FISH on the synchronized, double-strand-break-induced, and fixed G2 cells, to visualize via RASER-FISH the cutting sites targeted by the sgRNAs conjugated with Cas9. We also perform immunofluorescence targeting 53BP1, which will in our assay be considered as a general marker of repair, and RAD51, to specifically highlight repair foci undergoing homology-directed repair. Due to the insufficient RASER-FISH signal that some target sites provided, we only focused on 9 out of the 23 sites for this part of the project.

To assess the cut state and repair pathway choice in our setup, we draw regions of interest at the DNA FISH loci and measure the fluorescence intensity of both 53BP1 and RAD51. Thus, for each FISH locus, we obtain two measurements of fluorescence intensity, which we plot in a 2D scatterplot. From there, we set an intensity threshold for our two proteins of interest, based on the measurements when no targeted breaks are induced (two standard deviations over the mean). All the FISH loci displaying a higher value than the threshold will be considered “positive” for the according protein.

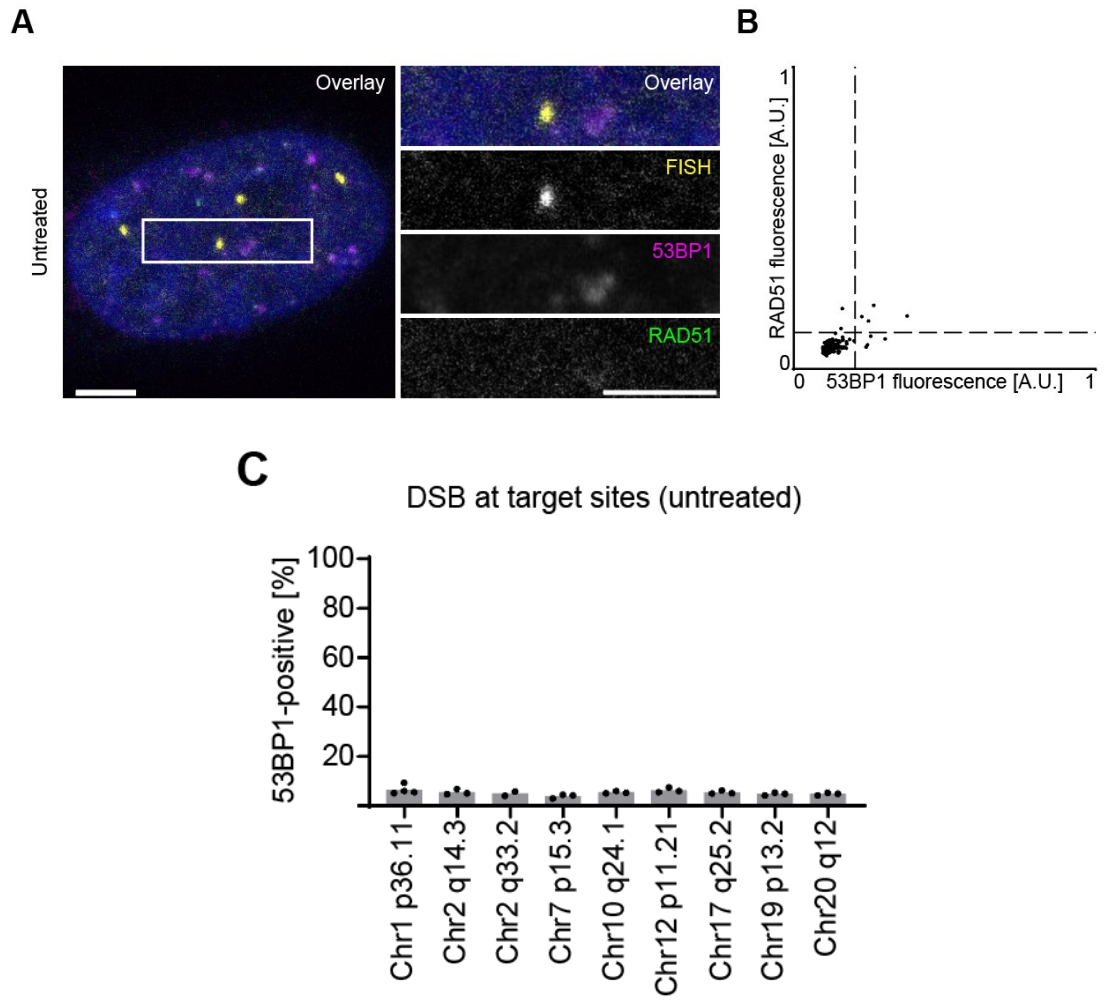

Figure 3.2.1. Repair proteins are absent from targeted cut sites in untreated conditions. From (Teloni et al., 2025). **(A)** Representative image of a G2 cell with immunofluorescence staining of 53BP1 (general repair marker) and RAD51 (specific to homologous recombination), combined with RASER-FISH at one target locus (chromosome 19 p13.2), in untreated conditions (no cuts induced). Scale bar: 5 μm. **(C)** Scatterplot displaying the fluorescence intensity measured at specific FISH loci of 53BP1 and RAD51, in untreated conditions (one dot represents one FISH locus). The dashed lines represent the threshold calculated on the untreated data, of two standard deviations over the mean. **(E)** Observed percentage of FISH loci that display a 53BP1 fluorescence intensity value that is over the threshold, in untreated conditions, at nine different target genomic positions. Each dot represents one experiment; the bars display the mean.

When no breaks are induced, we detect the targeted DNA loci via RASER-FISH, as expected, while little to no 53BP1 nor RAD51 signal is detectable (Figure 3.2.1). We also represented the fraction of FISH loci that displays an immunofluorescence signal over the set threshold (two standard deviations over the mean fluorescence intensity in cells without induction of double-strand breaks). In untreated conditions, neither of the studied loci displayed a higher than 5% fraction of 53BP1-positive loci, which is to be expected.

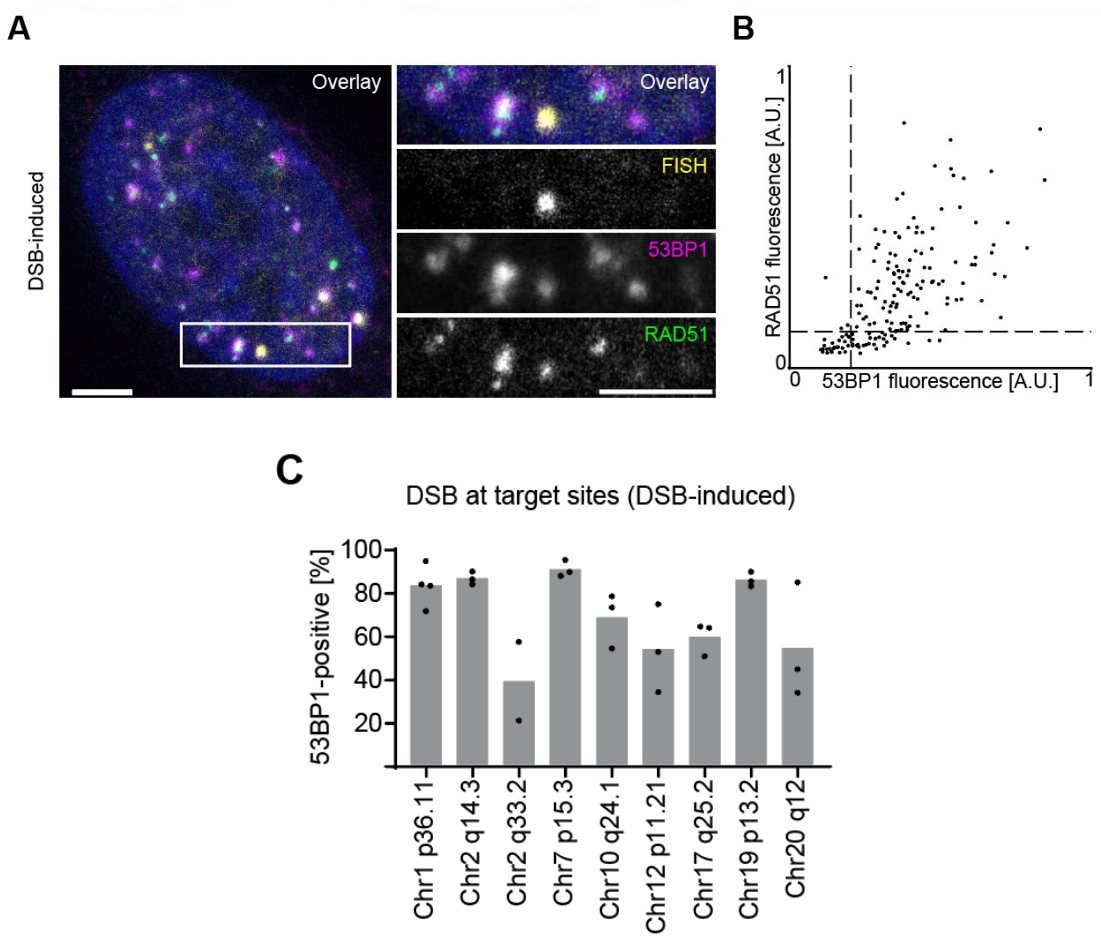

Figure 3.2.2. Site-specific induction of DNA damage repair. From (Teloni et al., 2025) **(A)** Representative image of a G2 cell with immunofluorescence staining of 53BP1 (general repair marker) and RAD51 (specific to homologous recombination), combined with RASER-FISH at one target locus (chromosome 19 p13.2), in double-strand break induced conditions. Scale bar: 5 µm. **(B)** Scatterplot displaying the fluorescence intensity measured at specific FISH loci of 53BP1 and RAD51, in cut conditions (one dot represents one FISH locus). The dashed lines represent the threshold calculated on the untreated data, of two standard deviations over the mean.

(C) Observed percentage of FISH loci that display a 53BP1 fluorescence intensity value that is over the threshold, in cut conditions, at nine different target genomic positions. Each dot represents one experiment; the bars display the mean.

When we transfect the cells with the sgRNAs, the 53BP1 fluorescence intensity at DNA FISH loci increases drastically. The fraction of 53BP1-positive loci ranges from 40% to 90%. This assay confirms the specificity of the induced DNA double-strand breaks, the efficiency of the cutting, and their detectability with our system (Figure 3.2.2).

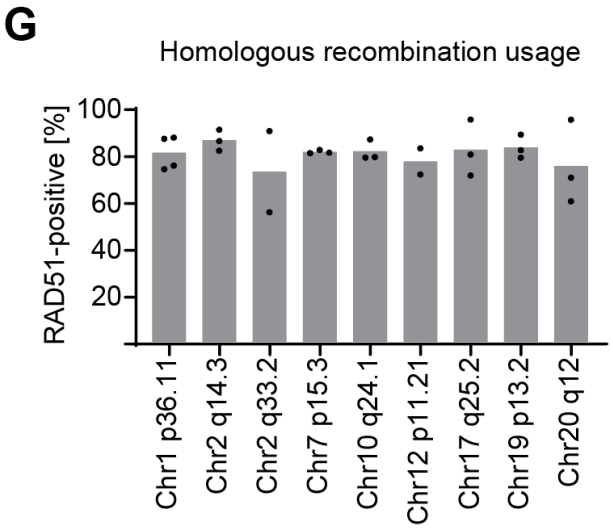

Figure 3.2.3. Homology-directed repair as a preferred repair pathway. Observed percentage of FISH loci, in cut conditions, that were 53BP1-positive and RAD51-positive. Each dot represents one experiment; the bars display the mean. From (Teloni et al., 2025)

Among the 53BP1-positive FISH loci, we also assessed the fraction that is positive for RAD51, since it is noticeable on the scatterplots that RAD51 fluorescence intensity also dramatically increased at the FISH loci. As opposed to the fraction of 53BP1-positive sites which was very variable depending on the targeted site, the fraction of 53BP1+ and RAD51+ FISH loci is consistently high, around 80% for all sites (Figure 3.2.3). This result not only confirms that our experimental set up allows for homologous recombination usage, but also that this repair pathway is predominant in

G2-synchronized HeLa cells, when the DNA double-strand breaks are induced by Cas9.

Although this approach provides us with adequate setup to address our questions of interest, we still wanted to shed some light on the functioning of Cas9 and on the potential biases it may introduce. Indeed, Cas9-mediated cutting allows for targeted and precise DNA double-strand break induction as we previously shown, which is a considerable advantage if we want to also target the sites with RASER-FISH. However, a supplementary challenge arises in the specific context of replicated genomes, which is the presence of an identical sister chromatid in the nucleus. Indeed, as the sister chromatids are sharing the same DNA sequence, it makes them both susceptible to Cas9-mediated cutting, but to model homologous recombination properly we need a single sister to be cut. The intact sister will then serve as a repair template, which constitutes the basis for homology-directed repair, and the focus of our project. To try and estimate the likelihood of 1 or 2 sisters being targeted by Cas9 and triggering a DNA damage response, we statistically modeled the situation with the help of Dmitry Mylarshchikov, a computational PhD in the lab. With this setup where we use light microscopy and label both sisters with the same fluorophore, the proximity between sister RASER-FISH loci cannot be resolved, and they appear as a single signal. From observations of the 53BP1 immunofluorescence signal (namely the cases where no 53BP1 signal is detected, signifying surely that 0 sisters are cut), we can estimate the probability of a single sister being cut. It is thus possible to decipher from one cutting frequency observation the relative probability of having a single sister being cut (see Materials and methods section). This modeling revealed that in 8 out of 9 targeted sites are predominantly cut on one sister only in our experimental conditions (Figure 3.2.4).

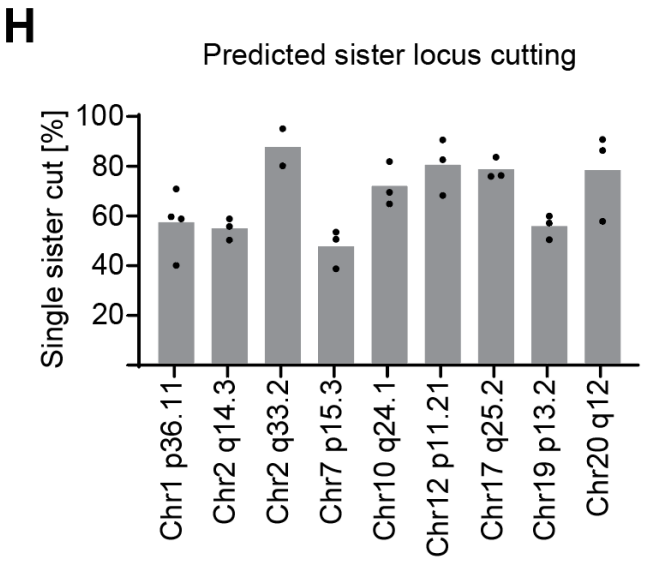

Figure 3.2.4. Estimation of Cas9-mediated cutting on one sister. Predicted percentage of single-sister cutting in different genomic positions, from statistical modelling and inference of observed cutting efficiency (fraction of 53BP1-positive FISH loci). From (Teloni et al., 2025).

This statistical modeling relies among other things on the assumption that Cas9-mediated cutting events are independent and happen stochastically. As we cannot be certain that this is the case, we wanted to try and estimate the stochasticity of allele cutting for different sgRNA concentrations. For this, the study relied on one genomic locus, the break site on chromosome 19 p13.2 and placed the focus of the question on nuclei. Indeed, for this region, we counted how many alleles displayed 53BP1 signal, out of the expected number of alleles in HeLa genomes (4 alleles for chromosome 19) (Figure 3.2.5).

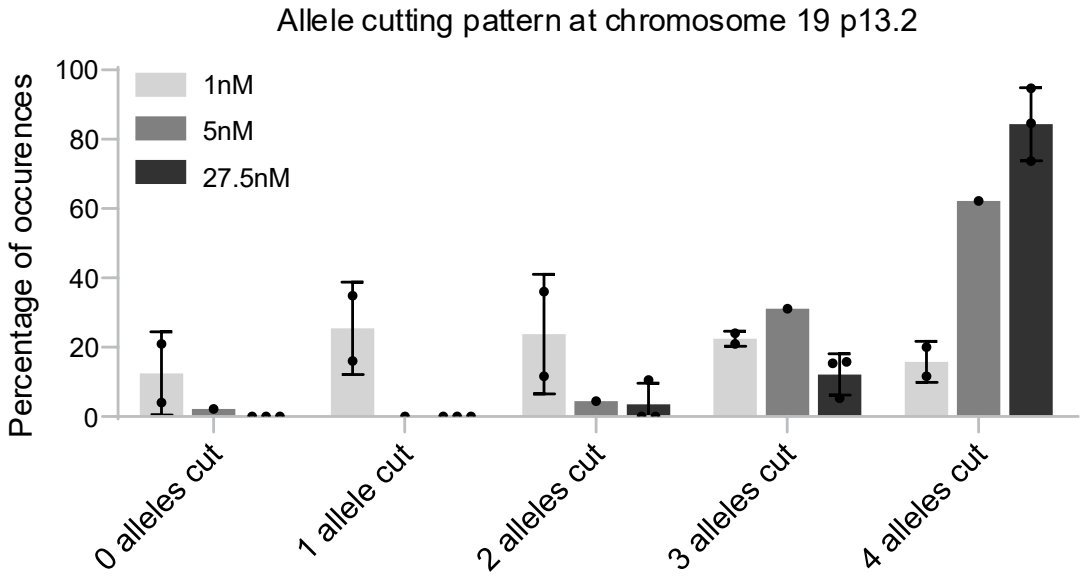

Figure 3.2.5 Allele cutting pattern of Cas9 for three sgRNA concentrations. This panel is not part of the (Teloni et al., 2025) publication. The bars display the mean count of "allele cut" situations, focusing on chromosome 19 p13.2, across three different sgRNA concentrations: 1 nM, 5 nM and 27.5 nM. Depending on the conditions, the value comes from 1 to three different replicates.

With this analysis, we see a correlation between sgRNA concentration and cutting on more alleles per nuclei: using a high sgRNA concentration leads to more frequent cutting on multiple, if not all, alleles in the nuclei. This suggests that Cas9 cutting pattern could be stochastic in our experimental conditions.

Taken together, these results show that the cutting efficiency, despite being locus-dependent, is high in our assay, and that there is a strong bias towards homology-directed repair when the DNA double-strand breaks are induced by Cas9. We also suppose that we are more likely to induce breaks in one sister chromatid rather that in both sisters.

3.3. Four-end labeling of sister chromatids enables separate tracking of double-strand break ends

Homology search and strand invasion are two crucial steps of homologous recombination that require simultaneously the movement of the DNA ends themselves but also the movement of the intact sister chromatid. Given that the success of these steps may be a determinant of a cell's survival, these intricate dynamics and synchronization represent a high stake. Yet, they are complex to study since they are happening at very short distances, which comes hand in hand with overcoming resolution restrictions specific to light microscopy. This knowledge gap made me particularly interested in deciphering how the DNA double-strand break ends are positioned relative to one another during homology-directed repair, and how they contact the sister chromatid repair template in the nuclear space. To tackle this question, we adapted our experimental setup, accordingly, using the full extent of technical possibilities offered by scsRASER-FISH. Indeed, this technique is not only developed to better protect DNA conformation by using milder denaturation steps, but it also allows us to target separately sister loci by the freeing sister chromatid strands, through the degradation of one of them. This is achieved by incorporating light-sensitive nucleotide analogues (BrdU and BrdC) in the previous cell cycle before cell fixation, that are further digested by an exonuclease. Given these characteristics, we designed an oligonucleotide pool that targets 21 out of the 23 cutting sites of the HS17 sgRNA. Each of these break sites is split into 4 different signals: on one hand, we have oligonucleotides that will hybridize to the upstream and downstream regions of the break, giving us access to what we call "cis" distances. On the other hand, we target the same locus but on the two sister chromatids, allowing us to measure what we call "trans" distances between the sisters (Figure 3.3.1). Each one of the four hybridization regions for oligonucleotides is 30kb-long and allows approximately 150 oligonucleotide probes bind. We designed these regions to start 5 kb away from the cut site; this span comprises the extent of resection, which is estimated to reach at maximum 3.5 kb in human cells (Canela et al., 2016; Zhou et al., 2014). This means that we are not directly looking at the invading portion of the DNA break ends, but rather at the very close proximity of it.

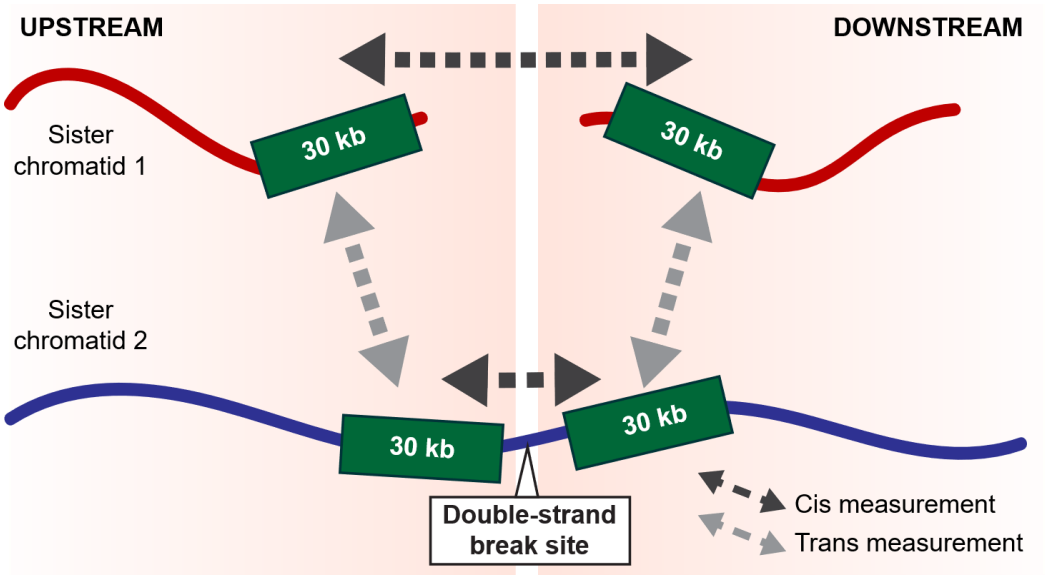

Figure 3.3.1. Concept of oligonucleotide pool design for four-end labeling of DNA double-strand breaks. The green boxes represent the targeted sites, or "four-end labeling", which contain approximately 150 probes each. Also depicted are the cis and the trans measurements that will be addressed later in the project to unveil the relative position of sister loci or DNA break ends.

The primary probes hybridize to their target sequences, and by design, remain bound throughout the whole experiment. In contrast, the secondary probes are applied sequentially, with each cycle involving hybridization, imaging, and stripping.

The oligonucleotides consist in one main hybridization sequence that will attach onto the DNA, and of two sets of two overhangs that will hybridize with fluorescently-labeled secondary oligonucleotides. The reason for the doubling of the two overhangs is to double the fluorescence signal detected by the microscope upon hybridization of the fluorescently-labeled oligonucleotides. One overhang (or barcode) is "regional" and will label at the same time the four ends of the double-strand break. The other one is "locus-specific" and labels differently the four ends (Figure 3.3.2).

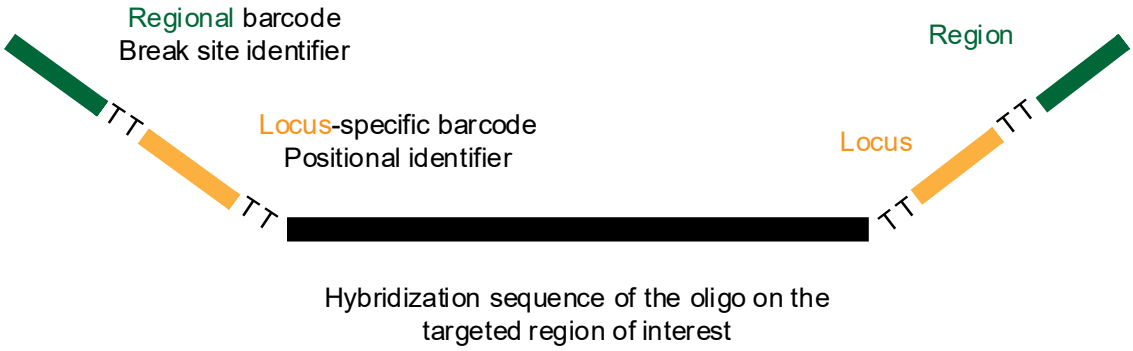

Figure 3.3.2. Dual-labeling oligonucleotide pool design strategy for increased signal and multiplexing. Scheme showing the design logic of each individual probe. The main hybridization sequence that will attach onto the DNA is represented in black. Regional barcodes are depicted here in green, and locus-specific barcodes are in yellow. Each of these segments is separated by a thymidine doublet.

The sequence of the regional barcode is the same for the four ends of every break site, but different between the break sites. For instance, a break site on chromosome 1 will be identified using sequence 1, so the four ends of this break site will each have two copies of sequence 1 on their oligonucleotides, as a regional barcode. Similarly, a break site on chromosome 2 will be identified using sequence 2, etc. This allows us to differentiate all break sites from one another.

The locus-specific barcode is not specific to the break site, but rather to one of the four positions targeted per break: namely the region upstream of the break on sister chromatid 1, the region upstream of the break on sister 2, the region downstream of the break on sister chromatid 1, and finally the region downstream of the break on sister chromatid 2.

Together, these barcodes constitute a dual-identification for all the targeted positions, allowing us to multiplex the experiment by repeating the same barcode sequences for several break sites. This has the advantage of limiting the number of hybridization cycles necessary to image all positions of interest, across all double-strand break sites, and thus the amount of data that each experiment generates (Figure 3.3.3 and supplementary Table S1). Indeed, the signal of the regional barcode defines an “area of interest” around which the detection of the locus-specific barcode is centered, even

though each locus-specific barcodes hybridizes simultaneously at multiple regions inside the nucleus.

Regional barcodes, unique for each break site:

Break site 1: **orange** Break site 2: **green**

Locus-specific barcodes, shared between break sites:

Sister 1 - Upstream: **brown** Sister 1 - Downstream: **pink**
Sister 2 - Upstream: **lime** Sister 2 - Downstream: **teal**

8 unique combinations, one for each position:

o+b	Break site 1 - S1 - Upstream	**g+b**	Break site 2 - S1 - Upstream
o+l	Break site 1 - S2 - Upstream	**g+l**	Break site 2 - S2 - Upstream
o+p	Break site 1 - S1 - Downstream	**g+p**	Break site 2 - S1 - Downstream
o+t	Break site 1 - S2 - Downstream	**g+t**	Break site 2 - S2 - Downstream

Figure 3.3.3. Example of dual-labeling in two break sites and advantages of multiplexing . It is possible to individually label all positions across all break sites by reusing the same locus-specific sequences. Without multiplexing, we would have needed 10 different oligonucleotide probes (2 sites + (2 sets * 4 ends)), while in this setting we only need 6 (2 sites + (1 set * 4 ends)). This labeling strategy is especially powerful when imaging multiple break sites. In our case, we have 21 break sites and 7 different sets of locus-specific quartets. Without multiplexing, we would have needed 105 different oligonucleotide probes (21 sites + (21 sets * 4 ends)), while in this setting we only need 49 (21 sites + (7 sets * 4 ends)).

Each experiment generates 3D multi-channel images, which are split into different time points, corresponding to the different rounds of hybridization of secondary probes. We then process this heavy dataset through our version of the LoopTrace pipeline, which

performs multiple processing steps, including nuclei segmentation, spot detection and Gaussian fitting. This allows us to retrieve the exact coordinates of the RASER-FISH signal, at sub-pixel resolution (around 30 nm), and measure distances between them. A resume scheme depicts the process (Figure 3.3.4).

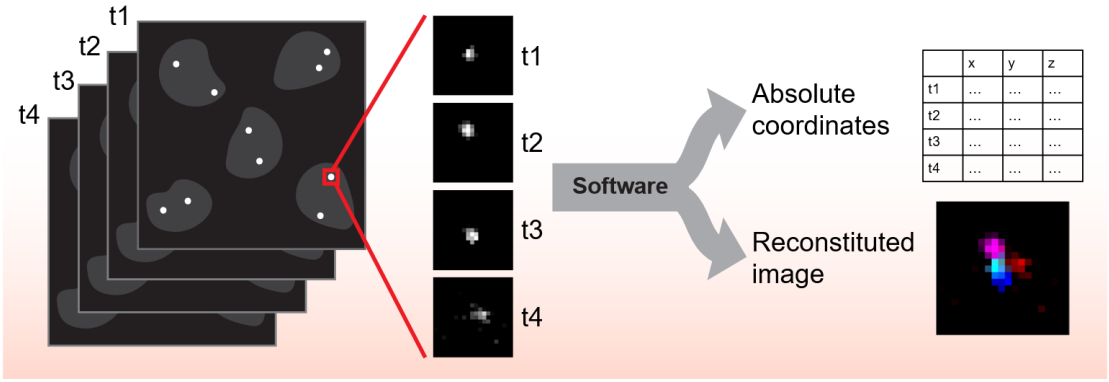

Figure 3.3.4. Experimental setup after image acquisition. From left to right, it shows that the multi-channel images where individual RASER-FISH probes were hybridized and imaged sequentially are fed into our version of the LoopTrace software. Two types of outcomes are expected: absolute coordinates, which are used to calculate distances, as in the rest of the project; and reconstituted images, which allow the user to visualize how the sisters are placed relative to each other.

The pipeline is still undergoing updates and implementations, perfecting this tool for further investigations, but it already provides us with the possibility to access "super-resolution" in our RASER-FISH loci, even with light microscopy, enabling discoveries about DNA double-strand break ends interactions during homology-directed repair.

3.4. Double-strand break induction leads to separation of broken ends

Since double-strand breaks represent a physical disconnection in a DNA molecule, they must be promptly and faithfully repaired, to avoid mutations, translocation, chromosome loss or apoptotic events. In non-homologous end-joining, one of the two

canonical repair pathways, the broken DNA ends are tethered together by the Ku70/Ku80 complex to protect them from degradation and prevent fusion with other DSB ends. Conversely, in homologous recombination, the ends must first be resected before they undergo repair. In this context, it is less intuitive how DNA double-strand break ends around a break are managed and protected before their repair. The factors recruited at break sites during homology-directed repair are known, but whether they affect distancing of the ends at a very local scale is not perfectly clear. Several research groups support the hypothesis of end tethering, also thought to facilitate sister chromatid invasion during homology search (Deshpande et al., 2014; Dumont et al., 2024; Phipps et al., 2025). This leads us to question how DNA double-strand break ends move inside the nucleus, relative to one another. To answer this question, we induced DNA double-strand breaks, and performed automated scsRASER-FISH, where we sequentially hybridized and imaged oligonucleotides.

These experiments were carried out on a subset of 8 sites out of the 21 sgRNA target sites, since they had the most consistent signal throughout repeats of the experiments. Since the repeats are very reproducible (Figure 3.4.2-3), from now on only one repeat will be displayed (the other ones are available in the Supplementary material section).

The coordinates of each measured locus were recorded once the data was processed by the LoopTrace software, and distances were measured, first in cis, between upstream and downstream regions of the targeted double-strand break sequence. The measurements from both sisters are then plotted in a 2D-scatterplot, illustrating how neighboring loci in cis are positioned (Figure 3.4.1). In this example, we are looking at the cut on chromosome 19 p13.2. In untreated conditions, where no breaks were induced, we can observe that the DNA “ends”, or neighboring DNA loci, are at very short distances from one another. Given that the DNA molecule should still be continuous, this phenotype is not surprising. Therefore, we set a “disjunction threshold” based on this condition,

For all distance measurements that are higher than the threshold, it is considered that the ends are “disjoined”: if this disjunction is only in one direction, that means that only one sister is disjoined. However, if both directions exceed the threshold, then both sisters are considered disjoined. This will help us to compare the extent of disjunction between untreated and double-strand break induced conditions.

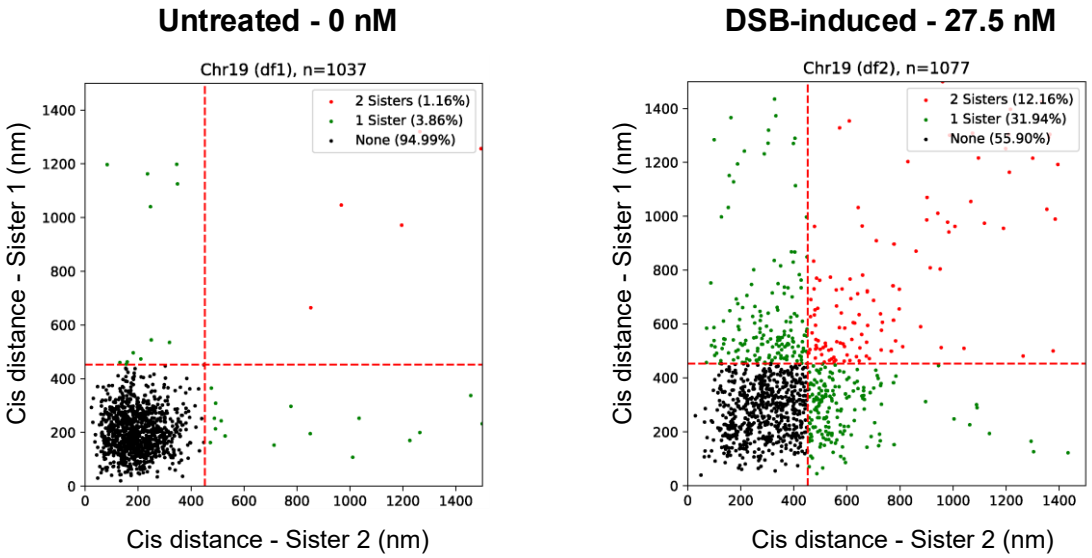

Figure 3.4.1. Double-strand break induction causes a distance increase between DNA ends. 2D-scatterplots displaying distances in cis, in chromosome 19 p13.2, before (left) and after (right) induction of Cas9-mediated double-strand breaks. The x axis shows the cis distances on one sister, while the y axis shows them on the other sister. Each point represents a single genomic locus, recording the cis distances in both sisters. The red dashed lines represent the disjunction threshold, where we exclude the 5% most extreme data points. It was calculated on the untreated (0 nM) control condition of the resented biological repeat to keep consistency between experiments. The labeling "1 sister" and "2 sister" refers to the disjunction state on the 4-end structure: "1 sister" means that only one of the two sisters is disjoined at the double-strand break site, and "2 sisters" mean that both are disjoined. "None" means that there is no detected disjunction at the break site.

Upon DNA damage, there is considerable increase in distance between the ends of the breaks in cis. This disjunction phenotype is not only noticeable for the break site on chromosome 19, but it can be generalized across all eight of the studied genomic locations (Figure 3.4.2, detailed data of all studied genomic loci can be found in Supplementary figures 7.2). The average change in distances compared to untreated conditions ranges from 80 nm to almost 200 nm. This distance increase in cis indicated that the DNA ends tend to disjoin after DNA double-strand break induction. This observation could be interpreted as a release of tension or relaxation at the break site upon Cas9-mediated cutting, at the immediate vicinity of the break site.

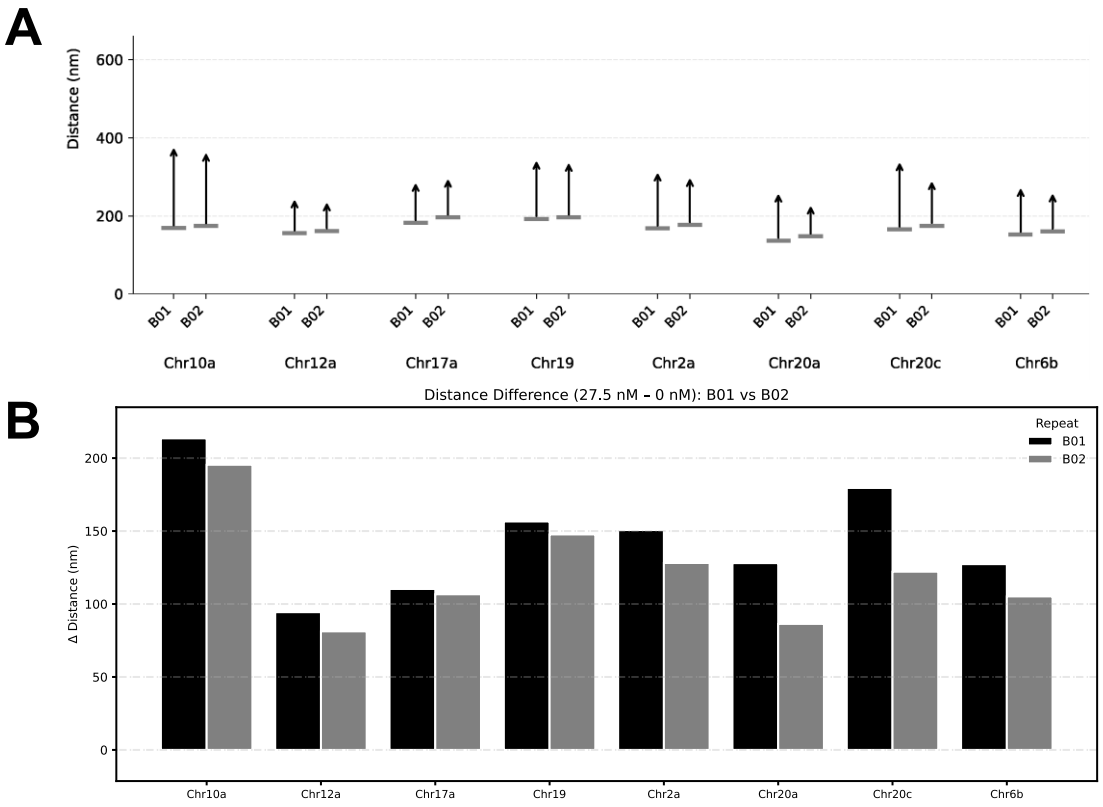

Figure 3.4.2. Cis distancing of DNA ends upon a break, across different genomic loci. (A) Medians of all observed distances between untreated condition (base of the arrow) and cut conditions (arrowhead), for 8 different genomic loci. B01 and B02 stand for two biological replicates. **(B)** Median displacement in cis of the DNA break ends, across 8 different genomic loci. B01 and B02 stand for two biological replicates

3.5. Double-strand break induction brings sister chromatids in proximity to each other

Finding the correct template for homology-mediated repair is crucial for the cell, as it is the only way to attempt error-free repair. After the repair machinery starts with homologous recombination, in response to a double-strand break, the resected broken ends start looking for their homologous locus in the cell. This will allow them to copy faithfully the sequence that was lost when the break occurred. In somatic cells, the repair template is in most cases the sister chromatid. Here, we want to assess if, with

the sensitivity of our system, we can detect sisters rearranging relative to one another when a break happens. For this, we measure trans distances either upstream or downstream of the DNA breaks.

Before any breaks were induced, we can assess the distance between sister chromatids in the nucleus. We observe that sisters are separated from roughly 300 nm to 520 nm, which aligns with previous work (Stanyte et al., 2018). When DNA double-strand breaks are induced, the median distance between the sister loci decreases down to 150 nm depending on the cut sites. From our observations, there is only one cut site that does not seem to get closer to its sister, on chromosome 17. The decrease of trans distances is in line with the process of homologous recombination, consisting in the invasion of the template sister by the broken one, to copy the correct DNA sequence during homology search. Our approach allows us to precisely probe this distance decrease, since the measured values after DNA double-strand break induction are very close, if not under, the usual resolution limit of classical light microscopy (around 200-300 nm).

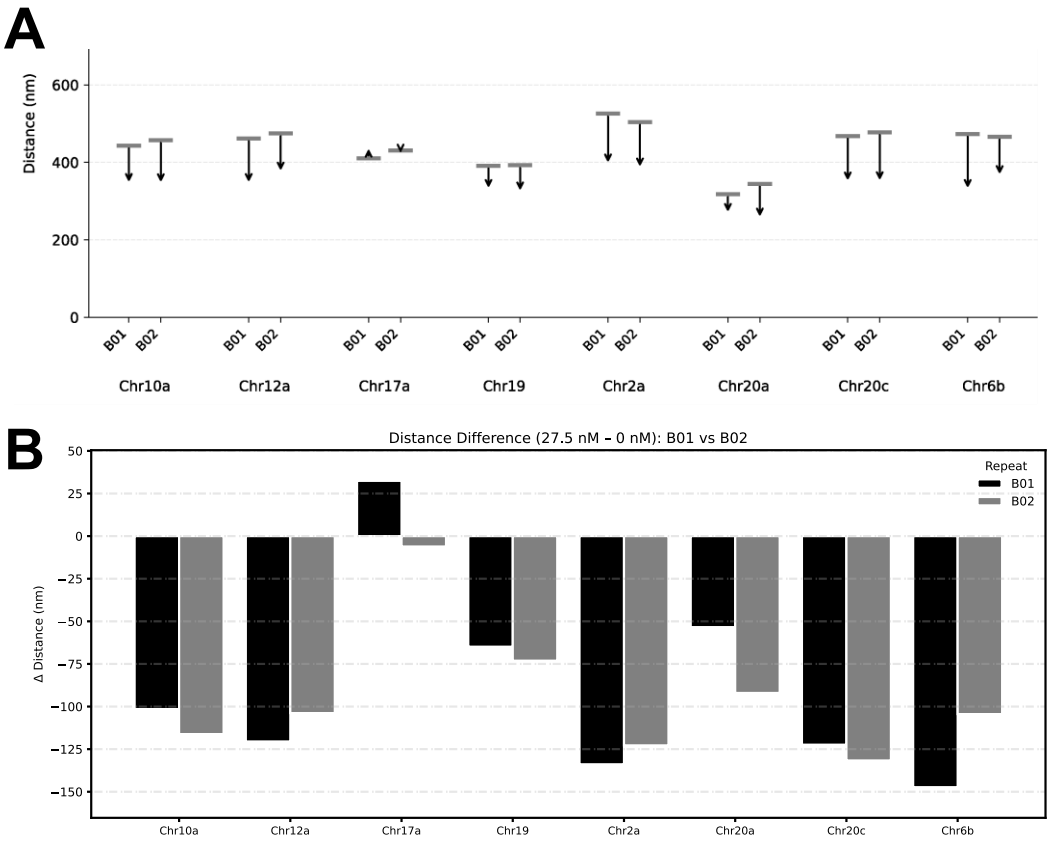

Figure 3.5. Increased proximity of sister loci upon double-strand break induction. **(A)** Median of all observed trans distances (between sister chromatids) between

untreated condition (base of the arrow) and cut conditions (arrowhead), for 8 different genomic loci. B01 and B02 stand for two biological replicates. **(B)** Median displacement in trans of the DNA break ends, across 8 different genomic loci. B01 and B02 stand for two biological replicates.

3.6. Double-strand break-induced end separation is dependent on loop-extruding cohesin

Cohesins shape the three-dimensional organization of the genome by extruding chromatin loops and by enforcing Sororin-dependent cohesion between sister chromatids after replication. Through these activities, cohesins control which loci preferentially interact and how sister chromatids are spatially arranged. Notably, cohesins are also recruited to DNA double-strand break sites, suggesting that they might modulate the behavior of broken ends during repair. We would therefore like to understand to what extent they are involved in the observed break end disjunction phenotype upon homology-mediated repair. To test their involvement, we propose to deplete the cells of cohesins, more precisely through inducible degradation of one of its subunits RAD21, a highly conserved kleisin common to both pools of cohesins. This is achieved by the generation of a Cas9-expressing HeLa Kyoto cell line, which has an auxin-inducible degron tag (AID tag) on RAD21. Upon addition of auxin in the culture medium, fast proteasome-mediated degradation of RAD21 occurs and depletes the cell of all cohesins functions (Teloni et al., 2025). We then performed scsRASER-FISH experiments with and without DNA double-strand break induction and compared our results with the wild-type condition where no depletion was induced.

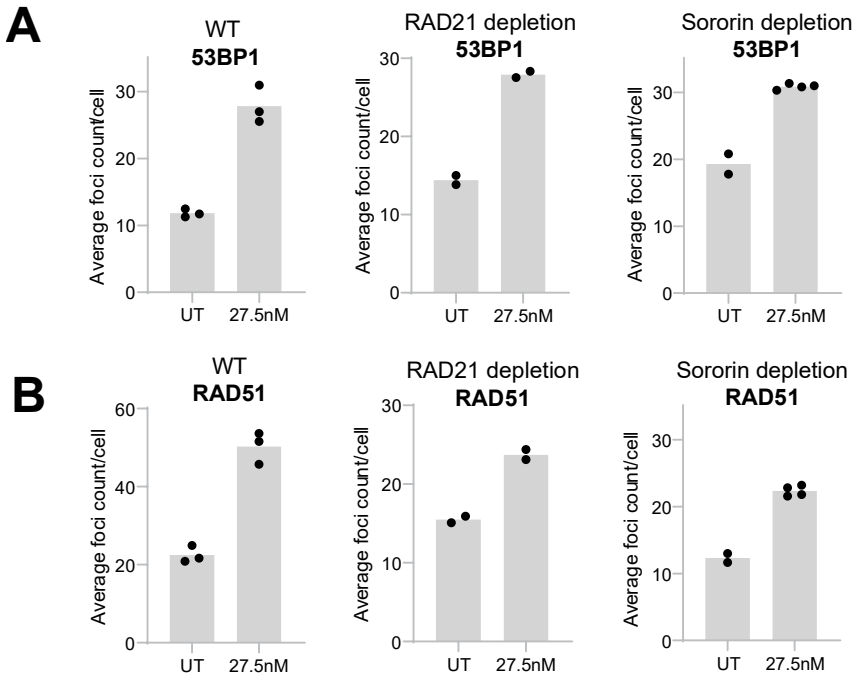

Figure 3.6.1. Cas-9 mediated DNA double-strand break induction in HeLa cells. (A,B) Comparison of WT, RAD21- and Sororin-depleted cells in their activation of the DNA damage response, through the quantification of 53BP1 foci per cell **(A)** and the usage of homologous as a repair pathway, through the quantification of RAD51 **(B)**. High RAD51 foci counts recorded in WT conditions come from variations in acquisition thus leading to differences in segmentation and automated foci count. The analysis parameters stayed consistent between the experiments.

By assessing the overall number of 53BP1 repair foci in the cells, we can see that we observe no difference between the WT and the RAD21 depleted cells, both displaying on average 28 repair foci per cell upon DNA double-strand break induction, showing that altering chromosome conformation does not impair Cas9-targeted cutting (Figure 3.6.1). We thus performed scsRASER-FISH on RAD21-depleted cells and assessed the cis distances around the break sites. Absence of all cohesins leads to drastically decreased distancing of DNA broken ends, as observed in individual loci, such as on the break site on chromosome 2 q14.3 (Figure 3.6.2. A). The fraction of non-disjoined DNA ends increases from 34.39% in wild-type conditions to 57.84% in RAD21-depleted conditions. This phenotype is generalized across multiple other genomic loci, with distances in cis ranging from 45 nm to 100 nm (Figure 3.6.2. B-C), suggesting that cis disjunction of broken ends relies on cohesins.

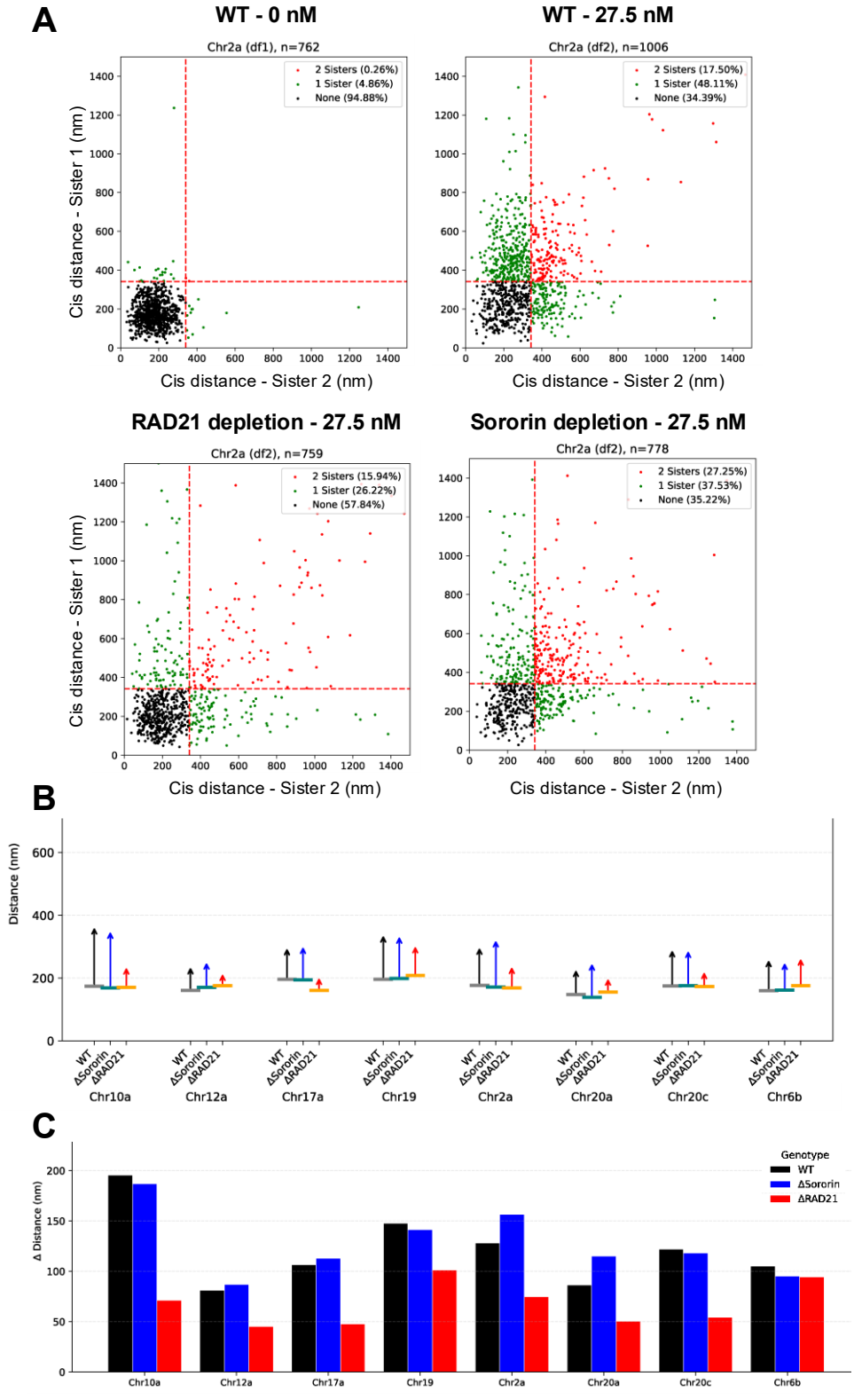

Figure 3.6.2 Cohesins are necessary for DNA end disjunction upon a double-strand break. (A) 2D-scatterplots displaying distances in cis, in chromosome 2 q14.3, in wild-type untreated, wild-type cut, RAD21-depletion cut and Sororin cut conditions. The x axis shows the cis distances on one sister, while the y axis shows them on the

other sister. **(B)** Median of all observed distances between untreated condition (base of the arrow) and cut conditions (arrowhead), for 8 different genomic loci, and for both Sororin (blue) and RAD21 (red) depletion conditions. **(C)** Median displacement in cis of the DNA break ends, across 8 different genomic loci in WT (black), Sororin (blue) and RAD21 (red) depletion conditions.

To try and separate the effect of loop-extruding and cohesive pools of cohesins, we performed the same experiments with Sororin depletion, which will abolish only cohesive cohesins that link sister chromatids together. Furthermore, when we perform the regular RASER-FISH procedure broadly targeting the break sites, some genomic loci display a division of the signal in two separate spots (Figure 3.6.3). This indicates that upon Sororin depletion, some genomic loci disjoin further than the resolution limit of confocal microscopy, confirming that Sororin depletion was effective. This separation phenotype is also observed in RAD21-depleted cells, confirming as well that RAD21 depletion is effective.

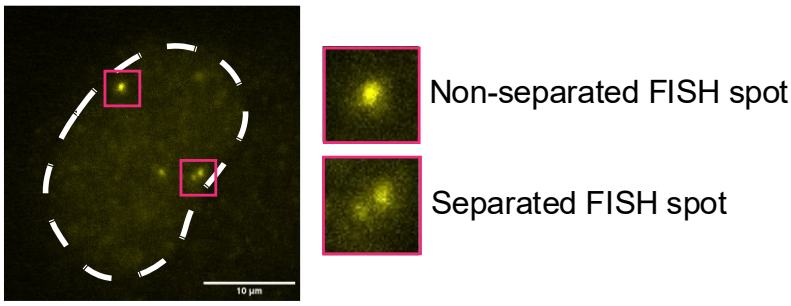

Figure 3.6.3. Sororin depletion leads to FISH loci dissociation. Representative image of FISH locus separation upon Sororin depletion. The image is a maximum intensity projection of 3 z slices. The dotted line represents the cell nucleus. Scale bar: 10 µm.

However, Sororin depletion does not change cis distances in our scsRASER-FISH assay, and end disjunction still takes place, as illustrated by the break site on chromosome 2 q14.3 (Figure 3.6.2. A). In this case, the fraction of non-disjoined DNA ends is very similar to wild-type conditions (34.39 % in wild-type, and 35.22 % in

Sororin depletion). The almost identical disjunction between these two contexts is once again noticeable across multiple genomic loci (Figure 3.6.2 B-C). This suggests that sister chromatid cohesion is not responsible for end disjunction.

Together, these results support the idea that cohesins are involved in shaping chromatin at the close vicinity of DNA double-strand break sites, affecting more precisely broken end disjunction during homologous recombination. This cohesin-mediated shaping is carried out solely by loop-extruding cohesin.

3.7. Double-strand break-induced sister chromatid proximity is independent of cohesion

During homologous recombination, the sister chromatids come into closer contact, as we were able to show through decreasing of the distance separating sister loci, at regions in the direct vicinity of the break site. In line with this, we were wondering whether cohesin disruption, and more precisely Sororin depletion, which is known to be essential for sister clamping in G2 (Zhang & Pati, 2012), would lead to the loss of the sister contacting phenotype in trans. We proceeded with the same depletion approach as described, depleting RAD21 (namely all cohesins) or Sororin (specifically targeting cohesive cohesins) and assessing the trans distance changes upon double-strand break induction (Figure 3.7.1).

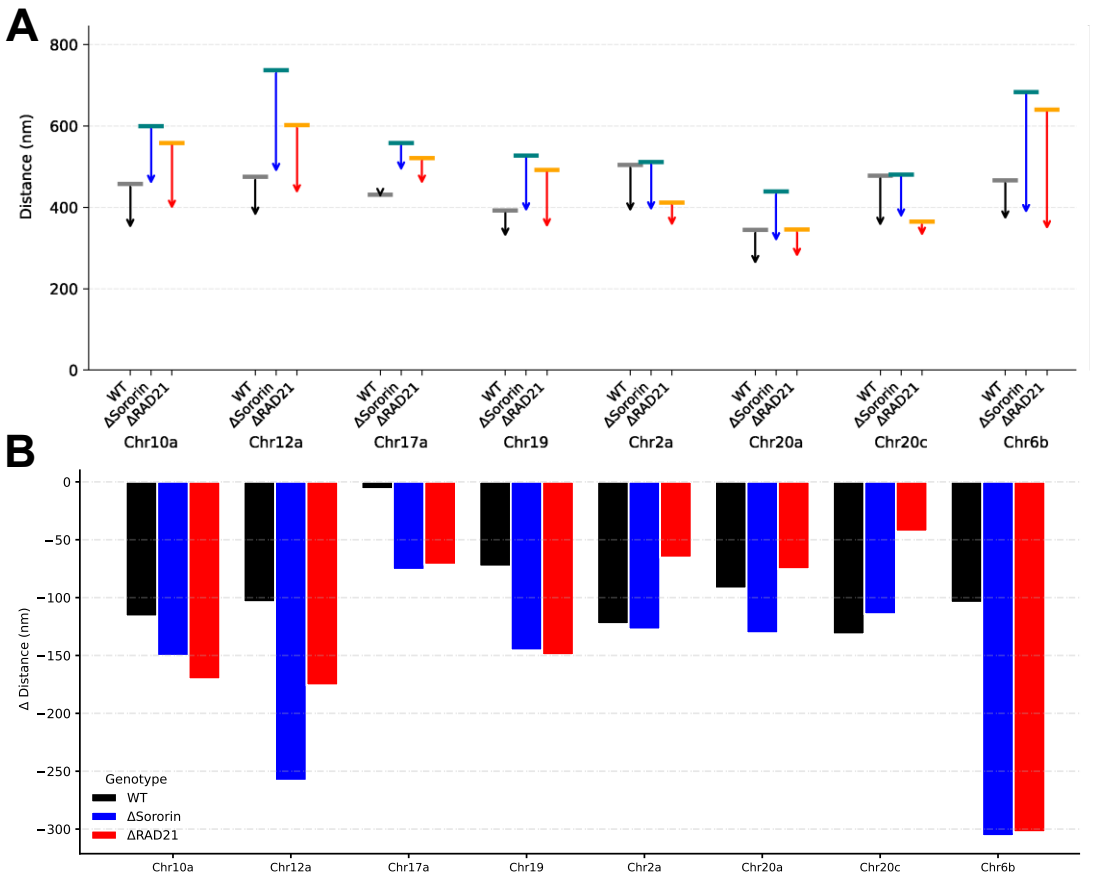

Figure 3.7.1. Maintenance of sister proximity upon double-strand break repair in cohesin-depleted conditions. (A) Median of all observed trans distances (between sister chromatids) between untreated condition (base of the arrow) and cut conditions (arrowhead), for 8 different genomic loci, and for both Sororin (blue) and RAD21 (red) depletion conditions. **(B)** Median displacement in trans of the DNA break ends, across 8 different genomic loci, in WT (black), Sororin (blue) and RAD21 (red) depletion conditions.

The first observation in both RAD21 and Sororin depletion is about the trans distance when no breaks are induced. In most of the observed sites, we notice that the distance separating sister loci is higher compared to wild-type cells, showing up to 240 nm of difference. This constitutes another confirmation that cohesin depletion was effective in our setup.

Depletion of cohesive cohesin, which we hypothesize to be responsible for sister proximity, surprisingly does not abolish the proximity behavior of DNA double-strand break ends. It even seems that the average distance change between uncut and cut cells

is even higher than in wild-type cells. Surely, since the distance between sisters before break induction is higher in Sororin depletion, even though the displacement is higher, Sororin depletion never leads to an even shorter physical distance between sisters compared to non-depleted conditions. This result is also reproduced in RAD21 depletion, where we observe sister loci coming in closer proximity upon a DNA double-strand break, even in the absence of genome organizers such as cohesins. A higher displacement observed in Sororin and RAD21 depletion can be explained by a higher mobility of the chromatin, since it is not restrained by cohesin loops anymore.

A recent study in our lab showed that Sororin-associated cohesin is localized at the double-strand break sites upon damage induction (whether by de novo recruitment or by sliding) (Teloni et al., 2025). This localization implies that the sister loci on the DNA are clamped together, potentially aiding the process of homology search and ultimately of accurate homology-directed repair. If we consider this being the case, then depletion of Sororin would abolish sister cohesion at break sites, and we would assume to observe a longer distance between them. In our assay, it seems that although the distance between sister loci is larger in cohesin depletion conditions, even after induction of damage, there is still a movement that reduces the distance between the sisters.

Together, these unexpected observations support the idea that neither cohesive cohesin nor loop-extruding cohesin are necessary for the two sister loci at the vicinity of a double-strand break to move closer to each other during homologous recombination.

Up until this point in the project, we were able to show that broken DNA ends, in a context of homologous recombination, disjoin in cis, and come closer to their homologous template locus on the sister chromatid. End disjunction in cis depends on the action of loop-extruding cohesins only, while approaching the sister does not require either loop-extruding or Sororin-associated cohesive cohesin. We wanted to shed more light on these processes, especially to try and understand what other factors could impact sister approach at DNA double-strand break ends during homologous recombination, and potentially understand the previously observed surprising phenotype in trans.

3.8. RAD51 filaments are not responsible for cis disjunction or sister proximity

Chromatin undergoing active DNA double-strand break repair could be very different to shape and regulate compared to chromatin undergoing replication or active transcription. Surprisingly, cohesins do not seem to be fully responsible for the changes in DNA conformation during homologous recombination. This result led us to explore the potential role of the repair machinery itself in shaping the chromatin, as it is repairing the break.

First, we wanted to question the potential role of RAD51 filaments in DNA double-strand break ends shaping. Indeed, RAD51 is a protein specific to homology-directed repair, that is loaded onto resected, RPA-coated, and single stranded DNA, at the vicinity of the breaks. The stiffened nucleoprotein RAD51-filament is responsible for homology search and capture once the repair template has been found. Given its central role in homologous recombination, we hypothesize RAD51, especially as stiff filaments, to lead to the separation of the regions flanking the resected DNA. Indeed, if the ends are only tethered at their tips, like it is suggested in (Friskes et al., 2025), and not at the base of the resection region (Dumont et al., 2024), then RAD51-mediated stiffening could push these regions apart. To test RAD51's involvement in cis end disjunction, we performed siRNA-mediated depletion of BRCA2, which is the factor responsible for replacing RPA with RAD51 at resected single-stranded DNA ends. By depleting BRCA2, we prevent RPA from being replaced by RAD51, thus no stiff RAD51 filaments would form at the DNA ends. If RAD51 is responsible for the stiffening and the end disjunction upon a break, we should lose the disjunction phenotype upon BRCA2 depletion and observe no distancing of the ends.

We first wanted to confirm the efficiency of BRCA2 depletion, which we did by assessing 53BP1 and RAD51 foci in damaged cells. The average of 53BP1 repair foci per cell is comparable between the wild-type and the BRCA2-depleted cells, however we can see that no RAD51 signal is detected, completely abolishing RAD51 loading on resected DNA ends, indicating that our depletion protocol is working.

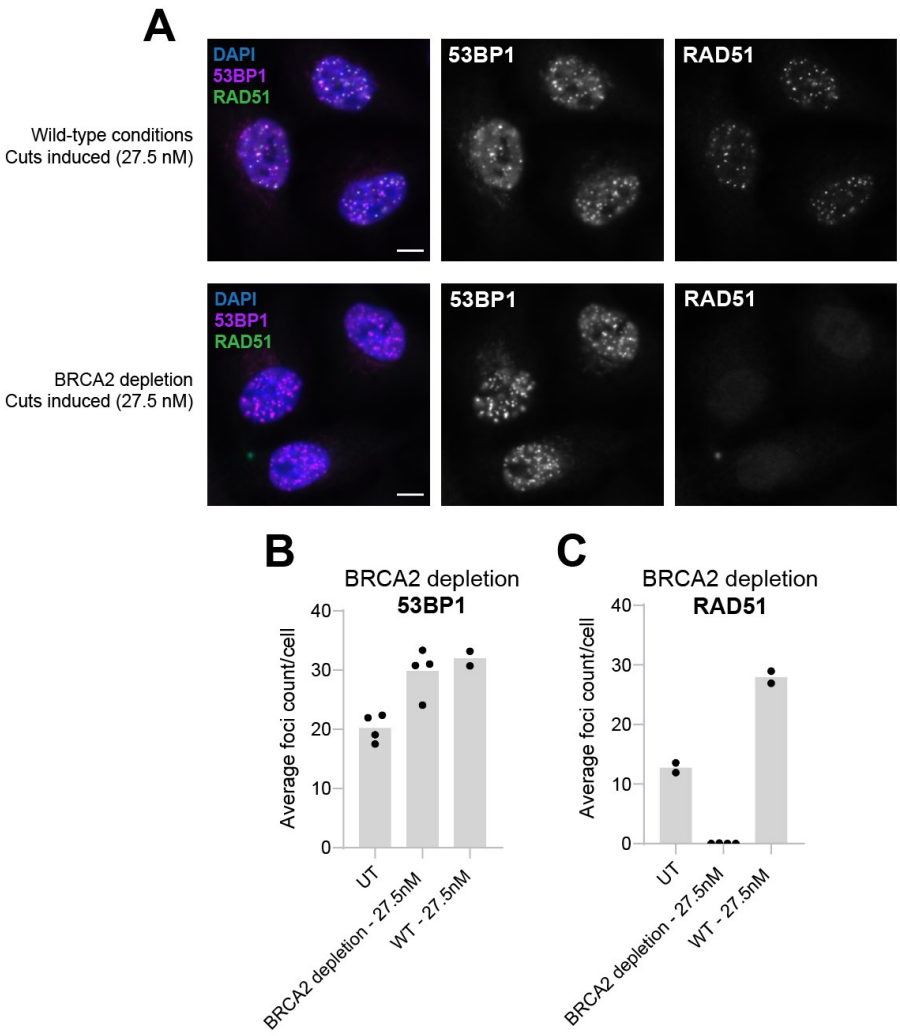

Figure 3.8.1. Efficient BRCA2 siRNA depletion leads to abolishment of RAD51 signal. (A) Representative images of HeLa cells in G2 with immunofluorescence staining of 53BP1 and RAD51 in double-strand break-induced cells, for WT and BRCA2 depleted conditions. All images are contrast-matched. Scale bar: 10 μm. **(B,C)** Quantifications of the average foci count for both 53BP1 **(B)** and RAD51 **(C)**, from several experiments. Each dot is an independent experiment, and the bars represent the mean.

We then carried out the scsRASER-FISH assay with BRCA2 depletion, and we saw minimal effect on the distancing of DNA ends in cis (Figure 3.8.2). Four out of our eight sites of interest showed a slightly decreased distancing in cis (up to 30 nm, which is generally below our resolution limit of 50 nm on average), and all the other sites displayed very similar distances. We thus did not show evidence of RAD51's contribution to DNA break end disjunction.

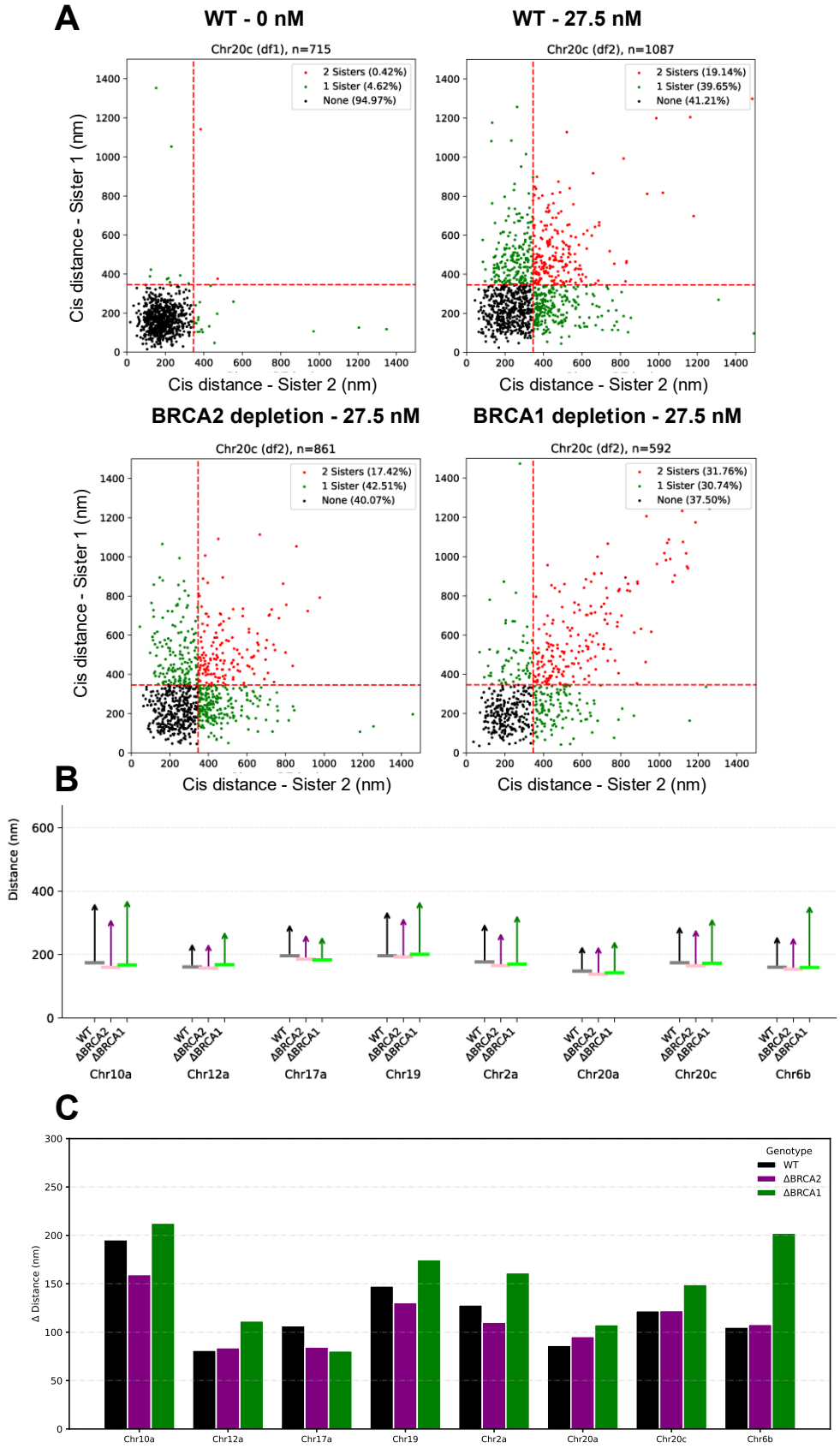

Figure 3.8.2. RAD51 filament formation is not responsible for DNA end disjunction upon double-strand break induction. **(A)** 2D-scatterplots displaying

distances in cis, in chromosome 20 q12, in wild-type untreated, wild-type cut, BRCA2-depletion cut and BRCA1-depletion cut conditions. The x axis shows the cis distances on one sister, while the y axis shows them on the other sister. **(B)** Median of all observed cis distances between untreated condition (base of the arrow) and cut conditions (arrowhead), for 8 different genomic loci, and for both BRCA2 (purple) and BRCA1 (green) depletion conditions. **(C)** Median displacement in cis of the DNA break ends, across 8 different genomic loci, in BRCA2 (purple) and BRCA1 (green) depletion conditions.

In trans (Figure 3.8.3), when assessing the distances between sister loci, we note that upon BRCA2 depletion, sister distances before break induction are very similar to the unperturbed conditions. Upon DNA double-strand break induction, only one site, on chromosome 10, displayed noticeably decreased approaching of the sister, with an average displacement of 60 nm less than in wild-type conditions. Otherwise, all the other sites have an average displacement within 30 nm of the one observed in wild-type cells, meaning that we are not detecting an effect of BRCA2 in trans distancing or approaching of the sisters with our assay.

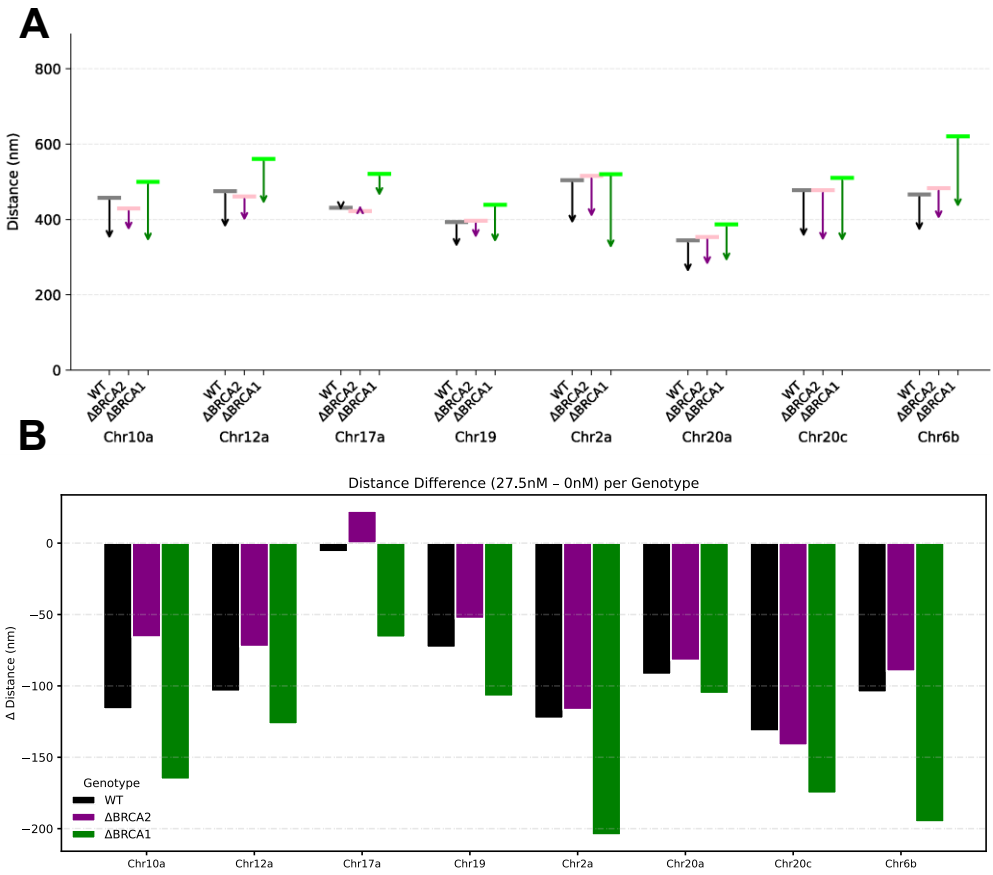

Figure 3.8.3 (A) Median of all observed trans distances between untreated condition (base of the arrow) and cut conditions (arrowhead), for 8 different genomic loci, and for both BRCA2 (purple) and BRCA1 (green) depletion conditions. **(B)** Median displacement in trans of the DNA break ends, across 8 different genomic loci, in BRCA2 (purple) and BRCA1 (green) depletion conditions.

Overall, BRCA2 depletion does not seem to alter the chromatin architecture at DNA breaks, neither in cis with end disjunction nor in trans with sister approaching. This observation suggests that RAD51 filaments, and therefore their stiffening effect when coating DNA, are not responsible for the conformational changes of DNA ends during homologous recombination.

3.9. Homologous recombination is not required for double-strand-break induced relocalizations in cis and trans

Since we did not observe that BRCA2 and RAD51 filaments are responsible for DNA double-strand break end disjunction in cis, or sister approaching in trans, we wanted to investigate the potential role of other homologous recombination factors in these processes, which arise earlier in the steps of repair. One hypothesis we make is regarding the role of the resection machinery (MRN, CtIP, ExoI). During this characteristic step of homologous recombination, the mass recruitment of these proteins could cause changes in chromatin shape and could be responsible for break ends disjoining, as previously observed. The distancing could be established at very early stages of the repair, at the same time as resection is taking place.

To test this hypothesis, we depleted BRCA1, a crucial factor during homologous recombination which allows the recruitment of the resection machinery (Chen et al., 2008; Zhong et al., 1999), namely proteins such as CtIP and the MRN complex. Without BRCA1, no resection can take place after the double-strand break, and homologous recombination stalls. Other non-canonical pathways are thought to take over the DNA repair in these extreme cases, such as microhomology-mediated end-joining (Ahrabi et al., 2016; Deng et al., 2014), a type of alternative end-joining, but they are prone to errors and a threat to genomic integrity. If indeed a component inherent to the homologous recombination pathway is responsible for the end disjunction phenotype, or sister approaching, such as the recruitment of proteins responsible for DNA resection or DNA resection itself, then we would not see these anymore in BRCA1 depletion conditions.

Similarly to BRCA2 depletion, we first wanted to assess the efficiency of BRCA1 depletion through imaging, and we observed loss of all RAD51 foci while still allowing 53BP1 accumulation as a general marker of repair (Figure 3.9.1).

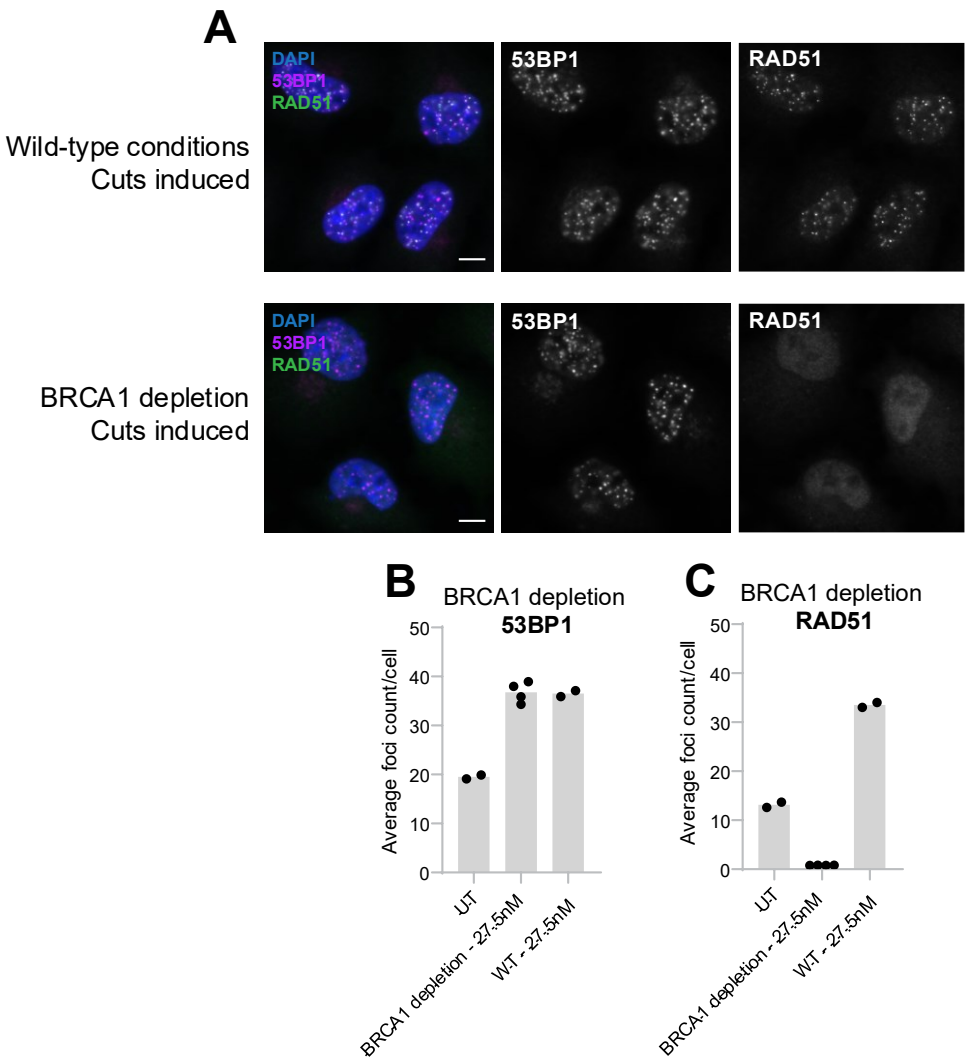

Figure 3.9.1. Efficient BRCA1 siRNA depletion leads to abolishment of RAD51 signal. (A) Representative images of HeLa cells in G2 with immunofluorescence staining of 53BP1 and RAD51 in cut cells, for WT and BRCA1 depleted conditions. All images are contrast-matched. Scale bar: 10 μm. **(B,C)** Quantifications of the average foci count for both 53BP1 **(B)** and RAD51 **(C)**, from several experiments. Each dot is an independent experiment, and the bars represent the mean.

After proceeding with the scsRASER-FISH protocol in BRCA1 depletion conditions (Figure 3.8.2), we observed no obvious difference between the average distances in cis between wild-type cells and BRCA1-depleted ones before and after double-strand break induction. The exceptions are two sites on chromosome 12 q24.31 and 19 p13.2 which displayed an average displacement in cis that was around 30 nm, and the site on chromosome 6 p21.2 had displacement that approached 90 nm. This leads us to the

conclusion that BRCA1 was not shown to be responsible for DNA end disjunction in cis upon DNA double-strand break induction.

Taken together, we conclude that BRCA1 is not responsible for changes in DNA end distances in cis during homologous recombination, however it could have a limiting effect in sister approaching.

4. Discussion

We have been able to show that when a DNA double-strand break takes place in G2 and homologous recombination starts, it results in the disjunction and separation of the DNA ends, in the direct vicinity of the break. We found that this disjunction relies on the presence of cohesins, especially the loop-extruding pool of cohesins. We also confirmed that DNA ends in this context approach their homologous locus, on the sister chromatid. However, this decrease in distance between the sisters is surprisingly independent from cohesive cohesins. All the observed chromatin architecture rearrangements and shape changes do not seem to be affected by perturbations in the homologous recombination pathway: first, the stiffening of the RAD51-bound ssDNA overhang is not necessary for DNA end disjunction. Also, DNA resection, a characteristic step illustrating the commitment to homologous recombination for repair, does not trigger DNA end disjunction, nor the mutual approach of sister loci.

4.1. Literature overview and comparison with our data

4.1.1. Reconciling Local End Disjunction with Cohesin-Mediated Loop Extrusion

Some research groups have hypothesized that loop-extruding cohesins constrict the movement range of DNA double-strand break ends (Yang et al., 2023), suggesting a tethering of the ends. This is thought to happen either through recruitment at break site and oligomerization of the cohesin complexes (Phipps et al., 2025), or through increased looping activity near the double-strand break to determine repair domains (Arnould et al., 2021; Yang et al., 2023). These results may seem contradictory to ours, since we show that DNA double-strand break ends disjoin upon a break, in a cohesin-dependent manner. However, it could be that the difference of scale in our approaches alters our interpretation, and that both scenarios can be correct and even complementary.

In our assay, we are looking at 30kb stretches of DNA that are 5kb away from the break site, so we are neither assessing the dynamics of surrounding chromatin, nor the resected filaments themselves. At a very local level, we observe a disjunction of DNA double-strand break ends of between 100nm and 200nm on average across 8 different loci. This displacement is limited and is explained by the disruption of the integrity of the DNA molecule. This relatively limited disjunction could still suggest that higher order architecture changes occur around the break, as proposed by other labs. Indeed, cohesins were shown to accumulate around break sites (Caron et al., 2012; Teloni et al., 2025) and in cis delimiting repair-prone regions. There is a contraction of the regions upstream and downstream of breaks. These larger-scale movements and compaction could participate in increased distancing at the direct vicinity of the break. Also, this would be supported by our RAD21 depletion condition, where in case of absence of cohesins, we do not have higher order architecture changes, thus neither upstream nor downstream regions of the break are pulling on the DNA double-strand break ends. Since loop-extrusion has been shown to be the mechanism responsible for locus contraction, altering the loop-extruding activity of cohesins would provide supplementary insights into this hypothesis.

4.1.2. Cohesive Cohesin and Sororin-Independent Sister Chromatid Proximity

For our trans observations, we were surprised to notice that Sororin was not necessary for the broken end to come closer to the repair template. Indeed, it has been shown that Sororin is accumulated in the direct vicinity of DNA double-strand breaks repaired by homologous recombination (Teloni et al., 2025), and that this accumulation causes an increase in contact probability between the ends and the repair template.

This could also be partly explained by the scale and the precision we are looking at. Indeed, during the homology search process, the broken end (or ends in case the search happens from both sides) scans the intact template (the sister chromatid) to find a homologous sequence. It could be that the locus is contracted overall, which causes the sisters to come in closer proximity, in a cohesin-independent process, meaning that the "repair-prone region" would include both sister chromatids in the vicinity of the break. However, cohesive cohesin allows the scanning to happen on the repair template, justifying its presence at the DNA break ends, but it could be that we are missing the effect of cohesive cohesin in homologous recombination repair since we are focusing on the immediate vicinity of the break site, and not extending the observations to nearby regions, where homology search is taking place. To understand sister chromatid dynamics during homology search, we may need to consider both cohesin-mediated processes (such as sister scanning during homology search) and cohesin-independent processes (such as overall repair locus contraction to create a repair-prone region).

Besides, in the HiC data from (Teloni et al., 2025), we can identify that there is an overall increase in contact probabilities between the sister chromatids near break ends, even in the absence of Sororin. This observation is also consistent with our data and conclusions. This statement could support the idea that cohesins are not the only regulator of chromosome architecture during homologous recombination. Since this is a very surprising conclusion, another potential interpretation of this observation would be that we are unable to achieve complete depletion of Sororin, with our AID system. In this case, sister chromatids coming in closer proximity during homologous recombination could be due to the action of residual Sororin-associated cohesins.

4.2. Limitations of the study

Although we are setting solid grounds for future investigations in the field of chromosome dynamics in the context of DNA repair, a few limitations remain in this study.

4.2.1. Effect of genomic context on Cas9-mediated double-strand break induction

First, we observe variable cutting efficiencies depending on the targeted loci with our sgRNA. This statement does not pose any issues and is expected, given the different compaction states and accessibility of the chromatin in the cell nucleus. However, we have not yet found a consistent pattern when we tried to correlate sequencing data of specific genomic regions and our imaging data and the observed cutting efficiency (quantification of the number of FISH loci per cell that accumulate 53BP1 upon the induction of a DNA double-strand break). Indeed, chromatin compaction state, TAD boundaries and expression levels do not seem to be obvious factors that in our case would lead to differential Cas9-mediated cutting. This aspect of the study needs to be further investigated.

4.2.2. Cas9-mediated single sister cutting

Another aspect that we would be very interested in elucidating is also relevant to the double-strand break induction process. Since we are using CRISPR/Cas9 as an induction method for DNA double-strand breaks, the guide RNA targets specific DNA sequences. In replicated genomes, these sequences happen to be the same on both sister chromatids, since the genomic content is faithfully copied. This poses a problem in the establishment of our model, in which we would ideally induce breaks in one sister only, leaving the second one intact to be used as a repair template. To address this question indirectly, we relied on a theoretical model and on experimental observations (Figure 3.2.4) and we could deduce that in most cases, only 1 sister is cut at the concentration

of sgRNA we are using in our assay. Lowering the concentration to 1 nM instead of 27.5 nM helps theoretically reduce the fraction of sites cut on two sisters, but the overall cutting efficiency is affected. We preferred to focus on conditions that allow a high cutting efficiency, while minimizing the risk of two sisters being cut, knowing that the fraction of two sisters cut was not equal to zero. Also, we used the same concentration as the one we used in this study (Teloni et al., 2025), and we wanted to be able to compare our results in the most accurate way possible. The topic of single-sister cutting is currently under investigation with our RASER-FISH approach, where Thomas Steinacker is trying to set up an assay to distinguish the cut sister from the repair template using immunofluorescence signal of RAD51 and its position relative to the DNA break ends. We hope to reach a clearer answer using this method.

4.2.3. Lack of efficient NIPBL depletion through auxin-inducible degron

Protein depletion through the auxin-inducible degron system is usually very efficient and allows for time-controlled depletion. Unfortunately, in some cases, the depletion is incomplete, and it is what happened with our cell line with NIPBL auxin-induced depletion. NIPBL is the loading factor of loop-extruding cohesins onto the DNA. Therefore, by not being able to deplete completely NIPBL, we could not disrupt loop-extrusion and abolish the structure of chromatin in cis specifically, whilst keeping sister chromatid cohesion intact. To counteract this issue, we simply relied on our RAD21-depleted cells, also through the auxin-inducible degron system, and got rid of the entire population of cohesins, both loop-extruding and cohesive. Assessing separately the role of these two pools through indirect depletion and deductions is not ideal, but in our case was the most reliable technique we had. Other depletion methods involving genetic engineering and cell line generation could be of use in this case, to induce a more efficient NIPBL depletion in our cellular context in further studies.

4.2.4. Precise time-resolution of Cas9-mediated double-strand break induction

In our setup, we are freezing the image at a point in time, 6 hours after inducing the DNA double-strand breaks. This timing allows us to maximize the number of G2 cells that have DNA double strand breaks. With transfection of the sgRNAs, we trigger their conjugation with Cas9, but it does not necessarily mean that all cuts happen at the exact same time. The incomplete control of the break induction timing signifies that we cannot follow the different steps of the break "state" through time, from the initial cutting to the repair and resolution of the break focus. We hypothesize that the distancing between the DNA ends observed after Cas9-mediated double-strand break induction regroups different stages of repair. Indeed, we observe a lot of genomic loci where the break ends are not disjoined, and we would like to understand whether that is due to variation in the stages of repair, or because of differences in the induction of chromatin architecture changes at different break sites.

4.3. Project outlooks and future work

This promising project is shedding light on the mechanisms of chromatin architectural changes in the specific context of homology-directed repair in replicated genomes.

4.3.1. Additional perturbations of the system

It will be further investigated through improvement of perturbation conditions (notably with the generation of a cell line providing more efficient NIPBL depletion) to more clearly decipher the role of loop-extruding cohesins in this restructuration.

Conditions of co-depletion would be very relevant for the study, especially through the combination of BRCA1 and RAD21 depletion, a context where neither pre-existing chromatin architecture nor the repair machinery will be able to induce changes in chromatin dynamics upon a double-strand break. This is technically achievable, since the modalities of depletion are different: for cohesin depletions we are using cell lines

that express AID-tagged cohesin subunits, while the BRCA1 depletion is carried out through siRNA transfection of the cells.

4.3.2. Precise time-resolution of cutting and study of movements over time

We would also like to be able to follow the dynamics of DNA break ends through time: from their formation upon Cas9-mediated cutting, through their homology-directed repair and finally until the resolution of the break foci following a successful repair. One method we wanted to explore towards this goal, to be able to dissect these different stages of the repair process, is the use of "caged" gRNAs, developed in this study (Liu et al., 2020). The transfection of the guides in Cas9-expressing cells is the same as in our protocol, however the guides are "caged", meaning that they can lead Cas9 at the break site, but this prevents the nuclease from cutting. Upon illumination with ultraviolet light, the sgRNAs are "liberated" from their cage, Cas9 becomes active and cuts the targeted sites. This technique allows for a very high time resolution of cutting, on the scale of the second. It is not trivial to implement it, since we must use another sgRNA to combine it with this technology, which also implies re-designing our RASER-FISH oligonucleotide pool to fit with the new break sites, explaining why it was not implemented yet. Performing a time-course experiment will help us characterize the dynamics of DNA double strand break ends upon cutting and through homologous recombination.

4.3.3. Study of protein accumulation at double-strand break sites and interaction with DNA ends

Assessing the cut state of sister chromatids independently has always been a challenge, whether it be in sequencing experiments or in imaging approaches, since they both share the same sequence and are very close in space. One technical advancement that is currently being investigated about cut state observation is the addition of immunofluorescence signal to our processing pipeline. This feature aims to measure fluorescence intensities of proteins involved in DNA repair, such as 53BP1 or RAD51,

and possibly record their position relative to FISH loci. For instance, studying specifically the positioning of the RAD51 signal relative to the four ends that are targeted by FISH would, among other things, allow the identification of sister chromatids based on their cut state.

As we are in early stages of development of this specific aspect of the project, the necessary processing steps to draw biological conclusions have yet to be implemented and functional. It is for this reason that the protein accumulation aspect of the research was not further developed in this thesis. However, all generated data during this work also includes immunofluorescence signal, and it will be possible to reprocess all of it once our software includes this aspect of the analysis.

4.3.4. Larger-scale chromatin spatial positioning and movements during homologous recombination

Finally, the biggest goal and follow-up of this project would be to extend our study, relying on the strong setup that we provided here, to not only focus on the direct vicinity of DNA double-strand break ends, but to rather assess the whole chromatin fiber, over few Mb-long domains. This great advancement will provide us with key insights about chromatin dynamics during homology-directed repair, and more specifically how the interactions with the repair template occur through the homology search process, to what extent the repair locus is contracted or insulated from the rest of the chromatin (as it is already suggested in sequencing-based projects) and how the interplay between the shapers of chromatin architecture and the repair machinery results in efficient and high-fidelity DNA repair.

5. Materials and methods

5.1. Cell culture

All cell lines were cultured under sterile conditions, at 37°C and with 5% CO2 in a humidified incubator and regularly tested negative for mycoplasma contamination. The parental HeLa cell line "Kyoto" was obtained from S. Narumiya (Kyoto University, Japan). The cells were cultured in Dulbecco's Modified Eagle's Medium (DMEM; IMP/IMBA/GMI Molecular Biology service/Media Kitchen), supplemented with 10% (v/v) fetal bovine serum (FBS; Gibco, 10270-106), 1% (v/v) GlutaMAX (Invitrogen, 35050038), and 1% (v/v) penicillin-streptomycin (Sigma-Aldrich, P0781). To activate the AID system (Auxin-induced degradation), the WT medium was supplemented with 500µM indole-3-acetic acid (Auxin; Sigma-Aldrich, I5148).

5.2. Cell line generation – Cas9-dox cell lines

The detailed list of the cell lines used in this thesis can be found in Supplementary Table S2. They were generated previously by Federico Teloni, the details are available in the corresponding publication (Teloni et al., 2025).

5.3. Cell synchronization to G2 phase and double-strand break induction

Multi-channel imaging slides (ibidi, 80607, µ-Slide VI 0.5 Glass bottom) were first coated with a solution of 0.01% of Poly-L-lysine (Sigma-Aldrich, P8920) for 1 hour and washed with H2O. Cells were subsequently seeded at a concentration of $1.5x10^5$ cells/mL (120µL per channel) in wild-type medium supplemented with 2mM of thymidine (Sigma-Aldrich, T1895), to achieve a first step of synchronization at the G1/S boundary. After 16 hours in thymidine, cells were washed four times with pre-warmed wild-type medium and left to recover and progress through the cell cycle for

8 hours. Both 3µg/mL of Aphidicolin (Sigma-Aldrich, A0781) and 0.2µg/mL of Doxycycline (Sigma-Aldrich, D9891) were added to the cells to respectively block the cells at the G1/S boundary and to induce Cas9 expression in the cells. At this step, 40µM BrdU/BrdC (3:1 ratio; Sigma-Aldrich, B5002; Santa Cruz Biotechnology, sc-284555) was also added in the medium, to allow nucleotide analog incorporation in case some cells slip in S phase despite the presence of aphidicolin. Aphidicolin release was performed 16 hours later by washing them four times with pre-warmed wild-type medium and are then kept in 40µM BrdU/BrdC. Cells were transfected at different times: 3 hours after release for wild-type cells, 2 hours after release for RAD21-AID cells and 1.5 hours after release for Sororin-AID cells (see section: sgRNA transfection). Cells were finally fixed at RT for 15 minutes with 4% PFA (Electron Microscopy Sciences, 15710) in PBS (1X final concentration) and quenched for 10 minutes with 100mM NH4Cl (Sigma-Aldrich, 326372).

5.4. sgRNA transfection for double-strand break induction

The sgRNA that was used in this project is described in this paper from (van den Berg et al., 2018), under the name HS17. Its sequence is the following: 5′-CAGACAGGCCCAGATTGAGG-3’. Transfections of sgRNA were performed with TrueGuide sgRNA (Thermo Fisher Scientific), using Lipofectamine RNAiMAX (Thermo Fisher Scientifis, 13778150), for up to 6 hours. Unless stated otherwise, the final concentration of the sgRNA was 27.5 nM.

5.5. siRNA transfection for BRCA2 and BRCA1 depletion

Transfections of siRNA for the depletion of BRCA2 and BRCA1 were performed with commercial siRNAs (Thermo Fisher Scientific), using Lipofectamine RNAiMAX, 48 hours before the time of fixation. The final concentration of the siRNA in the medium was 25 nM.

5.6. EdU pulse and staining

To assess the cell cycle stage in our synchronization protocol, we performed an EdU pulse before fixation of the cells, at different time points, after DNA double-strand break induction. 20 minutes before fixation, 10µM of EdU (5-ethynyl-2-deoxyuridine, Thermo Fisher Scientific, A10044) was added to the cells. Once the sample is fixed, the EdU staining was performed using the Click-iT^{TM} EdU Cell Proliferation Kit for Imaging, Alexa Fluor^{TM} 647 dye (Invitrogen, C10340), according to manual specifications.

5.7. Immunofluorescence and secondary fixation

Following their first fixation, the cells were permeabilized with 0.2% Triton X-100 (Sigma-Aldrich, 327371000) for 20 minutes at room temperature and then blocked with a solution of 2% Bovine Serum Albumine (BSA, Sigma-Aldrich, A7030) diluted in 1X PBS for 30 minutes at room temperature. Cells were then incubated with primary antibodies diluted in 2% BSA for 2 hours at room temperature, washed three times with 1X PBS for 5 minutes and then incubated with fluorescently-labeled secondary antibodies for 1 hour at room temperature, in the dark, also diluted in 2% BSA. Once the cells were washed three times with 1X PBS for 5 minutes, they were fixed for a second time, to ensure stability of the antibodies and the DNA structure, using 1mM Bis(NHS)PEG5 (Sigma-Aldrich, 803537) in 1X PBS for 30 minutes at room temperature, in the dark. The cells were then quenched for 10 minutes with 100mM NH4Cl (Sigma-Aldrich, 326372).

The primary antibodies that were used are anti-53BP1 (1:1000, Mouse; Millipore, MAB3802) and anti-RAD51 (1:1000, Rabbit, Abcam, ab176458). The secondary antibodies that were used are anti-Mouse IgG Alexa FluorTM 568 (1:1000, Goat; Invitrogen, A11004) and anti-Rabbit IgG Alexa FluorTM 488 (1:1000, Donkey; Invitrogen, A21206).

5.8. RASER-FISH methodology

Both RASER-FISH probe generation and hybridization was done following established protocols (Beckwith et al., 2025; Brunner et al., 2025) based on RASER-FISH (Brown et al., 2022) and oligonucleotide pool amplification (Mateo et al., 2021). Also, these methods were previously described in this publication: (Teloni et al., 2025).

5.8.1. RASER-FISH probe design and amplification

Probe design

Primary RASER-FISH oligonucleotide probe design was based on a HeLa Kyoto reference genome (hg19 with SNP correction, [ref]). We selected 21 of the 23 sgRNA target sites and designed probes upstream and downstream of the cutting site. To avoid probe hybridization onto resected RAD51-coated DNA filaments, we excluded the ±5 kb regions flanking the cut sites, and defined 30kb-region at the direct vicinity of the target site, starting from there. We used the OligoMiner pipeline [ref] to identify 36-42 bp unique target sequences (42 °C annealing temperature at 50% formamide concentration, 30–70% GC content, 0.25–0.99 LDA stringency, 5–20 k-mer filtering, and a 0.1 secondary structure filter). At least 150 probes covered each double-strand break site. Each unlabeled primary oligonucleotide carried short barcode sequences for binding to fluorescently labeled secondary oligonucleotides (see Figure 3.3.1 and Figure 3.3.2.), as well as flanking primers for oligonucleotide pool amplification containing the T7 in vitro transcription promoter. Oligonucleotide pools were ordered from GenScript (GenTitan™ Oligo Pools).

Probe amplification

RASER-FISH probes were amplified by qPCR using 2× Phusion High-Fidelity PCR Master Mix (Thermo Fisher Scientific, F531), 15 ng oligonucleotide pool, 0.5 µM forward and reverse primers, and 1× EvaGreen (Biotium, 31000). Samples were incubated at 98 °C for 3 min, followed by 98 °C for 10 s, 66 °C for 10 s, and 72 °C for 15 s in repeated cycles until near plateau. Amplified DNA was purified using the DNA Clean & Concentrator-25 kit (Zymo Research, D4033) and eluted in 50 µl ultrapure water. For the in vitro transcription, 1.5 µg PCR product was incubated overnight at

37°C using the HiScribe T7 Quick High Yield RNA Synthesis Kit (New England Biolabs, E2050) with 80 µl NTP buffer mix, 6.25 µl T7 RNA polymerase mix, 6.25 µl RNAsin Plus RNAse inhibitor (Promega, N2615), and ultrapure water to reach 160 µl. 150 µl of unpurified ssRNA was used directly for reverse transcription at 50 °C for 1 hour with 21 µl of 25 mM dNTP mix (final concentration 1.75 mM), 57 µl of 100 µM forward primer (final concentration 19 µM), 6 µl RNAsin Plus RNAse inhibitor, 6 µl Maxima H Minus Reverse Transcriptase (1,200 U, Thermo Fisher Scientific, EP0753), and 60 µl of 5× RT buffer. RNA was then degraded by incubation with 150 µl 0.5 M EDTA and 150 µl 1 M NaOH at 95 °C for 15 minutes. The ssDNA oligonucleotide pool was purified with a DNA Clean & Concentrator-100 kit (Zymo Research, D4030), eluted in 200 µl ultrapure water, and its concentration determined by Nanodrop.

Fluorescent secondary oligonucleotide generation

Fluorescently labeled secondary oligonucleotides were synthesized via Click chemistry (ClickTech Oligo Link Kit; baseclick, BCK-OL) with 3′-C3-azide oligonucleotides (Metabion) and an alkyne-modified ATTO647N fluorophore (ATTO-TEC, AD 647N). After purification with HPLC, labeled oligonucleotides were diluted in 1× TE buffer.

5.8.2. RASER-FISH procedure

Following the immunofluorescence procedure, nuclei were stained with 0.5 µg/mL DAPI (Thermo Fisher Scientific, 62248) in PBS (1× final concentration), for 15 minutes at room temperature, in the dark. Cells were then treated by UV illumination in a Vilber Bio-Link crosslinker (254 nm, 3.6 J/cm2) to induce nicks in BrdU- and BrdC-incorporated DNA strands, which were then digested by Exonuclease III (1 U/µL; New England Biolabs, M0206) during 15 minutes of incubation at 37°C. Cells were pre-incubated in FISH hybridization buffer at 37 °C for 1 hour (50% (v/v) Formamide; Thermo Fisher Scientific, AM9342; 10% (w/v) Dextran Sulfate; Merck, S4030; 2×SSC; Thermo Fisher Scientific, AM9763), followed by an overnight incubation at 42°C with primary FISH probes (~2 nM/probe) in the same buffer. After two 35 °C washes (5 min each) in 50% (v/v) formamide/2×SSC, cells were washed in 2×SSC+0.2% (v/v) Tween-20 (Sigma-Aldrich, P9416). RNA-DNA hybrids were

removed by RNase H digestion (0.05 U/µl; NEB, M0297) at 37 °C for 20 min, followed by 3 washes in 2×SSC+0.2% Tween-20, at room-temperature.

5.8.3. RASER-FISH secondary probe hybridization for manual experiments

For the data in the first two results, secondary FISH probe hybridization was performed manually, targeting only the regional barcodes (as explained in Result 3), to obtain the broad signal from the cut site. This was done at room temperature for 3 minutes, in a buffer containing 50% (w/v) Ethylene Carbonate (Sigma-Aldrich, E26258) and fluorescent secondary oligonucleotides (20 nM) in 2×SSC+0.2% Tween-20. Then, excess secondary oligonucleotides were removed by a 1-min wash at room temperature with 10% (v/v) Formamide in 2×SSC+0.2% Tween-20. Cells were then incubated in 2×SSC+0.2 µg/ml DAPI before imaging.

All experiments combining immunofluorescence and RASER-FISH in the first two results were imaged on a Zeiss LSM980 confocal system using a 63× NA 1.4 oil DIC Plan-Apochromat objective (ZEN Blue 2020 software v3.7). Images were collected in confocal mode with optimal sectioning (390 nm between z-slices).

A list of the genomic regions targeted by the sgRNA and our oligonucleotide pool can be found in Table S1.

5.8.4. scsRASER-FISH automated secondary probe hybridization

For the automated multiplexing data, in all results apart from the first two, secondary FISH probe hybridization was performed in an automated manner, combining a microfluidics system, robotics, and coordinated acquisition on the microscope.

First, cells were incubated with fiducial beads (TetraSpeck™ Microspheres, 0.1 µm; final dilution 1:250; Thermo Fisher, T7279) and 0.5 µg/mL DAPI in a 2×SSC solution, for 10 minutes at room temperature, in the dark. Then, excess beads were washed with

2×SSC, and the slide was connected to the microfluidics system and mounted onto the microscope. A 96-well plate was prepared and filled with secondary probe hybridization buffer (50% (w/v) Ethylene Carbonate and fluorescent secondary oligonucleotides (20 nM) in 2×SSC+0.2% Tween-20), each well with a different fluorescent oligonucleotide. The robot would then automatically perform the washing, imaging and stripping incubations, by pumping the corresponding buffers from wider plates.

- The *wash buffer* was prepared as previously mentioned: 10% (v/v) Formamide in 2×SSC+0.2% Tween-20. (See: Secondary probe hybridization for manual experiments).

- The *imaging buffer* is an oxygen-scavenging system (100 mM Tris-HCl pH8.0, 10% (w/v) D-(+)-Glucose (Sigma-Aldrich, G8270), 2 mM Trolox (Sigma-Aldrich, 238813), 0.5 µg/mL Glucose oxidase (Sigma-Aldrich, G7141-10KU), 40 µg/mL Catalase (Fisher Scientific, 11463070) in 2×SSC), and is covered with pure mineral oil (Thermo Fisher, 415080010) to prevent oxygen from coming into contact with the buffer.

- The *stripping buffer* contains a higher Formamide concentration compared to the wash buffer, to destabilize the interaction between primary and secondary probes, and is prepared as follows: 50% (v/v) Formamide in 2×SSC+0.2% Tween-20. It is left to incubate for 3 minutes on the sample before being washed with the wash buffer.

5.8.5. RASER-FISH image analysis

Quantification of regional RASER-FISH

The images that were acquired with regional RASER-FISH loci only were processed with an in-house automated pipeline (v0.9.0; https://github.com/gerlichlab/reparafil), except for a small subset of images which were analyzed manually. Nuclei are first segmented based on DAPI staining in Fiji. These nuclear regions (stored as ImageJ .roi files) are used as input in the processing pipeline and used to exclude non-nuclear FISH signals. Fluorescent puncta (FISH loci) were identified using a pixel-intensity threshold approach via the spotfishing package (https://github.com/gerlichlab/spotfishing).

Immunofluorescence intensities were collected from 10x10-pixel boxes around each FISH locus centroid in the relevant z-slice. To classify a FISH locus as 53BP1-positive, a signal threshold was set to the mean plus two standard deviations of the 53BP1 intensity in non-cut controls. This threshold was determined independently for each target site. Loci exceeding the threshold were tagged as 53BP1-positive. For these 53BP1-positive loci, homologous recombination was assessed by RAD51 intensity, using the same thresholding approach. Independent experiment quantifications were plotted using GraphPad Prism (v10.1.1).

Image analysis and quantification of automated multiplexing experiments

The data from the third result and on, generated using automated microfluidics and imaging, are processed through a pipeline that is part of a software called LoopTrace. It was initially created by the Ellenberg Lab (https://git.embl.de/grp-ellenberg/looptrace), but it was further developed and built on in the lab to best fit our specific needs. The multi-channel raw images, containing all rounds of secondary hybridizations and several fields of view, are submitted as input to the pipeline, and undergo multiple steps of analysis, among which are nuclei segmentation, image registration, and spot detection with gaussian fitting. These steps allow for sub-pixel resolution of the detected RASER-FISH loci, which are as an output associated with a set of corrected and precise coordinates. The distance measurements between untreated and double-strand-break-induced data stem form calculations on these coordinates. The thresholds for disjunction assessment calculated on the untreated (0 nM) control condition of the second biological repeat. It is set to exclude 5% of the most extreme data points.

5.9. Quantitative image-based cytometry (QIBC)

Quantitative image-based cytometry was performed as described previously (*88*) using an Olympus ScanR Screening System (Olympus IX83 microscope). Images were acquired with a Hamamatsu ORCA-FLASH 4.0 camera (16-bit, 2,048 × 2,048 pixels, 6.5 µm pixel size) using a 40× air objective (0.75 NA, 0.5mm WD). For each condition at least 400 cells were imaged. The acquisition and the analysis were performed using

the Olympus ScanR software (v3.5.0). A dynamic background correction was applied, nuclei were segmented based on DAPI intensity, 53BP1 and RAD51 foci were detected inside the nuclear masks, using a built-in spot detection module. Cell stage tags were attributed based on DAPI and EdU intensities.

5.10. Quantification of them frequency of single and double-sister cutting events in replicated chromosomes

To quantify how frequently sgRNA target sites on replicated chromosomes are cleaved on either one or both sister chromatids, we applied a statistical model based on the assumption that DNA double-strand breaks occur independently and stochastically at each sgRNA target site. If we define p as the probability that a cut occurs at a single target site on one chromatid, then the probability of no cuts occurring is $(1 - p)$. We can then obtain these three probabilities:

- p^2 if two sister chromatids are cut;
- $2p(1 - p)$ if only one sister chromatid is cut;
- $(1 - p)^2$ if no sister chromatids are cut.

The estimation of p was performed using the observed fraction of 53BP1-negative FISH target sites, in which case we assume that these are uncut sites. p was estimated by solving the equation $(1 - p)^2 = fraction\ of\ 53BP1\text{-}negative\ foci$. We used this to calculate the probabilities of single- and double-cutting in all sgRNA target sites analyzed by RASER-FISH and immunofluorescence.

5.11. Analysis of allele cutting efficiency at low concentrations of sgRNA

To determine the stochasticity of Cas9-induced cutting among several copies of the same genomic loci per nucleus, we focused our analysis of RASER-FISH images on the nuclei. We selected the nuclei that displayed the expected number of FISH loci for

two sites (3 alleles were expected for chromosome 2 and 4 alleles for chromosome 19). The number of 53BP1-positive alleles within each nucleus was manually recorded, using the 53BP1 thresholding calculated in all cells., and each nucleus was categorized depending on the number of 53BP1-positive alleles. Each dot represents the percentage of cells in each replicate that have 0/1/2/3/4 53BP1-positive FISH loci. The height of the bar is the average of the 3 replicates.

6. References

Ahrabi, S., Sarkar, S., Pfister, S. X., Pirovano, G., Higgins, G. S., Porter, A. C. G., & Humphrey, T. C. (2016). A role for human homologous recombination factors in suppressing microhomology-mediated end joining. *Nucleic Acids Research*, *44*(12), 5743–5757.

Arnould, C., Rocher, V., Finoux, A.-L., Clouaire, T., Li, K., Zhou, F., Caron, P., Mangeot, P. E., Ricci, E. P., Mourad, R., Haber, J. E., Noordermeer, D., & Legube, G. (2021). Loop extrusion as a mechanism for formation of DNA damage repair foci. *Nature*, *590*(7847), 660–665.

Arnould, C., Rocher, V., Saur, F., Bader, A. S., Muzzopappa, F., Collins, S., Lesage, E., Le Bozec, B., Puget, N., Clouaire, T., Mangeat, T., Mourad, R., Ahituv, N., Noordermeer, D., Erdel, F., Bushell, M., Marnef, A., & Legube, G. (2023). Chromatin compartmentalization regulates the response to DNA damage. *Nature*. https://doi.org/10.1038/s41586-023-06635-y

Aten, J. A., Stap, J., Krawczyk, P. M., van Oven, C. H., Hoebe, R. A., Essers, J., & Kanaar, R. (2004). Dynamics of DNA double-strand breaks revealed by clustering of damaged chromosome domains. *Science (New York, N.Y.)*, *303*(5654), 92–95.

Batty, P., Langer, C. C., Takács, Z., Tang, W., Blaukopf, C., Peters, J.-M., & Gerlich, D. W. (2023). Cohesin-mediated DNA loop extrusion resolves sister chromatids in G2 phase. *The EMBO Journal*, *42*(16), e113475.

Beckwith, K. S., Ødegård-Fougner, Ø., Morero, N. R., Barton, C., Schueder, F., Tang, W., Alexander, S., Peters, J.-M., Jungmann, R., Birney, E., & Ellenberg, J. (2025). Nanoscale 3D DNA tracing in non-denatured cells resolves the Cohesin-dependent

loop architecture of the genome in situ. *Nature Communications*, *16*(1). https://doi.org/10.1038/s41467-025-61689-y

Birkenbihl, R. P., & Subramani, S. (1992). Cloning and characterization of rad21 an essential gene of Schizosaccharomyces pombe involved in DNA double-strand-break repair. *Nucleic Acids Research*, *20*(24), 6605–6611.

Brown, J. M., De Ornellas, S., Parisi, E., Schermelleh, L., & Buckle, V. J. (2022). RASER-FISH: non-denaturing fluorescence in situ hybridization for preservation of three-dimensional interphase chromatin structure. *Nature Protocols*, *17*(5), 1306–1331.

Brunner, A., Morero, N. R., Zhang, W., Hossain, M. J., Lampe, M., Pflaumer, H., Halavatyi, A., Peters, J.-M., Beckwith, K. S., & Ellenberg, J. (2025). Quantitative imaging of loop extruders rebuilding interphase genome architecture after mitosis. *The Journal of Cell Biology*, *224*(3). https://doi.org/10.1083/jcb.202405169

Burma, S., Chen, B. P., Murphy, M., Kurimasa, A., & Chen, D. J. (2001). ATM phosphorylates histone H2AX in response to DNA double-strand breaks. *The Journal of Biological Chemistry*, *276*(45), 42462–42467.

Canela, A., Sridharan, S., Sciascia, N., Tubbs, A., Meltzer, P., Sleckman, B. P., & Nussenzweig, A. (2016). DNA breaks and end resection measured genome-wide by end sequencing. *Molecular Cell*, *63*(5), 898–911.

Caron, P., Aymard, F., Iacovoni, J. S., Briois, S., Canitrot, Y., Bugler, B., Massip, L., Losada, A., & Legube, G. (2012). Cohesin protects genes against γH2AX Induced by DNA double-strand breaks. *PLoS Genetics*, *8*(1), e1002460.

Ceccaldi, R., Rondinelli, B., & D'Andrea, A. D. (2016). Repair pathway choices and consequences at the double-strand break. *Trends in Cell Biology*, *26*(1), 52–64.

Chen, L., Nievera, C. J., Lee, A. Y.-L., & Wu, X. (2008). Cell cycle-dependent complex formation of BRCA1.CtIP.MRN is important for DNA double-strand break repair. *The Journal of Biological Chemistry*, *283*(12), 7713–7720.

Covo, S., Westmoreland, J. W., Gordenin, D. A., & Resnick, M. A. (2010). Cohesin Is limiting for the suppression of DNA damage-induced recombination between homologous chromosomes. *PLoS Genetics*, *6*(7), e1001006.

Cremer, T., & Cremer, M. (2010). Chromosome territories. *Cold Spring Harbor Perspectives in Biology*, *2*(3), a003889.

de Luca, K. L., Rullens, P. M. J., Karpinska, M. A., de Vries, S. S., Gacek-Matthews, A., Pongor, L. S., Legube, G., Jachowicz, J. W., Oudelaar, A. M., & Kind, J. (2024).

Genome-wide profiling of DNA repair proteins in single cells. *Nature Communications*, *15*(1), 9918.

Deng, S. K., Gibb, B., de Almeida, M. J., Greene, E. C., & Symington, L. S. (2014). RPA antagonizes microhomology-mediated repair of DNA double-strand breaks. *Nature Structural & Molecular Biology*, *21*(4), 405–412.

Deshpande, R. A., Williams, G. J., Limbo, O., Williams, R. S., Kuhnlein, J., Lee, J.-H., Classen, S., Guenther, G., Russell, P., Tainer, J. A., & Paull, T. T. (2014). ATP-driven Rad50 conformations regulate DNA tethering, end resection, and ATM checkpoint signaling. *The EMBO Journal*, *33*(5), 482–500.

Dion, V., Kalck, V., Horigome, C., Towbin, B. D., & Gasser, S. M. (2012). Increased mobility of double-strand breaks requires Mec1, Rad9 and the homologous recombination machinery. *Nature Cell Biology*, *14*(5), 502–509.

Dion, V., Kalck, V., Seeber, A., Schleker, T., & Gasser, S. M. (2013). Cohesin and the nucleolus constrain the mobility of spontaneous repair foci. *EMBO Reports*, *14*(11), 984–991.

Dumont, A., Mendiboure, N., Savocco, J., Anani, L., Moreau, P., Thierry, A., Modolo, L., Jost, D., & Piazza, A. (2024). Mechanism of homology search expansion during recombinational DNA break repair in Saccharomyces cerevisiae. *Molecular Cell*, *84*(17), 3237-3253.e6.

Friskes, A., Snoek, M., Oldenkamp, R., van den Broekb.vd., B., Nahidiazar, L., Koob, L., Dick, A. E., Mertz, M., Harkes, R., Rowland, B. D., Jalink, K., & Medema, R. H. (2025). Visualizing homology search in living cells. In *bioRxiv* (p. 2025.03.01.640932). https://doi.org/10.1101/2025.03.01.640932

Gelot, C., Guirouilh-Barbat, J., Le Guen, T., Dardillac, E., Chailleux, C., Canitrot, Y., & Lopez, B. S. (2016). The Cohesin Complex Prevents the End Joining of Distant DNA Double-Strand Ends. *Molecular Cell*, *61*(1), 15–26.

Gerlich, D., Koch, B., Dupeux, F., Peters, J.-M., & Ellenberg, J. (2006). Live-cell imaging reveals a stable cohesin-chromatin interaction after but not before DNA replication. *Current Biology: CB*, *16*(15), 1571–1578.

Goodwin, E., & Meyne, J. (1993). Strand-specific FISH reveals orientation of chromosome 18 alphoid DNA. *Cytogenetics and Cell Genetics*, *63*(2), 126–127.

Graham, T. G. W., Walter, J. C., & Loparo, J. J. (2016). Two-stage synapsis of DNA ends during non-homologous end joining. *Molecular Cell*, *61*(6), 850–858.

Guirouilh-Barbat, J., Huck, S., Bertrand, P., Pirzio, L., Desmaze, C., Sabatier, L., & Lopez, B. S. (2004). Impact of the KU80 pathway on NHEJ-induced genome rearrangements in mammalian cells. *Molecular Cell*, *14*(5), 611–623.

Hartlerode, A. J., & Scully, R. (2009). Mechanisms of double-strand break repair in somatic mammalian cells. *Biochemical Journal*, *423*(2), 157–168.

Hochegger, H., Takeda, S., & Hunt, T. (2008). Cyclin-dependent kinases and cell-cycle transitions: does one fit all? *Nature Reviews. Molecular Cell Biology*, *9*(11), 910–916.

Hustedt, N., & Durocher, D. (2016). The control of DNA repair by the cell cycle. *Nature Cell Biology*, *19*(1), 1–9.

Jackson, S. P., & Bartek, J. (2009). The DNA-damage response in human biology and disease. *Nature*, *461*(7267), 1071–1078.

Johnson, R. D., & Jasin, M. (2000). Sister chromatid gene conversion is a prominent double-strand break repair pathway in mammalian cells. *The EMBO Journal*, *19*(13), 3398–3407.

Khalil, A., Grant, J. L., Caddle, L. B., Atzema, E., Mills, K. D., & Arneodo, A. (2007). Chromosome territories have a highly nonspherical morphology and nonrandom positioning. *Chromosome Research: An International Journal on the Molecular, Supramolecular and Evolutionary Aspects of Chromosome Biology*, *15*(7), 899–916.

Kuru-Schors, M., Haemmerle, M., & Gutschner, T. (2021). The cohesin complex and its interplay with non-coding RNAs. *Non-Coding RNA*, *7*(4), 67.

Lee, M., Lipfert, J., Sanchez, H., Wyman, C., & Dekker, N. H. (2013). Structural and torsional properties of the RAD51-dsDNA nucleoprotein filament. *Nucleic Acids Research*, *41*(14), 7023–7030.

Litwin, I., Pilarczyk, E., & Wysocki, R. (2018). The Emerging Role of Cohesin in the DNA Damage Response. *Genes*, *9*(12). https://doi.org/10.3390/genes9120581

Liu, Y., Zou, R. S., He, S., Nihongaki, Y., Li, X., Razavi, S., Wu, B., & Ha, T. (2020). Very fast CRISPR on demand. *Science (New York, N.Y.)*, *368*(6496), 1265–1269.

Lukas, J., Lukas, C., & Bartek, J. (2011). More than just a focus: The chromatin response to DNA damage and its role in genome integrity maintenance. *Nature Cell Biology*, *13*(10), 1161–1169.

Mao, Z., Bozzella, M., Seluanov, A., & Gorbunova, V. (2008). DNA repair by nonhomologous end joining and homologous recombination during cell cycle in human cells. *Cell Cycle (Georgetown, Tex.)*, *7*(18), 2902–2906.

Mason, J. M., Dusad, K., Wright, W. D., Grubb, J., Budke, B., Heyer, W.-D., Connell, P. P., Weichselbaum, R. R., & Bishop, D. K. (2015). RAD54 family translocases counter genotoxic effects of RAD51 in human tumor cells. *Nucleic Acids Research*, *43*(6), 3180–3196.

Mateo, L. J., Sinnott-Armstrong, N., & Boettiger, A. N. (2021). Tracing DNA paths and RNA profiles in cultured cells and tissues with ORCA. *Nature Protocols*, *16*(3), 1647–1713.

Michaelis, C., Ciosk, R., & Nasmyth, K. (1997). Cohesins: chromosomal proteins that prevent premature separation of sister chromatids. *Cell*, *91*(1), 35–45.

Miné-Hattab, J., & Rothstein, R. (2012). Increased chromosome mobility facilitates homology search during recombination. *Nature Cell Biology*, *14*(5), 510–517.

Mitter, M., Gasser, C., Takacs, Z., Langer, C. C. H., Tang, W., Jessberger, G., Beales, C. T., Neuner, E., Ameres, S. L., Peters, J.-M., Goloborodko, A., Micura, R., & Gerlich, D. W. (2020). Conformation of sister chromatids in the replicated human genome. *Nature*, *586*(7827), 139–144.

Nakamura, K., Saredi, G., Becker, J. R., Foster, B. M., Nguyen, N. V., Beyer, T. E., Cesa, L. C., Faull, P. A., Lukauskas, S., Frimurer, T., Chapman, J. R., Bartke, T., & Groth, A. (2019). H4K20me0 recognition by BRCA1-BARD1 directs homologous recombination to sister chromatids. *Nature Cell Biology*, *21*(3), 311–318.

Nick McElhinny, S. A., Snowden, C. M., McCarville, J., & Ramsden, D. A. (2000). Ku recruits the XRCC4-ligase IV complex to DNA ends. *Molecular and Cellular Biology*, *20*(9), 2996–3003.

Nishiyama, T., Ladurner, R., Schmitz, J., Kreidl, E., Schleiffer, A., Bhaskara, V., Bando, M., Shirahige, K., Hyman, A. A., Mechtler, K., & Peters, J.-M. (2010). Sororin mediates sister chromatid cohesion by antagonizing Wapl. *Cell*, *143*(5), 737–749.

Pannunzio, N. R., Watanabe, G., & Lieber, M. R. (2018). Nonhomologous DNA end-joining for repair of DNA double-strand breaks. *The Journal of Biological Chemistry*, *293*(27), 10512–10523.

Phipps, J., & Dubrana, K. (2022). DNA Repair in Space and Time: Safeguarding the Genome with the Cohesin Complex. *Genes*, *13*(2). https://doi.org/10.3390/genes13020198

Phipps, J., Toulouze, M., Ducrot, C., Costa, R., Brocas, C., & Dubrana, K. (2025). Cohesin complex oligomerization maintains end-tethering at DNA double-strand breaks. *Nature Cell Biology*, *27*(1), 118–129.

Piazza, A., Bordelet, H., Dumont, A., Thierry, A., Savocco, J., Girard, F., & Koszul, R. (2021). Cohesin regulates homology search during recombinational DNA repair. *Nature Cell Biology*, *23*(11), 1176–1186.

Qi, Z., Redding, S., Lee, J. Y., Gibb, B., Kwon, Y., Niu, H., Gaines, W. A., Sung, P., & Greene, E. C. (2015). DNA sequence alignment by microhomology sampling during homologous recombination. *Cell*, *160*(5), 856–869.

Rao, S. S. P., Huang, S.-C., Glenn St Hilaire, B., Engreitz, J. M., Perez, E. M., Kieffer-Kwon, K.-R., Sanborn, A. L., Johnstone, S. E., Bascom, G. D., Bochkov, I. D., Huang, X., Shamim, M. S., Shin, J., Turner, D., Ye, Z., Omer, A. D., Robinson, J. T., Schlick, T., Bernstein, B. E., … Aiden, E. L. (2017). Cohesin Loss Eliminates All Loop Domains. *Cell*, *171*(2), 305-320.e24.

Rao, S. S. P., Huntley, M. H., Durand, N. C., Stamenova, E. K., Bochkov, I. D., Robinson, J. T., Sanborn, A. L., Machol, I., Omer, A. D., Lander, E. S., & Aiden, E. L. (2014). A 3D map of the human genome at kilobase resolution reveals principles of chromatin looping. *Cell*, *159*(7), 1665–1680.

Rogakou, E. P., Pilch, D. R., Orr, A. H., Ivanova, V. S., & Bonner, W. M. (1998). DNA double-stranded breaks induce histone H2AX phosphorylation on serine 139. *The Journal of Biological Chemistry*, *273*(10), 5858–5868.

Roukos, V., Voss, T. C., Schmidt, C. K., Lee, S., Wangsa, D., & Misteli, T. (2013). Spatial dynamics of chromosome translocations in living cells. *Science (New York, N.Y.)*, *341*(6146), 660–664.

Saleh-Gohari, N., & Helleday, T. (2004). Conservative homologous recombination preferentially repairs DNA double-strand breaks in the S phase of the cell cycle in human cells. *Nucleic Acids Research*, *32*(12), 3683–3688.

Sanders, J. T., Freeman, T. F., Xu, Y., Golloshi, R., Stallard, M. A., Hill, A. M., San Martin, R., Balajee, A. S., & McCord, R. P. (2020). Radiation-induced DNA damage and repair effects on 3D genome organization. *Nature Communications*, *11*(1), 6178.

Schwarzer, W., Abdennur, N., Goloborodko, A., Pekowska, A., Fudenberg, G., Loe-Mie, Y., Fonseca, N. A., Huber, W., Haering, C. H., Mirny, L., & Spitz, F. (2017). Two independent modes of chromatin organization revealed by cohesin removal. *Nature*, *551*(7678), 51–56.

Scully, R., Panday, A., Elango, R., & Willis, N. A. (2019). DNA double-strand break repair-pathway choice in somatic mammalian cells. *Nature Reviews. Molecular Cell Biology*, *20*(11), 698–714.

Scully, R., & Xie, A. (2013). Double strand break repair functions of histone H2AX. *Mutation Research*, *750*(1–2), 5–14.

Sikorska, N., & Sexton, T. (2020). Defining functionally relevant spatial chromatin domains: It is a TAD complicated. *Journal of Molecular Biology*, *432*(3), 653–664.

Stanyte, R., Nuebler, J., Blaukopf, C., Hoefler, R., Stocsits, R., Peters, J.-M., & Gerlich, D. W. (2018). Dynamics of sister chromatid resolution during cell cycle progression. *The Journal of Cell Biology*, *217*(6), 1985–2004.

Ström, L., Lindroos, H. B., Shirahige, K., & Sjögren, C. (2004). Postreplicative recruitment of cohesin to double-strand breaks is required for DNA repair. *Molecular Cell*, *16*(6), 1003–1015.

Teloni, F., Takacs, Z., Mitter, M. M., Langer, C. C. H., Prlesi, I., Steinacker, T. L., Reuter, V. P., Mylarshchikov, D., & Gerlich, D. W. (2025). Cohesin guides homology search during DNA repair via loops and sister chromatid linkages. *BioRxiv: The Preprint Server for Biology*.

Unal, E., Heidinger-Pauli, J. M., & Koshland, D. (2007). DNA double-strand breaks trigger genome-wide sister-chromatid cohesion through Eco1 (Ctf7). *Science*, *317*(5835), 245–248.

van den Berg, J., G Manjón, A., Kielbassa, K., Feringa, F. M., Freire, R., & Medema, R. H. (2018). A limited number of double-strand DNA breaks is sufficient to delay cell cycle progression. *Nucleic Acids Research*, *46*(19), 10132–10144.

Wilson, T. E., Grawunder, U., & Lieber, M. R. (1997). Yeast DNA ligase IV mediates non-homologous DNA end joining. *Nature*, *388*(6641), 495–498.

Wutz, G., Várnai, C., Nagasaka, K., Cisneros, D. A., Stocsits, R. R., Tang, W., Schoenfelder, S., Jessberger, G., Muhar, M., Hossain, M. J., Walther, N., Koch, B., Kueblbeck, M., Ellenberg, J., Zuber, J., Fraser, P., & Peters, J.-M. (2017). Topologically associating domains and chromatin loops depend on cohesin and are regulated by CTCF, WAPL, and PDS5 proteins. *The EMBO Journal*, *36*(24), 3573–3599.

Yang, J. H., Brandão, H. B., & Hansen, A. S. (2023). DNA double-strand break end synapsis by DNA loop extrusion. *Nature Communications*, *14*(1), 1913.

Zhang, N., & Pati, D. (2012). Sororin is a master regulator of sister chromatid cohesion and separation. *Cell Cycle (Georgetown, Tex.)*, *11*(11), 2073–2083.

Zhong, Q., Chen, C. F., Li, S., Chen, Y., Wang, C. C., Xiao, J., Chen, P. L., Sharp, Z. D., & Lee, W. H. (1999). Association of BRCA1 with the hRad50-hMre11-p95

complex and the DNA damage response. *Science (New York, N.Y.)*, *285*(5428), 747–750.

Zhou, Y., Caron, P., Legube, G., & Paull, T. T. (2014). Quantitation of DNA double-strand break resection intermediates in human cells. *Nucleic Acids Research*, *42*(3), e19.

7. Supplementary material

7.1. Tables

Chromosome		Genomic position	Abbreviation	Selected for FISH	Regional-specific barcode	Locus-specific probe set
Chr1	p36.21	16119503	Chr1a	-	1	Set 1
Chr1	p36.11	27306872	Chr1b	-	2	Set 2
Chr2	**q14.3**	**122416332**	**Chr2a**	**X**	**3**	**Set 3**
Chr2	q33.2	204055719	Chr2b	-	4	Set 4
Chr2	p11.2	85101949	Chr2c	-	5	Set 5
Chr6	**p21.2**	**37059304**	**Chr6b**	**X**	**6**	**Set 6**
Chr7	p15.3	22921728	Chr7	-	7	Set 6
Chr8	p11.23	37840790	Chr8	-	8	Set 6
Chr10	**p15.1**	**5904349**	**Chr10a**	**X**	**9**	**Set 3**
Chr10	q24.1	99069499	Chr10b	-	10	Set 4
Chr10	q21.3	69634394	Chr10c	-	11	Set 5
Chr12	**q24.31**	**121354761**	**Chr12a**	**X**	**12**	**Set 7**
Chr12	p11.21	32101483	Chr12b	-	13	Set 1
Chr13	q21.33	69228918	Chr13	-	14	Set 2
Chr14	q12	31260411	Chr14	-	15	Set 2
Chr17	**q23.2**	**58511366**	**Chr17a**	**X**	**16**	**Set 7**
Chr17	q25.2	78950467	Chr17b	-	17	Set 1
Chr19	**p13.2**	**13269385**	**Chr19**	**X**	**18**	**Set 7**
Chr20	**p11.23**	**19804371**	**Chr20a**	**X**	19	**Set 3**
Chr20	q13.2	53691398	Chr20b	-	20	Set 4
Chr20	**q12**	**40176277**	**Chr20c**	**X**	**21**	**Set 5**

Table S1: Targeted sites by the sgRNA and oligonucleotide pool design for scsRASER-FISH. Here are indicated the chromosome number and genomic positions of all break sites that we targeted with RASER-FISH probes. In bold are highlighted the genomic positions studied in the presented this thesis, that yielded good signal. The two columns on the right represent the labelling strategy for the multiplexed design of the RASER-FISH probes.

Name	Genotype	Plasmid used	Base cell line used	Resistance marker
HeLa Kyoto Cas9-dox	FKBP12F36V-5xGly-3xFLAG-Cas9 (PiggyBac integration)	FKBP12F36V-5xGly-3xFLAG-Cas9 (piggyBac with tetracycline response promoter) Super PiggyBac Transposase	HeLa Kyoto	G418
HeLa Kyoto RAD21-AID Cas9-dox	mEGFP-AID-SCC1TIR1-3xMyc-T2A-Puro (lentiviral integration)FKBP12F36V-5xGly-3xFLAG-Cas9 (PiggyBac integration	mEGFP-AID-SCC1 repair template TIR1-3xMyc-T2A PuroL entivirus sgRNA expressing / Cas9D10A expressing to tag SCC1 FKBP12F36V-5xGly-3xFLAG-Cas9 (piggyBac with tetracycline response promoter) Super PiggyBac Transposase	HeLa Kyoto SCC1-mEGFP-AID	Puromycin, G418
HeLa Kyoto Sororin-AID Cas9-dox	EGFP-AID-SororinTIR1-3xMyc-T2A-Puro (lentiviral integration)FKBP12F36V-5xGly-3xFLAG-Cas9 (Piggyback integratio	EGFP-AID-Sororin repair template TIR1-3xMyc-T2A PuroL entivirus sgRNA expressing / Cas9D10A expressing to tag Sororin FKBP12F36V-5xGly-3xFLAG-Cas9 (piggyBac with tetracycline response promoter) Super PiggyBac Transposase	HeLa Kyoto Sororin-AID	Puromycin, G418

Table S2: Cell lines used in this study. Generation of the cell lines is published in this publication (Teloni et al., 2025).

7.2. Supplementary plots for scsRASER-FISH

In this section, all 2D-scatterplots of the studied sites in the comparison figures are presented. They provide the detail of cis distance changes upon double-strand break induction, across different genotypes or depletion conditions. The left column always refers to the control condition, where no breaks were induced (0 nM) and the right column corresponds to conditions where Cas9-mediated double-strand breaks were induced (27.5 nM). Each genomic location is indicated by its abbreviated form, over each scatterplot.

These are all results from one biological replicate, the one used to set the common threshold. All the experiments were repeated at least twice, but replicate data is not presented in this thesis.

The x axis shows the cis distances on one sister, while the y axis shows them on the other sister. Each point represents a single genomic locus, recording the cis distances in both sisters. The red dashed lines represent the disjunction threshold, specific to each genomic location, where we exclude the 5% most extreme data points. It was calculated on the untreated (0 nM) control condition of the presented biological repeat to keep consistency between experiments.

The labeling “1 sister” and “2 sister” refers to the disjunction state on the 4-end structure: “1 sister” means that only one of the two sisters is disjoined at the double-strand break site, and “2 sisters” mean that both are disjoined. “None” means that there is no detected disjunction at the break site.

7.2.1. Wild-type conditions

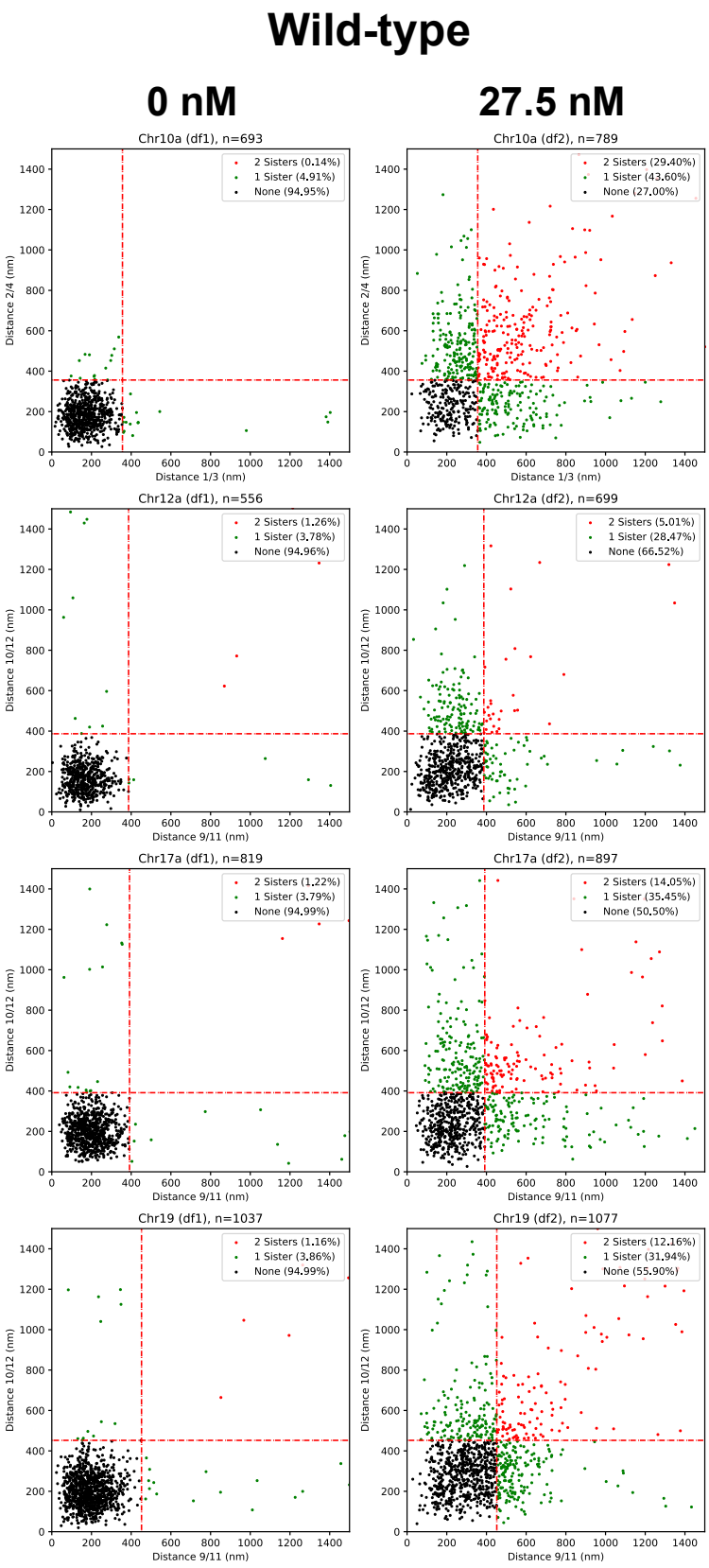

Wild-type

0 nM

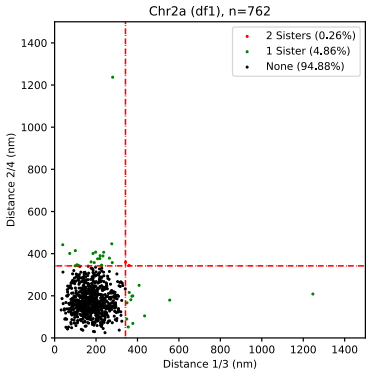

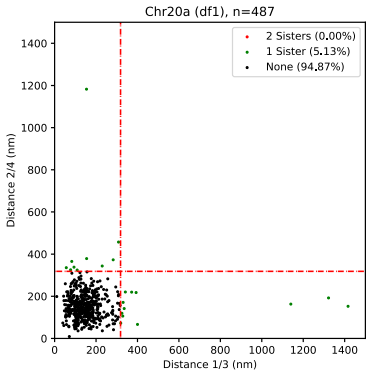

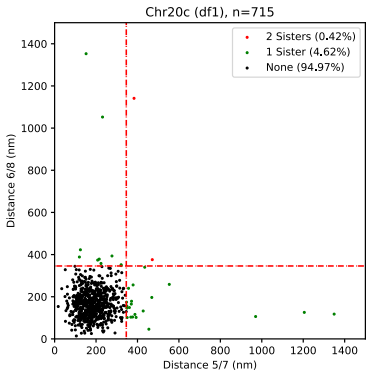

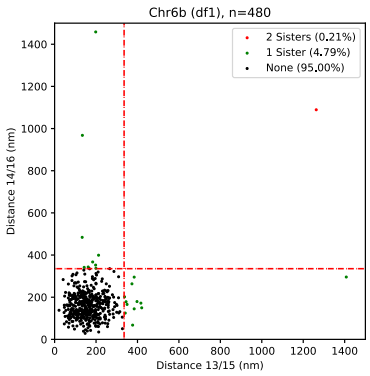

27.5 nM

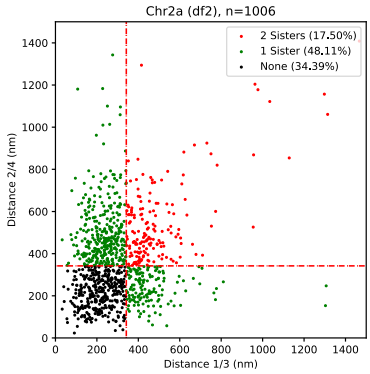

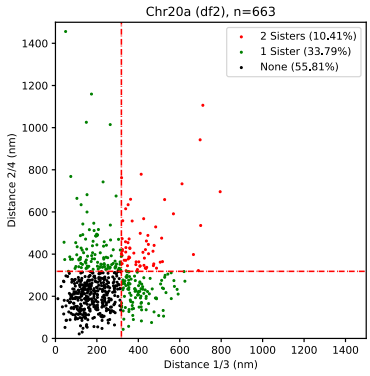

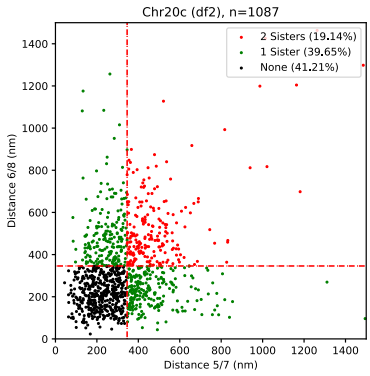

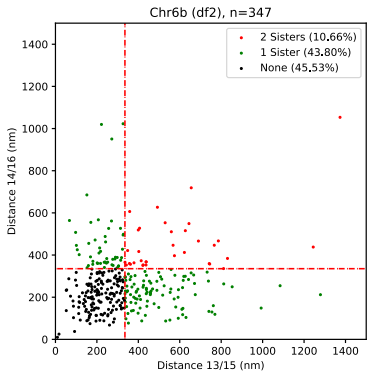

7.2.2. RAD21-depletion condition

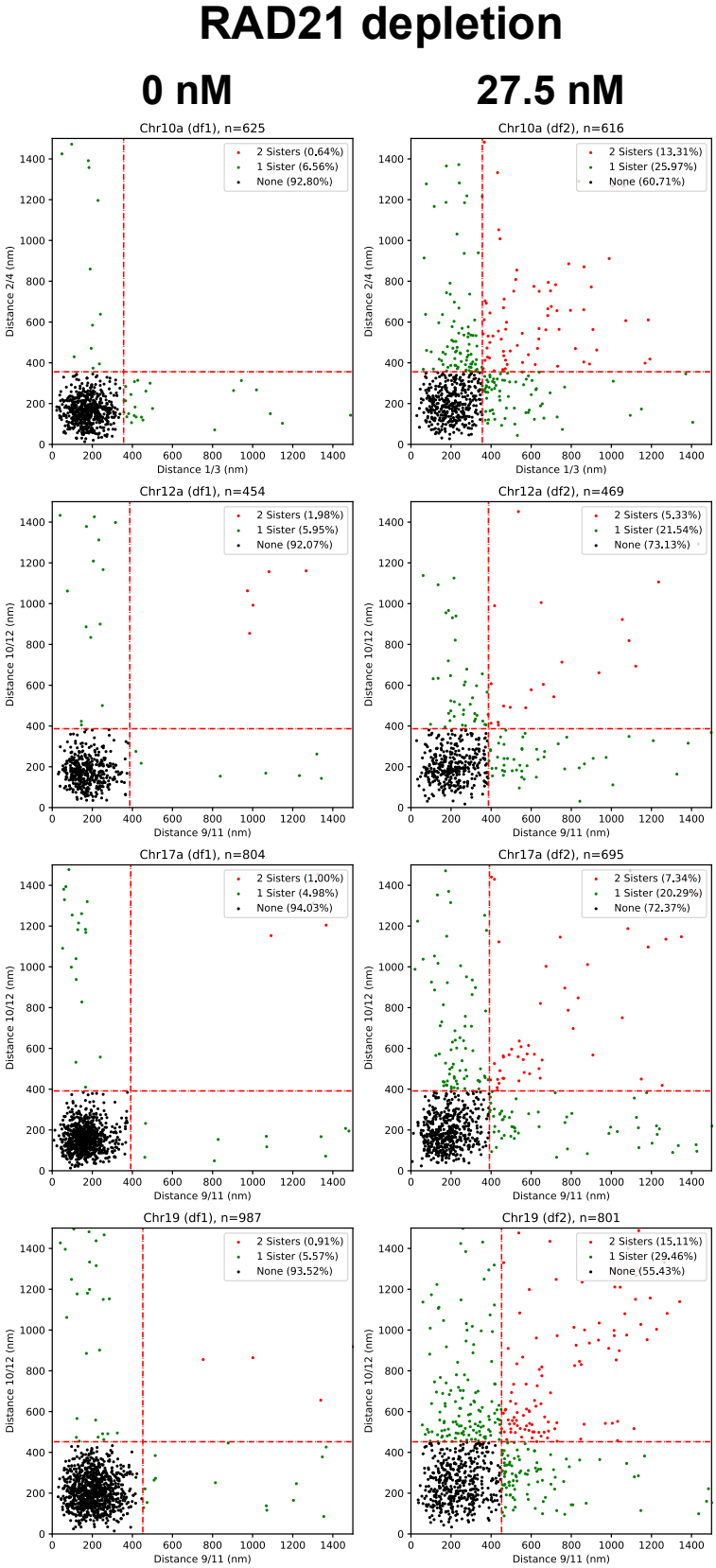

RAD21 depletion

0 nM

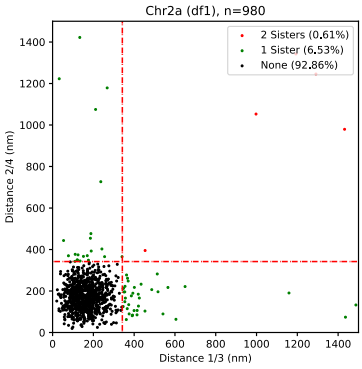

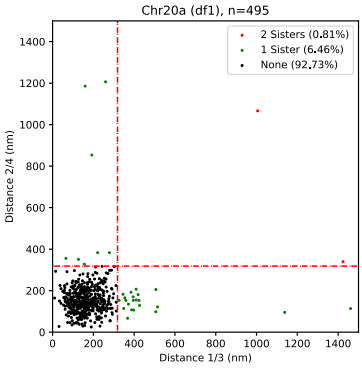

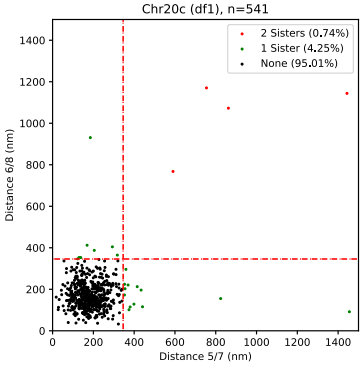

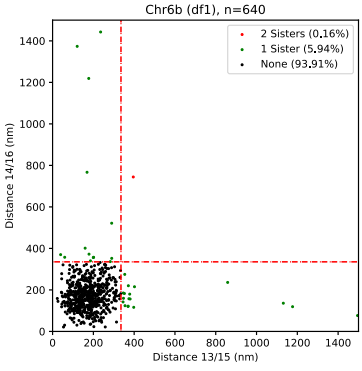

27.5 nM

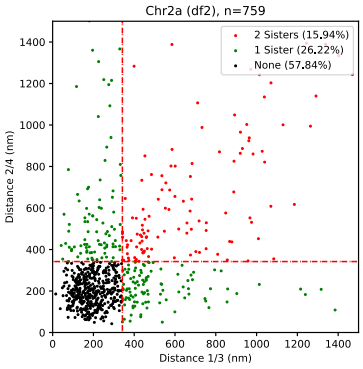

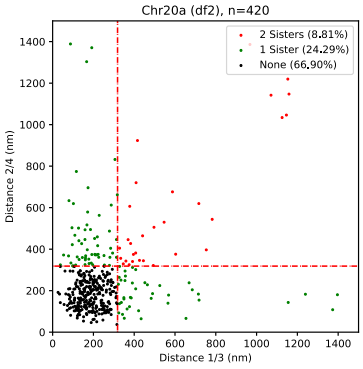

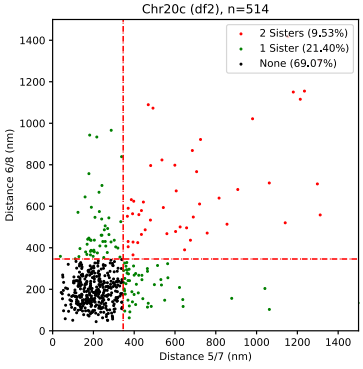

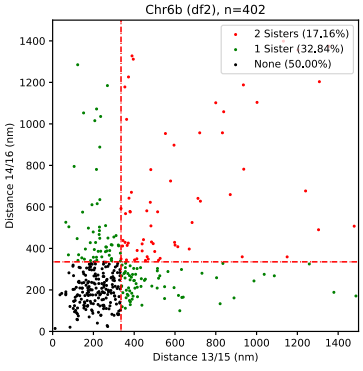

7.2.3. Sororin-depletion condition

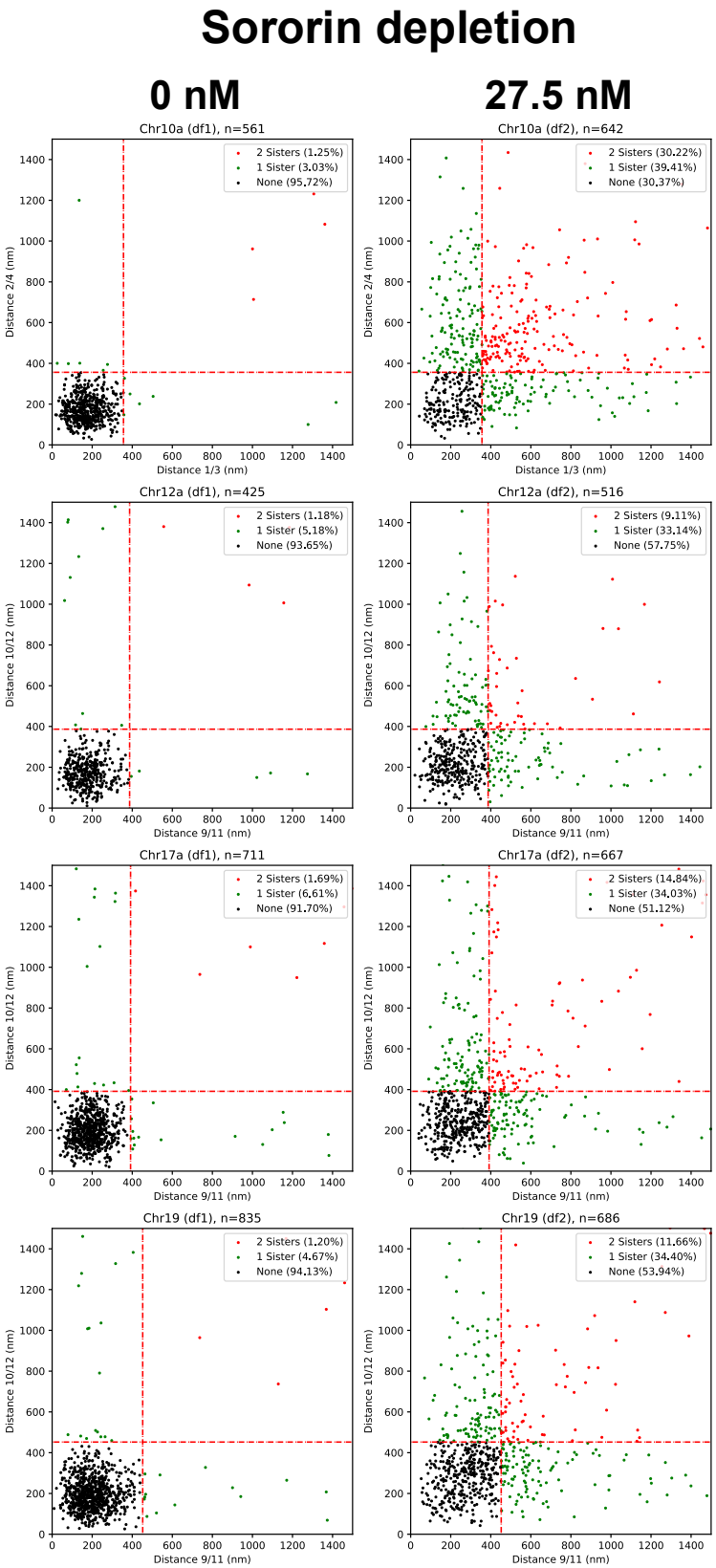

Sororin depletion

0 nM

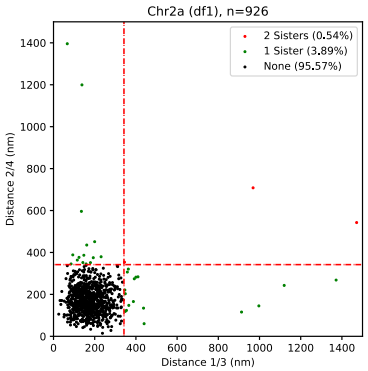

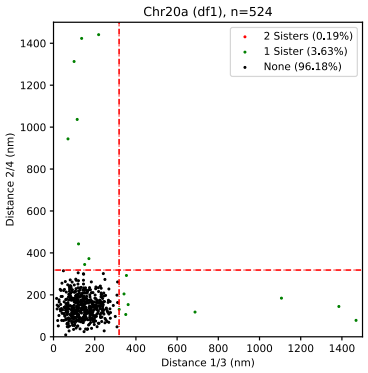

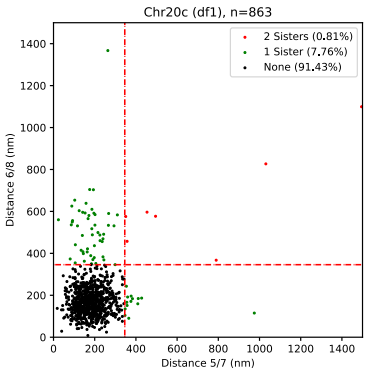

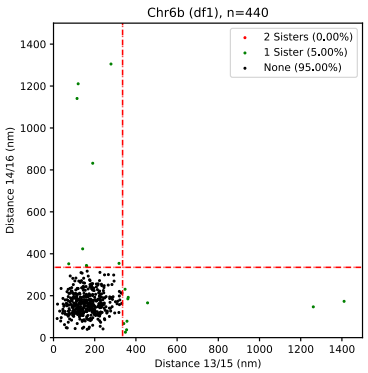

27.5 nM

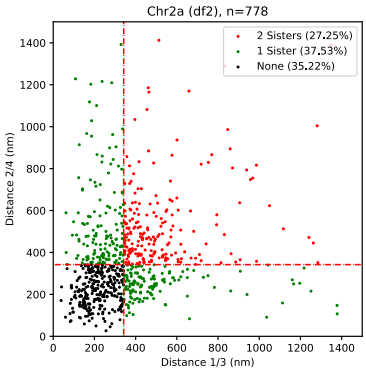

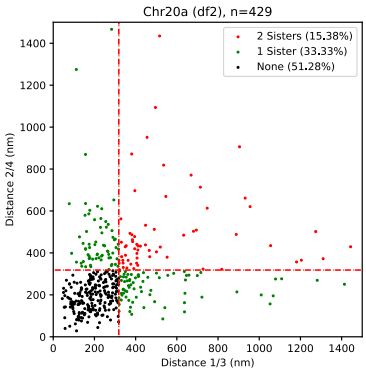

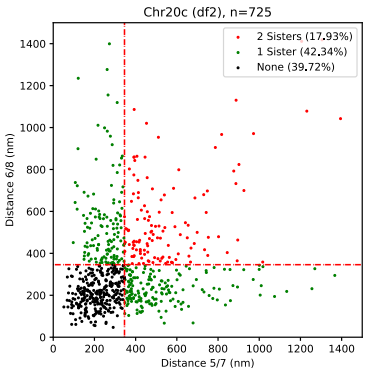

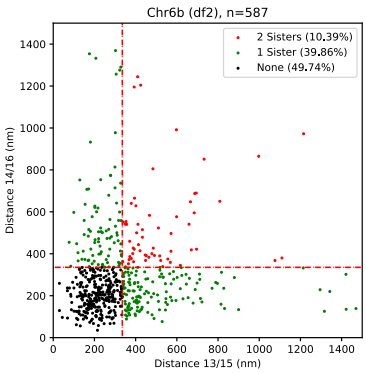

7.2.4. BRCA2-depletion condition

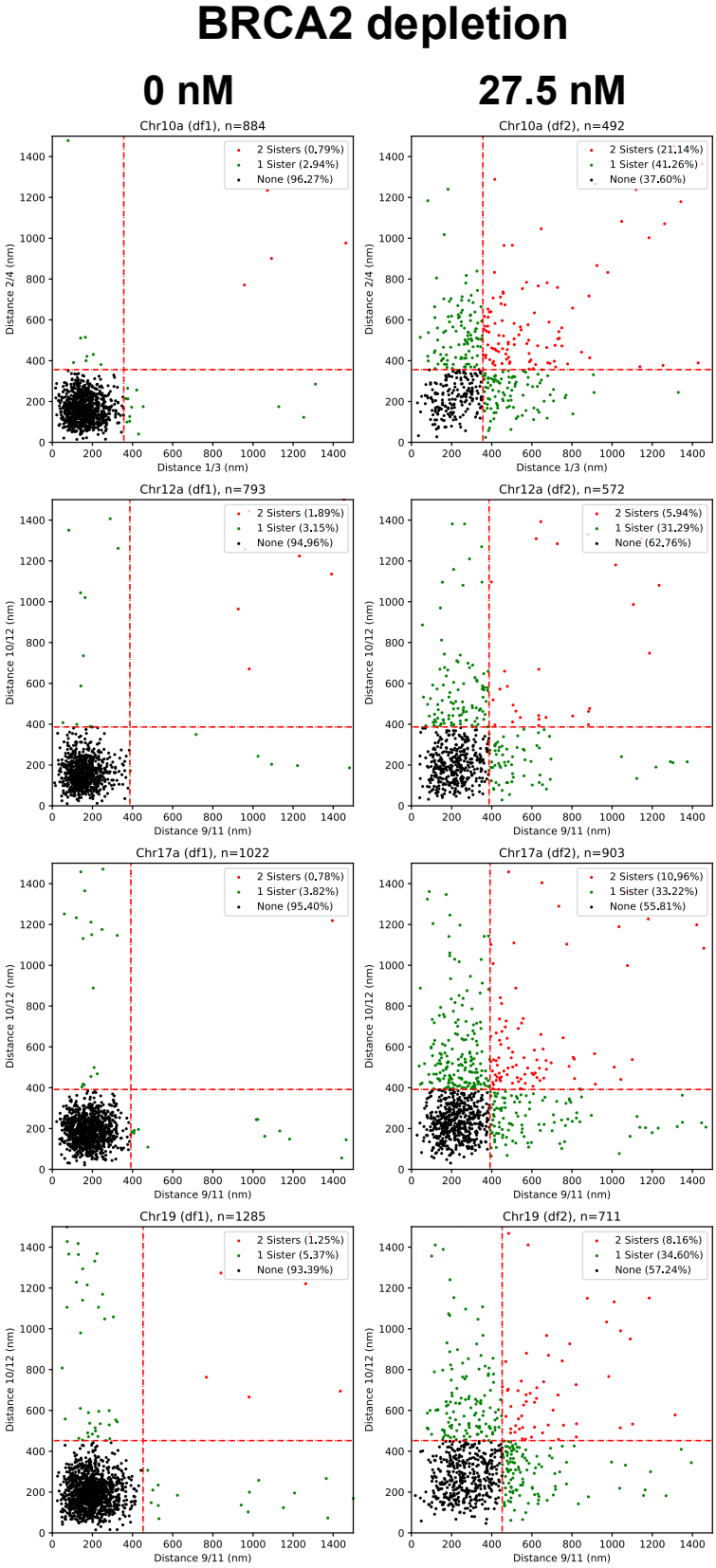

BRCA2 depletion

0 nM

27.5 nM

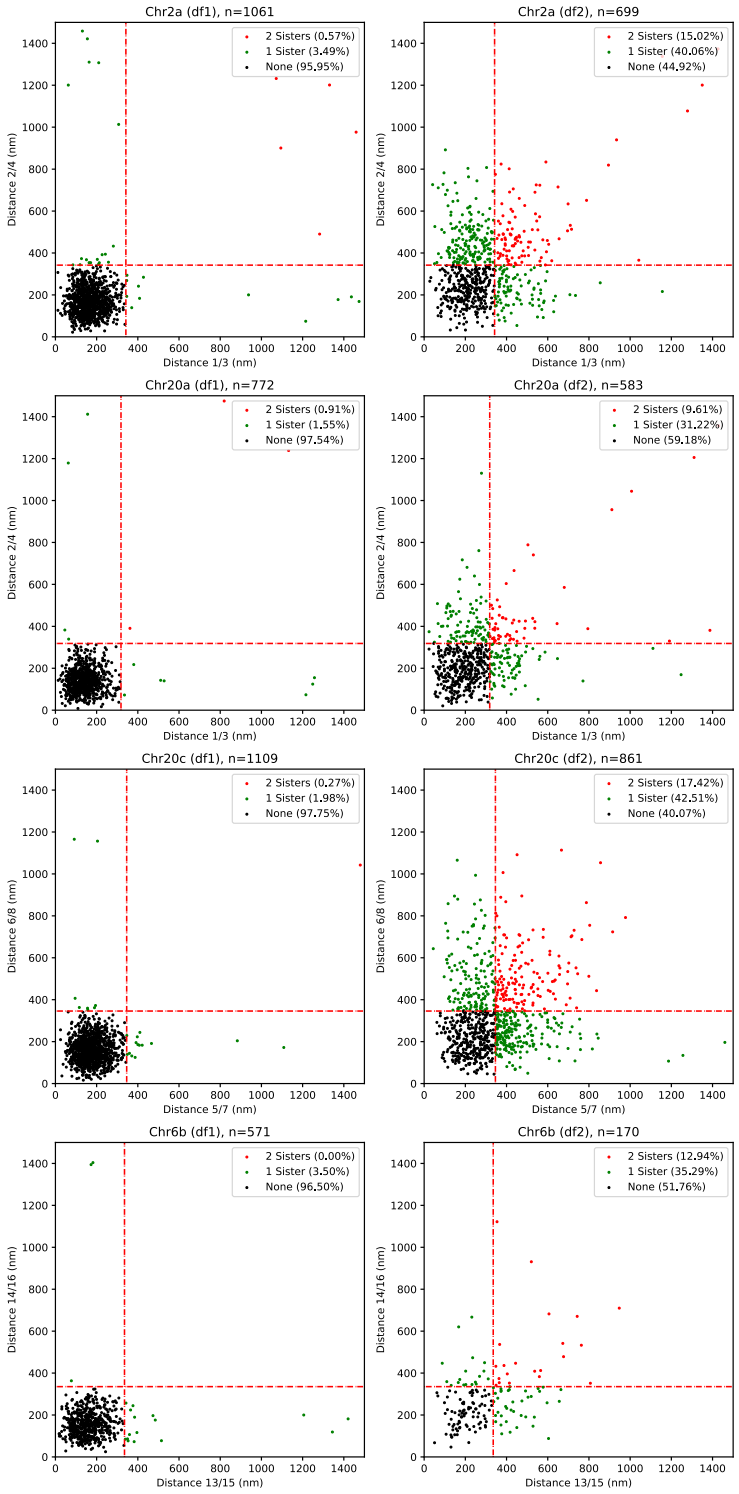

7.2.5. BRCA1-depletion condition

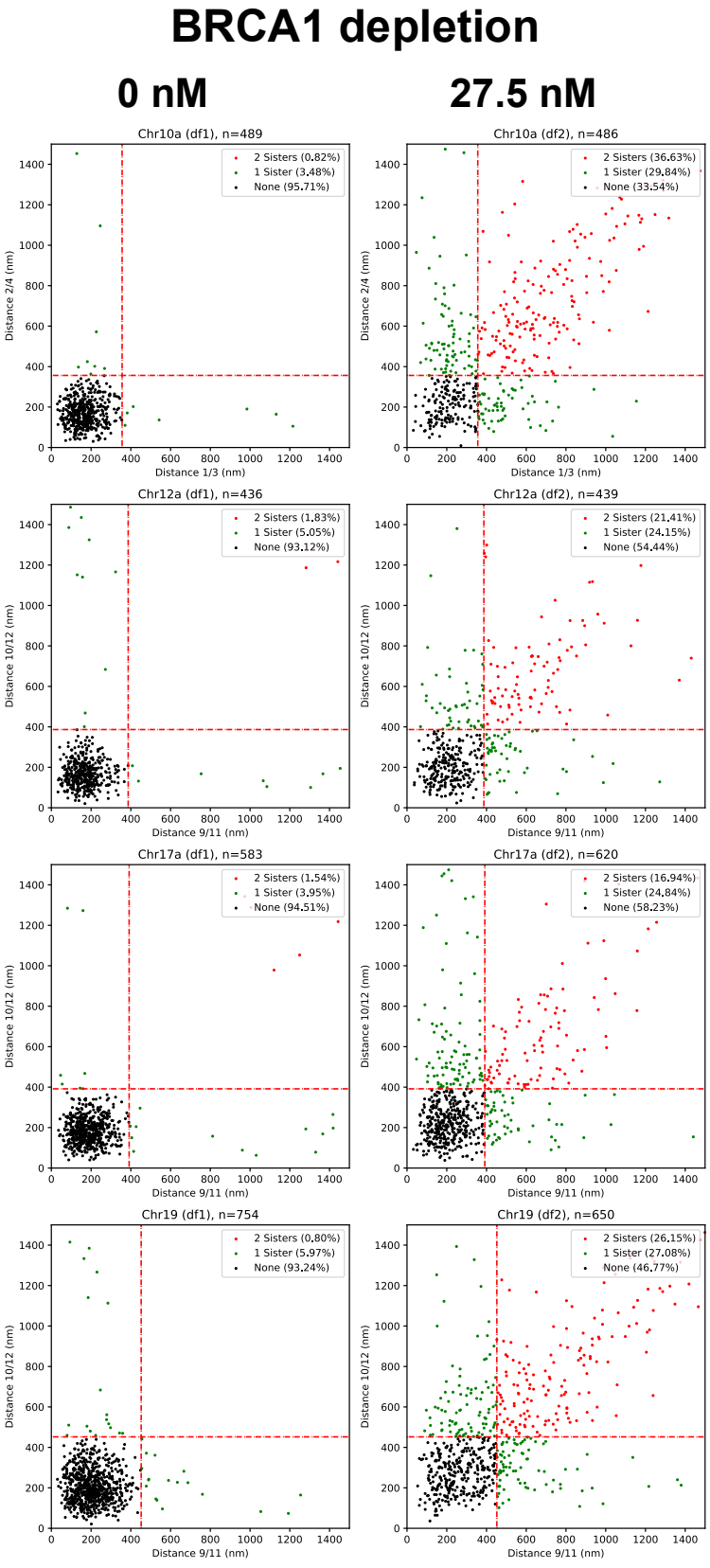

BRCA1 depletion

0 nM

27.5 nM